

Department of Physics and Astronomy

University of Heidelberg

Diploma thesis

in Physics

submitted by

Maren Hellwig

born in Lüdenscheid

- 2011 -

**Measurement of Multiplicity Distributions in
Limited Pseudo-Rapidity Windows in pp and
Pb–Pb collisions with the ALICE Detector**

This diploma thesis has been carried out by Maren Hellwig

at the

Physikalisches Institute Heidelberg

under the supervision of

PD Dr. Klaus Reygers

Measurement of Multiplicity Distributions in Limited Pseudo-Rapidity Windows in pp and Pb–Pb collisions with the ALICE Detector

This thesis presents the analysis of multiplicity distributions in limited pseudo-rapidity windows in high-energy pp and Pb–Pb collisions. Multiplicity distributions contain information about the produced particles like their correlation strength. Therefore they are important tools to investigate the particles production mechanism. Possible interpretations can be grouped into two models: The cascade model which claims that groups of particles are emitted in individual clusters which fragment and models which prefer partially stimulated emission of particles. Furthermore, the concept of intermittency and multifractality will be discussed.

In addition, for Pb–Pb collisions it is of great interest to obtain a reliable observable which can probe the phase transition to the Quark-Gluon Plasma. This study examined the $\alpha\xi$ observable of the Ginzburg-Landau framework in the context of particle collisions for this purpose. Unfortunately, up to this point this observable gives no clear evidence of a phase transition.

Messung von Multiplizitätsverteilungen in limitierten Pseudorapiditäts-Fenstern in pp und Pb–Pb Kollisionen mit ALICE

Diese Arbeit präsentiert die Analyse von Multiplizitätsverteilungen in limitierten Pseudorapiditäts-Fenstern in relativistischen pp und Pb–Pb Kollisionen. Multiplizitätsverteilungen enthalten Informationen über die in einer Kollision produzierten Teilchen, wie z.B. deren Korrelationsstärke. Daher sind diese Verteilungen besonders nützlich, um den Mechanismus der Teilchenproduktion zu untersuchen. Gängige Interpretationen der Teilchenproduktion können zwei Gruppen zugeordnet werden: Zum einen dem Kaskadenmodell, welches behauptet, dass Teilchen in Gruppen von individuellen Anhäufungen emittiert werden und danach fragmentieren und zum anderen dem Modell, welches teilweise stimulierte Emission von Teilchen bevorzugt. Desweiteren werden Konzepte wie Periodizität und Multifraktalität im vorliegenden Kontext diskutiert.

In Pb–Pb Kollisionen ist es zudem von großem Interesse eine Messgröße zu erhalten, welche den Phasenübergang zum Quark-Gluon-Plasma signalisieren kann. Daher wird in diese Arbeit die $\alpha\xi$ Messgröße der Ginzburg-Landau Theorie im Kontext von Teilchenkollisionen untersucht. Bedauerlicherweise kann man mit dieser Messgröße zu diesem Zeitpunkt keine eindeutige Aussage über die Existenz eines Phasenüberganges machen.

Contents

1. Introduction	9
2. The ALICE Experiment	11
2.1. The Large Hadron Collider	11
2.2. The ALICE detector	12
2.2.1. Detector layout	13
2.2.2. The Silicon Pixel Detector	15
2.3. The AliRoot Framework	18
2.4. Event Generator	19
3. Theoretical Framework	21
3.1. Quantum Chromodynamics	21
3.2. Quark-Gluon Plasma	22
3.3. QCD phase diagram	23
3.4. Ginzburg-Landau framework	25
3.5. Multiplicity Distribution	28
3.5.1. The Negative Binomial Distribution	29
3.5.2. The NBD k parameter and the Ginzburg-Landau frame- work	31
3.5.3. Convolution property of the NBD	33
3.5.4. Clan Model	34
3.5.5. Intermittency and Multifractality	35
3.6. Collision centrality in nucleus-nucleus collisions	37
3.6.1. The Glauber Monte Carlo Calculation	37
4. Data Analysis	41
4.1. Proton-Proton collisions	41
4.1.1. Trigger and Event selection	41
4.1.2. Measurement of multiplicity distributions	44
4.1.3. Correction through unfolding methods	44
4.1.4. Extraction of NBD k parameter	49
4.2. Pb-Pb collisions	50
4.2.1. Event and Trigger Selection	50
4.2.2. Centrality selection	51
4.2.3. Correction	53

Contents

4.2.4. Extraction of NBD k and $\alpha\xi$ parameters	54
5. Results	55
5.1. Proton-Proton collisions	55
5.1.1. Measured distributions	55
5.1.2. Corrected distributions	57
5.1.3. NBD k parameter versus $\delta\eta$	62
5.1.4. Comparison to MC predictions	69
5.2. Pb–Pb collisions	72
5.2.1. Measured multiplicity distributions	72
5.2.2. Correction of multiplicity distributions	73
5.2.3. Clan model	75
5.2.4. The Ginzburg-Landau Fit	76
6. Summary and Outlook	81
A. Acronyms	83
B. Multiplicity Distributions	85
Bibliography	100

1. Introduction

'I'm still confused, but on a higher level.'

Enrico Fermi

It is part of the human nature to question things which surround them and to make an effort to get a further understanding of them. As Enrico Fermi once stated, it is possible that one gains a deeper insight into certain things however, new questions tend to grow. Driven by the desire to investigate the constituents of matter and their dynamics, high-energy particle colliders and multi-purpose detector-systems have been build.

ALICE [Ali08] (A Large Ion Collider Experiment) which is positioned at an intersection point of the Large Hadron Collider (LHC) and located at the European Organization for Nuclear Research (CERN) has taken data of proton-proton collisions since the end of 2009. The obtained data is still being analysed in order to gain a greater understanding of the detector performance, to check if already proofed observables can be reproduced and to extract reference data for the heavy-ion program. The heavy-ion program of the LHC with the ALICE detector as its designated measurement facility is designed to break world records in the experimentally highest ever probed energy region. Its goal is to study strongly-interacting matter, primarily the Quark-Gluon Plasma as well as the related phase transition.

Recently, the ALICE detector has again drawn much attention with the first nucleus-nucleus collisions on the 8th of November 2010 at a center-of-mass energy per nucleon pair of $\sqrt{s_{NN}} = 2.76$ TeV; the highest ever achieved energy for this collision type.

This diploma thesis will have a closer look at a fundamental observable: multiplicity distributions of charged particles. Multiplicity distributions contain a huge amount of information of the produced final state particles like their production mechanism and their correlation strength. The correction of the

1. Introduction

measured spectra will be done for pp collisions with two individual unfolding techniques, namely the χ^2 - and the Bayesian unfolding. They are able to eliminate detector effects. The correction of multiplicity distributions of Pb–Pb collisions is done by correcting for fake tracklets as well as for the detector acceptance.

The following analysis will have a look at pp and Pb–Pb collisions and will put an emphasis on particle correlations. Both collision types will have a slightly different focus. In pp the top priority was put upon the particle production mechanism like cascading processes and the concept of intermittency. In Pb–Pb collisions the focus lies upon the investigation of a possible phase transition. Therefore the two-point particle correlation function which is predicted to be of the form of $\alpha e^{-\frac{|\eta_1 - \eta_2|}{\xi}}$ [Adl07], is of great interest. There α is the correlation strength, $|\eta_1 - \eta_2|$ the one dimensional distance in pseudo-rapidity and $\xi \propto |T - T_c|^{-\frac{1}{2}}$ the spatial correlation length. By analysing these two-particle density correlations in pseudo-rapidity one can get a observable which is a possible indicator for a phase transition in Pb–Pb collisions at LHC energies.

2. The ALICE Experiment

This chapter will briefly introduce the experimental setup of the particle collider as well as of the ALICE detector. This detector was used to measure the experimental observables which will be analysed in this analysis. Special emphasis is put on the Silicon Pixel Detector (SPD) which was mainly used for the data extraction.

2.1. The Large Hadron Collider

The Large Hadron Collider (LHC) [Eva08] is located at the border of France and Switzerland at the Conseil Européen pour la Recherche Nucléaire (CERN) close to Geneva. This high-energy particle collider is capable to collide protons with protons, nuclei with nuclei and protons with nuclei at the highest center-of-mass energies ever achieved in the world. It is the most powerful tool to answer open questions and fundamental issues in the high-energy regime of particle physics. Today, protons collide with a center-of-mass-energy of $\sqrt{s} = 7$ TeV and heavy ions at $\sqrt{s_{NN}} = 2.76$ TeV per nucleon pair. The design values for pp collisions with $\sqrt{s} = 14$ TeV and Pb–Pb collisions with $\sqrt{s_{NN}} = 5.74$ TeV per nucleon pair are not yet reached because data taking just started at the end of 2009 with lower energies. The energy will be carefully increased over the next years. At the moment the luminosity for colliding protons is $\mathcal{L} = 4.67 \times 10^{32} \text{ cm}^{-2}\text{s}^{-1}$. It is planned to reach a luminosity of $\mathcal{L} = 10^{34} \text{ cm}^{-2}\text{s}^{-1}$ for protons and $\mathcal{L} = 10^{27} \text{ cm}^{-2}\text{s}^{-1}$ for heavy ions within the next years which corresponds to a bunch crossing rate of 40 MHz.

The LHC is a scientific environment which exhibits a variety of world records. It starts with the spatial dimension of the LHC which consists of two adjacent parallel beam pipes which were build in the old Large Electron Positron (LEP) tunnel. The tunnel has a circumference of 27 kilometres and is located 50 to 175 metres underground. The parallel beam pipes where the particles counter-rotate through, intersect at the four interaction points at which the experiments ALICE, ATLAS, CMS and LHCb were installed. The particles are kept on their path by 1,232 dipole and 392 quadrupole magnets which make in total around 1632 superconducting magnets. Before particles are injected into the LHC tunnel they need to be pre-accelerated successively in order to reach a speed close to the speed-of-light [Wik11a]. The acceleration of protons starts at the linear accelerator LINAC 2 which generates 50 MeV protons. Next the

2. The ALICE Experiment

Proton Synchrotron Booster (PBS) boosts them to 1.4 GeV and feeds them to the Proton Synchrotron (PS) which accelerates them to 25 GeV. In a last step the Super Proton Synchrotron (SPS) increases their speed up to 450 GeV before injecting the beam into the LHC. The pre-acceleration for Pb–Pb collisions varies a bit from that procedure in the first two steps. The lead ions are first accelerated by the linear accelerator LINAC 3 and next injected into the Low-Energy Ion Ring which stores and cools the ions. Then they are fed to the PS from which on the same procedure as for protons remains. The final velocity of each beam which is 99.9% of the speed-of-light for pp collisions at 14 TeV is achieved by the LHC itself. After the beams have reached their final velocity they are brought to collision in the four experiments. Further information can be found in [Eva08].

2.2. The ALICE detector

ALICE [Aam08] stands for A Large Ion Collider Experiment and is a dedicated multi-purpose heavy-ion experiment which focuses on various observables such as multiplicity, transverse or zero-degree energy flow, the impact parameter, the shape as well as the orientation of the collision volume and the number of interacting nucleons. The strength of ALICE lies in the low p_t region of particles as well as on the particle identification. This is caused by the low magnetic field of 0.5 T. As a result ALICE will be able to gain a deeper understanding of Quantum Chromodynamics (QCD) which is the theory of the strong interaction in the Standard Model.

Therefore, driven by the physics requirements, ALICE had an important design constraint: the extreme particle multiplicity. The expected charged particle multiplicity density at mid-rapidity in central Pb–Pb collisions varied from $dN_{ch}/d\eta = 2000$ to $dN_{ch}/d\eta = 8000$. These values are up to three orders of magnitudes larger than in typical pp collisions at the same energy and two to five times above the highest multiplicities ever achieved at the Relativistic Heavy Ion Collider (RHIC). Due to more recent extrapolations of RHIC data the design of ALICE was optimized to a value of $dN_{ch}/d\eta = 4000$. The recently measured $dN_{ch}/d\eta$ in Pb–Pb collisions at a center-of-mass energy per produced nuclei of 2.76 TeV is lower than expected with $dN_{ch}/d\eta = 1600$ at mid-rapidity [Aam10c].

Another significant feature of this experiment is its large momentum range which goes over more than three orders of magnitude from a few MeV/ c up to some 100 GeV/ c . This region needs to be covered in order to be able to investigate collective effects over several length scales, to have a good acceptance for resonance decays as well as to be able to do jet physics. The combination of a small material budget with a large tracking coverage solves these special needs. Having a small material budget helps to reduce the possibility of mul-

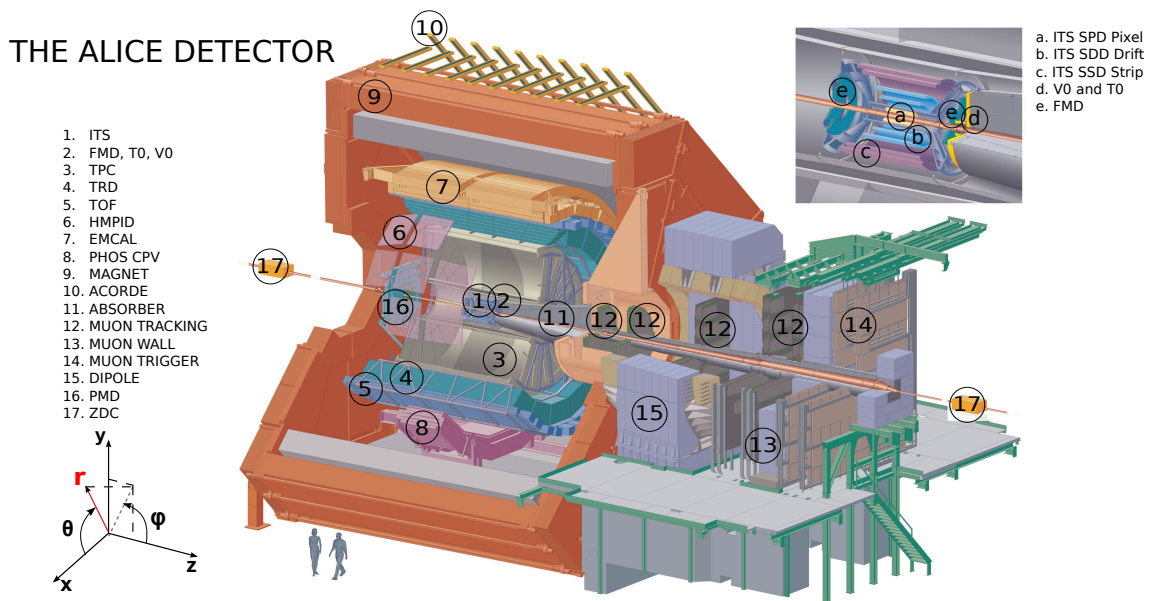


Figure 2.1.: A Large Ion Collider Experiment (ALICE) [Ali08]

multiple scattering in the low p_t region. Whereas the large tracking lever arm of up to 3.5 m provides a good resolution at high p_t . Therefore it was made sure that this broad momentum range can be covered.

The particle identification (PID) over the covered momentum range is another challenge for ALICE which is of key importance. Since many observables are mass or flavor dependent one can identify single particle species in order to specify the investigated particle environment more precisely. Given that, ALICE utilizes various PID techniques like the identification of particles through the specific ionization energy loss dE/dx , the time-of-flight, the transition and the Cherenkov radiation. On top of that the electromagnetic calorimeters, the muon filters and the reconstruction of topological decays play an important role for the PID.

2.2.1. Detector layout

In order to fulfill the broad range of physics requests mentioned before ALICE is constructed out of various detectors which are wrapped around the beam pipe and exhibit a shell like structure. The sub-detectors are dedicated to tracking, particle identification, triggering and energy counting.

Figure 2.1 shows a schematic view of ALICE. Staring at the inside from the beam pipe and going to the outside particles will first be detected by the Inner Tracking System (ITS). In the upper right corner of Figure 2.1 a close-up of the systems bordering the beam pipe is depicted. These detectors are the ITS,

2. The ALICE Experiment

the V0, the T0 and the FMD. The ITS consists of six cylindrical layers which are wrapped around the beam pipe. The V0, T0 and the Forward Multiplicity Detector (FMD) are located in forward direction to the beam pipe. Looking back at the main picture it can be seen that these detectors are surrounded by the Time Projection Chamber (TPC), the Transition Radiation Detector (TRD) and the Time-Of-Flight detector (TOF). All these inner systems except the Forward detectors cover the full azimuthal angle once all the modules are installed. In the next layer the Photon Spectrometer (PHOS), the Electromagnetic Spectrometer (EMCAL) and the High-Momentum Particle Identification Detector (HMPID) are located. The ALICE Cosmic Ray Detector (ACORDE) is placed on top of the magnet which fully surrounds the just mentioned detector systems and has a total weight of 7800 tons. Still left outside the magnet are the Muon spectrometer and the Forward detectors like the Zero Degree Calorimeter (ZDC) and the Photon Multiplicity Detector (PMD). Each detector system has its own assignment to help achieving a better understanding of the collided system.

Tracking The ITS, the TPC and the TRD are the dedicated inner tracking detectors. A component detector of the ITS will be described in detail in the next section given the fact that this sub-detector, the Silicon Pixel detector (SPD), is crucial for the following analysis due to its wide pseudo-rapidity coverage of $|\eta| < 1.4$. The ITS and TPC are able to reconstruct the primary vertex as well as the secondary vertex of heavy flavor and strange particle decays and are capable of doing particle identification. Tracking in the low momentum region is done by the ITS. ALICE's main tracking detector is the TPC which provides a robust and efficient tracking. In addition, it especially improves the particle identification in the region of the relativistic rise up to 50 GeV/ c . Furthermore, the TPC is optimized for a 'good double-track resolution and minimum space charge induced distortions' [Aam08]. The TRD supports the other tracking detectors in improving the resolution in the high transverse momentum region.

Particle Identification Particle identification over a large pseudo-rapidity and momentum range for many different particles is done via the Time-Projection Chamber (TPC), the Time-Of-Flight (TOF) array, the High-Momentum Particle Identification Detector (HMPID) and the Transition Radiation Detector (TRD). TOF can separate pions, kaons and protons event-by-event up to 3 GeV/ c when it is combined with the ITS and the TPC. This allows invariant mass studies of identified kaons, the investigation of open heavy-flavour states and vector-meson resonances. The HMPID is able to identify hadrons whose transverse momentum is larger than 1 GeV/ c . Light nuclei and anti-nuclei like

d, t, ^3He and α can be identified by the TPC and the TRD. The TRD is also dedicated to the identification of electrons above 1 GeV/ c to probe production rates of quarkonia and heavy quarks close to mid-rapidity.

Trigger detectors Trigger detectors are special systems which measure global event characteristics. ALICE has several trigger detectors which can be combined in different trigger schemes. Further information about the online trigger procedure is given in section 4.1.1 and will give an overview over offline triggering as well. Possible online trigger detectors are the T0, V0, ACORDE, FMD and ZDC. The T0 evaluates the event time by Cherenkov counters whereas the V0 scintillators can be used as minimum bias triggers and reject beam-gas background. ACORDE triggers on cosmic rays for calibration and alignment reasons. The FMD provides information about multiplicity and spatial distribution of photons and the ZDC measures the impact parameter of a collision.

Electromagnetic Calorimeters ALICE has two different electromagnetic calorimeters: PHOS and EMCAL. PHOS measures the photons from thermal processes, from hard QCD processes and from neutral mesons. It can reject charged particles. EMCAL was built in order to account for the fact that interactions and energy loss of high energy partons contain interesting information in high energy collisions. Using the EMCAL, which has a lower granularity and energy resolution than PHOS, it is possible to measure the properties of jets like their production rates more precisely than PHOS. Besides that EMCAL is able to estimate fragmentation functions together with other detector systems.

Muon Spectrometer The Muon Spectrometer is dedicated to measure the production of heavy-quark resonances like the J/Ψ and Υ families with a mass resolution that allows to separate all resonances. Due to the absorber which reduces hadron contamination, the muon spectrometer provides only a good resolution of the low p_t region at small angles. This is caused by the fact that muons are Lorentz boosted at large rapidity ranges.

2.2.2. The Silicon Pixel Detector

The Silicon Pixel Detector (SPD) is the inner part of the Inner Tracking System (ITS) and is composed out of two cylindrical layers of hybrid silicon pixel components. They are located at a radial distance of 3.9 and 7.6 cm from the beam line and contain a total of 9.8×10^6 pixels. They cover an active area of 12.8 mm in $r\varphi$ and 70.7 mm in z -direction which are read out by 1200 electronic chips.

The SPD is dedicated to the reconstruction of the primary vertex position and

2. The ALICE Experiment

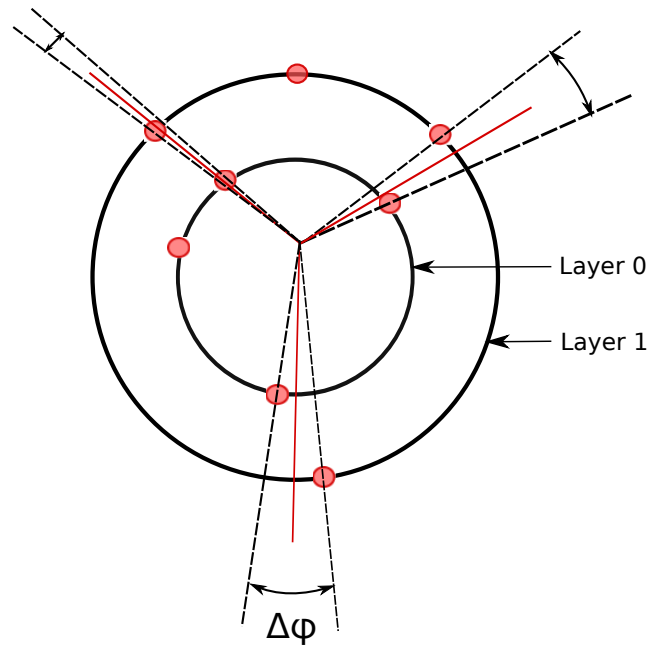


Figure 2.2.: Schematic view of the reconstruction procedure of SPD tracklets

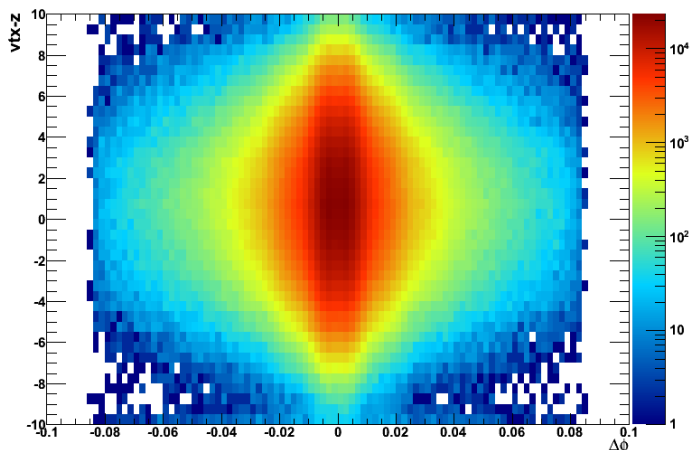
the determination of the impact parameter from secondary tracks coming from weak decays of strange, charm and beauty particles. Coming along with the location of the SPD relative to the interaction point (IP) the track density in the layers is in the order of $50 \text{ tracks}/\text{cm}^2$ in heavy-ion collisions. At this location the radiation level is very high too. Therefore the SPD needed to have a very low material budget in order to be able to operate for an acceptable time period. The material was reduced up to the point where a track coming perpendicular out of the detector surface exhibits around 1% of the radiation length per layer.

Reconstruction of tracklets

The SPD is of key importance for the reconstruction of tracklets which are needed for the measurement of the charged-particle multiplicity. If a particle hits one of the layers of the SPD with an energy over a given threshold, a cluster is formed.

In order to form tracklets, both layers 0 and 1 have to have clusters. Figure 2.2¹ sketches the reconstruction procedure. Each cluster of layer 0 is connected with a straight line to each cluster in layer 1. At the point where the majority of lines from combined clusters cross, one has found the primary vertex. The next step is the selection of candidate tracklets. All candidate tracklets which are formed with clusters from both layers and which end in the reconstructed

¹Figure 2.2 is closely related to Figure 4.10 (a),(b) in [Gro09]

Figure 2.3.: $\Delta\varphi(z)$ distribution of SPD tracklets

primary vertex, are kept. A further selection is made by setting a threshold for the azimuthal difference $\Delta\varphi$ between clusters in layer 0 and layer 1 of a found tracklet. This azimuthal difference needs to be below a maximum value in order to suppress combinatorial background coming from fake tracklets. The threshold of the $\Delta\varphi$ value can be found through the $\Delta\varphi(z)$ distribution in Figure 2.3. One can extract out of this illustration that the majority of found tracklets are in the region of $|\Delta\varphi(z)| < 0.03$ rad. Although going to $|\Delta\varphi(z)| < 0.05$ rad the counting rate drops for a order of magnitude, this region is still acceptable. From $|\Delta\varphi(z)| > 0.05$ the number of tracklets is drastically dropping and the combinatorial background increases. To reduce the bias introduced by combinatorial background a cut of $|\Delta\varphi(z)| < 0.05$ was chosen. Due to this procedure one can reconstruct the tracklets which appear in the event as well as at the primary vertex. The procedure of finding the primary vertex introduces a dispersion in its actual position in polar direction. This dispersion needs to be kept small for analysis purposes and has an acceptable maximum value of $\Delta\theta = 0.02$ rad.

Tracklets which are used in this analysis are primary tracklets. Those are tracklets from particles which are not only formed by the particles produced in the collision but also by the clusters from their decay particles. These produced particles include the products of strong and electromagnetic decays as well as weak decays of beauty and charm particles. Excluded are products from strange weak decays as well as other secondary particles like γ conversions and their products.

If a cut of $|\Delta\varphi| < 0.05$ rad is applied, one can be certain that 99% of the reconstructed particles stem from primary particles [Gro09]. Therefore one has a very low contamination from secondary particles and a high efficiency for selecting primaries. Followed by this, the $\Delta\varphi$ cut is a quality parameter

2. The ALICE Experiment

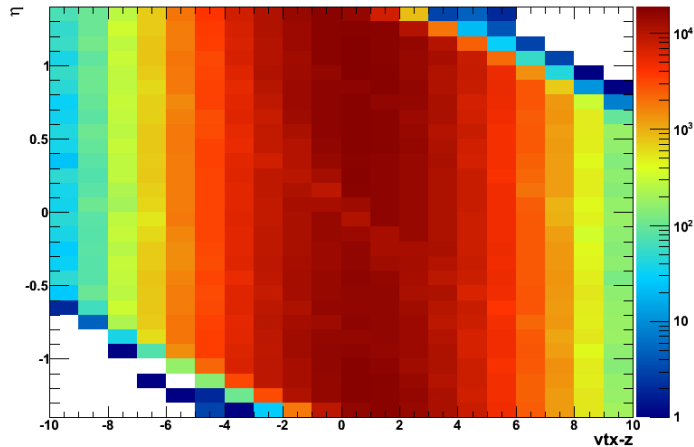


Figure 2.4.: SPD acceptance of pseudo-rapidity versus the z position

for primary tracklets.

Acceptance of the SPD

The SPD has full coverage in azimuthal direction but is limited in pseudo-rapidity space η . The innermost layer covers $|\eta| < 2$ and the outer layer $|\eta| < 1.4$. In the tracklet and primary vertex reconstruction both layers are needed. As a result the maximum pseudo-rapidity coverage is reduced to $|\eta| < 1.4$ in this analysis. It was checked if the SPD covers the full η -area of the fiducial z -region of ± 10 cm. It was observed that η is dependent on z . As illustrated in Figure 2.4 the acceptance has a somewhat twisted band structure going from the upper left corner to the lower right corner. Therefore it is necessary to carefully take the SPD acceptance in η through the application of cuts in z direction into account. Especially one has to put an emphasis on these cuts in strongly pseudo-rapidity dependent analysis like in the following case.

2.3. The AliRoot Framework

The AliRoot Framework [Car08] is built upon the ROOT system [Bru97] and customized for ALICE in order to be able to simulate, reconstruct and analyse physics events in the given high-energy regime. AliRoot is more powerful than ROOT by itself due to its various and highly specific analysis classes which enable advanced data selection and processing.

The Monte Carlo simulation of primary interactions is done via event generators like PYTHIA [Sjö06] (see section 2.4) or PHOJET. The produced set

of simulated particles are afterwards propagated through the sub-detectors by the use of the transport packages GEANT3, GEANT4 and FLUKA. As output one gets a kinematic tree which stores the information of the particles momenta, their decay history and their production vertex. During the particles propagation through the sub-detectors they produce so called hits. Hits correspond to energy depositions in the detector at a given point and are saved in Monte Carlo labels which contain the information of the particle ancestor besides other details. Each detector system has its own definition of a hit, but can be generally assigned into one of the following two groups. The first group refers to a hit when it discovers a energy deposition in an active detector volume like EMCAL and PHOS and the second group triggers a hit whenever the energy deposition is above a specific threshold like ITS and TOF. In a next step the detector response is factorized and the hits are converted into summable digits. Afterwards this information is stored in formats acceptable for reconstruction.

The reconstruction framework processes digits, digitized signals at a specific time, and clusters which are sets of adjacent digits in space and/or time. Clusters most likely stem from the same particle which was sensed by adjacent active areas. First, the space point where the particle crossed these sensitive elements is reconstructed. So that the reconstructed clusters are located in the center of gravity of all adjacent fired chips. Next, the track or tracklet is reconstructed with a set of parameters through the particles trajectory and the covariance matrix of the given space point. It follows the reconstruction of the vertex and the particle identification. The results of the reconstruction process are stored in the Event Summary Data (ESD).

The analysis done with AliRoot always has a special physical focus and therefore cannot be characterized in a more general way.

2.4. Event Generator

An event generator [Sjö06] is capable of simulating physics events that are produced in high-energy collisions. Software libraries store the information of processes of various physics aspects. These aspects can be very different regarding the state of an event. Monte Carlo techniques use the relevant probability distribution to make sure that the final events are randomly distributed. The sub-processes covered by event generators are initial-state compositions of the colliding particles (like the flavour and the initial energy), the sub-structure, initial-state parton showers, hard processes, resonance decays, final-state showers, associated semi-hard processes as well as hadronization and further decay processes.

2. *The ALICE Experiment*

The procedure of assigning the realistic development of an event to the initial state is unfortunately limited by the current knowledge of the underlying physics. This lack of knowledge needs to be approximated because event generators are used to correct the bias on data introduced by the detector through simulation of physics events. The approximation of physics events is done via a combination of perturbative QCD and phenomenological approaches.

Event generator produce outputs that have the form of events and behave like real data. These events can be used to predict the result.

PYTHIA One possible event generator for the simulation of ALICE MC data is PYTHIA. There the hard interactions are described via perturbative QCD if the partons have a momentum transfer that is above a tunable minimal p_T cut-off value. Soft interactions need to be treated differently because the strong coupling constant $\alpha_s \rightarrow 1$ and therefore perturbative QCD is not valid any more. This gives rise to the use of the Regge theory with the Pomeron and the Reggeon exchange to describe soft interactions. Their exchange explains the experimentally seen rise of cross sections in higher center-of-mass systems. Further details about the Regge theory can be found in [Col77] .

3. Theoretical Framework

This chapter introduces the theoretical baseline of the presented analysis. First it will give a brief impression of the Quantum Chromodynamics (QCD) which solved the quest of the constituents of hadronic matter and their dynamical relation to each other at normal conditions. Special emphasis is made on the QCD phase diagram and one of its phases called the Quark-Gluon Plasma (QGP). In the past decade it was of great importance to probe this plasma with collider experiments. Therefore the Ginzburg-Landau theory first known from superconductivity will be introduced in the context of heavy-ion collisions in order to suggest a possible experimental observable which might be capable of indicating a phase transition to the QGP. This observable can be extracted out of charged-particle multiplicity distributions which are described by the negative binomial distribution (NBD). This dependence between multiplicity distributions and the NBD gives the opportunity to investigate the underlying particle production mechanism with the clan model and to examine particle density correlations with the NBD convolution property as well as to investigate intermittency and multifractality. Furthermore, the centrality classification of ultra-relativistic heavy-ion collisions with the Glauber Monte Carlo approach will be addressed and later on used to analyse multiplicity distributions in different centrality classes.

3.1. Quantum Chromodynamics

Quantum Chromodynamics (QCD) [Shu04] [Wik11b] is the theory of the color force which is part of the Standard Model of particle physics. This fundamental force is mediated by gluons which act as gauge bosons on color-charged fermions (quarks and antiquarks) as well as on themselves. Gluon-gluon interactions are possible due to the fact that gluons carry color charge. The force confines quarks into composite particles (hadrons) which appear to have the size close to 1 fm at room temperature and density. Besides this QCD merges two important features of the strong interaction: The first one is confinement and the second feature is asymptotic freedom. Confinement means that one has to induce an infinite amount of energy into the separation of two bound quarks. They are never found to occur individually in order to conserve color charge. The asymptotic freedom on the other hand is related to a different energy scale. Whenever one approaches very high energies and therefore high

3. Theoretical Framework

momentum transfers the distance between quarks and gluons is getting small and they start to interact weakly with each other. This feature is owed to the self coupling of the gluons and is expressed with α_s , the so called running or strong coupling constant. The crossover between confined and quasi-free quarks can be approximated by the QCD cut-off parameter $\Lambda_{QCD} \approx 200$ MeV which is the inverse of the nucleus radius. Therefore confinement dominates at low energies which means a spacing of more than 1 fm between particles and asymptotic freedom dominates at high energies with smaller distances than 1 fm. Consequently this exhibits the highly nonlinear behaviour of the strong nuclear force.

QCD is a gauge theory of the SU(3) gauge group and defines a local symmetry. Local symmetries act independently on each point in space time and require a gauge boson which appears to be the gluon. The symmetry of the strong interaction has approximately flavour symmetry because it does not differentiate between the flavours but is broken by the different quark masses. Another symmetry which occurs in this context of confined (hadronic) and deconfined matter (freed quarks and gluons) is the chiral symmetry which distinguishes between left- and right-handed particles. The handedness of a moving particle is defined by its helicity which is spin and momentum dependent. For a massive particle which moves slower than the speed-of-light in the vacuum, the helicity changes when the reference frame moves faster than the particle. Thus, the explicit chiral symmetry breaking gives the particles to a huge amount its mass and forces independent transformation of the two types of handedness. Further information can be found in [Kle04]. In summary, the chiral symmetry is broken in the confined phase and predicted to be restored in the deconfined phase.

3.2. Quark-Gluon Plasma

The deconfined phase in which the aforementioned chiral symmetry is restored is called the Quark-Gluon Plasma (QGP) [Bra07]. This plasma exists at extremely high temperatures and high or low densities and therefore cannot be found in every day life where matter is hadronized. But at the beginning of its evolution the universe was extremely dense and had a very high temperature. Therefore scientists believe that shortly after the Big Bang the universe consisted for roughly 10 microseconds out of this phase, before it started to cool down and expand. Due to this assumption much research in recent years has focussed on the investigation of the strongly interacting Quark-Gluon Plasma (sQGP) by going backwards in the evolution with collider experiments like CERN SPS, RHIC and most recently the LHC.

The QGP is a phase of QCD and consists of hadrons melted into their con-

stituents, the quarks and gluons. It is characterized as a plasma because the color charge of the quarks and gluons is dynamically screened in long range interactions due to other mobile charges. Only at a very short range quarks and gluons interact weakly with each other and are therefore quasifree. As stated before chiral symmetry at a temperature below the critical temperature T_c of a phase transition is broken and will be restored when a transition from the confined to the deconfined phase occurs. Lattice QCD simulations predict a phase transition at $T_c \cong 170$ MeV [Baz10]. This critical temperature corresponds to an Bjorken energy density of $\varepsilon_c \cong 1$ GeV fm⁻³ [Sne03]. The QGP has a finite volume and is color neutral from outside.

Since the quantities of a sQGP are obviously not easy to access it is even harder to learn more about the evolution of our universe. Today it could exist in neutron stars which cannot be probed up to this point. That leaves as the last possibility the creation of a sQGP in heavy-ion collisions in a high-energy particle collider like at the LHC in the ALICE experiment. The plasma created in heavy-ion collisions is expected to be very short lived due to the rapid expansion of the system which cools down after its initial thermalization.

This system can be investigated through several hard or soft observables which by themselves cannot guarantee a stand-alone detection of the sQGP. The most prominent observables are jet quenching and J/Ψ -suppression or -enhancement. Jet quenching is a hard probe which is sensitive to the early state of the collision and corresponds to the suppression of particles at high transverse momentum. High p_t particles are damped whenever they traverse a plasma and thus can give information of the crossed state of matter. J/Ψ -enhancement on the other hand means that due to the color screening the attractive force between bound states of initially formed $c\bar{c}$ pairs is reduced. Thus, lower excitations of $c\bar{c}$ pairs are more suppressed than the recombination to a J/Ψ at the freeze-out. The J/Ψ takes around 1 fm to evolve from lower configurations which gives it the possibility to escape out of the sQGP if it has a high transverse momentum or if the sQGP expands rapid enough [Zap05]. An enhancement of J/Ψ in the final state would therefore be an indicator for a sQGP.

Because the formed final state is very likely to be highly dependent on its initial conditions which determines the chemical potential μ_B , it is interesting to study the possible phase transitions as well as their transition orders to the sQCD.

3.3. QCD phase diagram

In non-perturbative QCD, matter has a rich phase structure. Nuclei and strong interacting matter can be parametrized by the temperature T and the baryochemical potential μ_B to form a phase diagram. The baryochemical potential basically is a measure of the nucleon density or, more precisely, the imbalance

3. Theoretical Framework

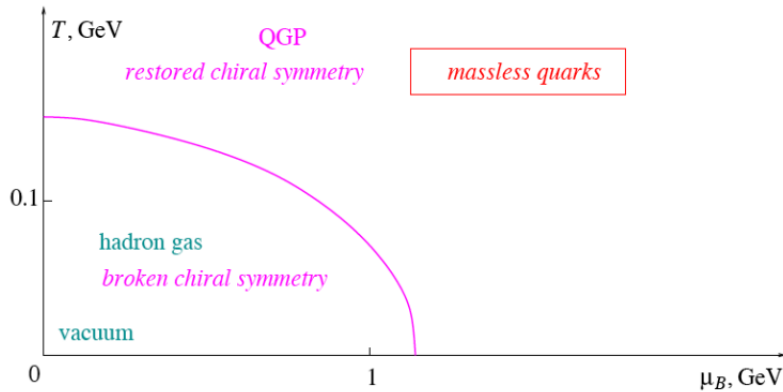


Figure 3.1.: QCD phase diagram [Ste06]

between quarks and antiquarks in a system.

Based upon this diagram one can make assumptions of the evolution of the early universe coming from high T and $\mu_B \ll 1$ and expanding while cooling down after the Big Bang. Hence, it is of great interest in nuclear physics to investigate the QCD phase diagram further.

Having a closer look at the phase diagram in Figure 3.1 one can separate it in two distinct regions. In one region at a small baryochemical potential μ_B and low temperatures the quarks and gluons are confined and form hadronic matter. In the other region at either high μ_B or high T and low μ_B the constituents of the matter are deconfined and form a QGP. The separation of phases brings up the question with what kind of phase transition one is dealing with. If the system has a baryochemical potential $\mu_B > 0$ which favors quarks over antiquarks and a temperature $T \approx 0$ a first order transition could exist between hadronic matter and the QGP. At $\mu_B = 0$ and $T > 0$ a smooth crossover transition from low to higher temperatures and therefore from normal to extremely dense matter is expected due to the finite masses of the quarks. As a result thermal fluctuations break up the pions and form a gas in this crossover region. It is expected that at the end of the first order phase transition line a critical end-point (CEP) exists. The determination of the exact location of the CEP would be a milestone in QCD. Numerical calculations of the location using lattice gauge theory exist as well as model calculations which are still diverging from each other [Adl07]. Consequently, it is of great interest to experimentally pin down the location of the CEP and its properties via fundamental observables.

In pp and Pb–Pb collisions at LHC energies a bulk of high density matter is created with the expectation that the initial temperature of the thermalized state is larger than the critical temperature T_c at which the phase transition occurs. Although it is questionable if it is possible to form a QGP with a pp

collision system because it provides less multiplicity than heavy-ion collision systems. But still it is not neglected that it might occur in pp collisions as well.

Therefore it is worthwhile to study the phase transition in relation to the temperature of the system. A possibility to distinguish the properties of phase boundaries is the measurement of different order parameters. They are strongly depend on the system's temperature as well as the critical temperature T_c and thus being an excellent observable to probe the crossover transition.

This thesis will have a closer look onto spatially dependent multiplicity fluctuations from their mean value and will make use of the Ginzburg-Landau framework in order to extract the number of participating nucleons N_{part} at the phase transition. If one could determine N_{part} it would be possible to make an estimate of the critical temperature T_c via the Bjorken energy density.

3.4. Ginzburg-Landau framework

The Ginzburg-Landau framework (GL) [Adl07, Hom06] in the Ornstein-Zernike¹ picture for a scalar order parameter describes a relation of the free energy density f and an order parameter ϕ as a function of the system temperature T through

$$f(T, \phi, h) = f_0(T) + \frac{1}{2}A(T)(\nabla\phi)^2 + \frac{1}{2}a(T)\phi^2 + \frac{1}{4}b\phi^4 + \dots - h\phi \quad . \quad (3.1)$$

The first term f_0 represents the equilibrium value of the free energy, the second term is a spatial inhomogeneous term caused by $(\nabla\phi)^2$ and the last term describes an external field h . Terms with odd powers are neglected due to the symmetry of order parameters. The parameter b plays a significant role because its sign is used to categorize the order of the transition. For first order transitions one will get $b < 0$, for second order transitions $b > 0$ and at the critical point $b = 0$.

Order parameters should vanish above the critical temperature T_c for that reason the coefficient $a(T)$ equals $a_0|T - T_c|$. At the same time b is supposed to be constant in the vicinity of the critical temperature. Higher orders than the second order terms are neglected too, because this situation is equal to $\phi \approx 0$ in a region far away from T_c . Therefore this approximation is only sensitive to the behavior of the system with T if $T \approx T_c$.

Like in [Hom06] the scalar order parameter ϕ is equal to the multiplicity density fluctuation ρ from the mean density $\langle\rho\rangle$. The following derivations

¹The Ornstein-Zernike equation is originally applied in statistical mechanics and describes the correlation of two molecules between each other and the indirect correlation generated by a third molecule.

3. Theoretical Framework

are taken from [Adl07, Hom06]. The order parameter ϕ can be written as a function of the one dimensional rapidity point y and has the form

$$\phi(y) = \rho(y) - \langle \rho(y) \rangle \quad . \quad (3.2)$$

Mostly in high-energy physics, density fluctuations in rapidity space are approximated with the pseudo-rapidity η . Rapidity needs the information of the transverse momentum p_T of the particles and their masses. Compared to rapidity it is easier to obtain the information of the pseudo-rapidity because no mass information is needed and therefore no particle identification has to be done before. As a consequence, the following derivations are expressed via pseudo-rapidity

$$\eta = -\ln \tan \frac{\theta}{2} \quad (3.3)$$

with θ being the angle between the beam axis and the xy -plane like indicated in Figure 2.1. In order to express spatial fluctuations from the equilibrium value one can use the deviation of the free energy density $\frac{\Delta F}{Y}$

$$\frac{\Delta F}{Y} = \frac{1}{Y} \int (f - f_0) dy = \frac{1}{2} \sum_{\omega} |\phi_{\omega}|^2 (a(T) + A(T)\omega^2) \quad (3.4)$$

where a Fourier expansion was applied to the density fluctuation through

$$\phi(\eta) = \sum_{\omega} \phi_{\omega} e^{i\omega\eta} \quad (3.5)$$

with ω being the wave number and Y the total pseudo-rapidity range corresponding to a one dimensional volume. This deviation of the free energy only contains terms up to the second order to approximate the region around the vicinity of the critical point [Hom06]. The goal was to study the temperature dependence of the free energy deviation and therefore the statistical weight w for fluctuations of $\phi(\eta)$ in relation to the systems temperature T is established by the form

$$w(\phi(\eta)) = N e^{-\frac{\Delta F}{T}} \quad . \quad (3.6)$$

Thus, the statistical average of the square of the density fluctuation of wave number ω is

$$\langle |\phi_{\omega}|^2 \rangle = \int_{-\infty}^{+\infty} |\phi_{\omega}|^2 w \left(\sum_{\omega} \phi_{\omega} e^{i\omega\eta} \right) d\phi_{\omega} = \frac{NT}{Y} \frac{1}{a(T) + A(T)\omega^2} \quad . \quad (3.7)$$

Eq. 3.7 plays an important role in this analysis because $\langle |\phi_{\omega}|^2 \rangle$ is related to the experimental observable G_2

$$G_2(\eta_1, \eta_2) = \langle (\rho(\eta_1) - \langle \rho \rangle)(\rho(\eta_2) - \langle \rho \rangle) \rangle \quad (3.8)$$

which is the two point density correlation function. $\rho(\eta_i)$ represents the density for a given sub-volume $d\eta_i$ in G_2 . In order to simplify it the case of self correlation at zero distance between the two sub volumes is excluded. So that one can multiply $e^{-i\omega\eta} = e^{-i\omega(\eta_2-\eta_1)}$ to both sides of Eq. 3.8 and integrate over the two sub-volumes $d\eta_1$ and $d\eta_2$:

$$Y \int G_2(\eta) e^{-i\omega\eta} d\eta = \langle |\int (\rho(\eta) - \langle \rho \rangle) e^{-i\omega\eta} d\eta|^2 \rangle = \langle |\phi_\omega|^2 \rangle \quad . \quad (3.9)$$

Via Eq. 3.9 and Eq. 3.7 the correlation G_2 can be determined with the calculation of the inverse Fourier transformation of $\langle |\phi_\omega|^2 \rangle$. The one dimensional case is of the form

$$G_2(\eta) = \frac{NT}{2Y^2 A(T)} \xi(T) e^{-\frac{|\eta|}{\xi(T)}} \quad (3.10)$$

where for the first time the correlation length $\xi(T)$ is introduced in this theory. This observable corresponds to the temperature dependent order parameter $\Phi(T)$ and will therefore play an important role in the following analysis due to the fact that

$$\xi(T)^2 = \frac{A(T)}{a_0 |T - T_c|} \quad (3.11)$$

and thus is dependent on the critical temperature T_c .

Another approach of the GL-theory can be made by using the wave number dependent susceptibility in the long wavelength limit as an order parameter. The connection can be derived by Eqs. 3.1, 3.2 and 3.4. Then the wave number dependent susceptibility $\chi_\omega(T)$

$$\chi_\omega(T) = -\frac{\delta^2 f}{\delta h^2} = \left(\frac{\delta h}{\delta \Phi_\omega} \right)^{-1} = \frac{1}{a_0 (T - T_c) (1 + \omega^2 \xi(T)^2)} \quad . \quad (3.12)$$

of the long wavelength limit with $\omega = 0$ is defined as

$$\chi_{\omega=0}(T) = \frac{1}{a_0 |T - T_c|} = \frac{2Y^2}{NT} \xi(T) G_2(0) \quad (3.13)$$

with the total pseudo-rapidity range corresponding to a 1-dimensional volume Y and G_2 as the two-point correlation function at $\omega = 0$.

It turns out that the application of the Ginzburg-Landau framework to spatial density fluctuations from the mean value is a powerful tool in the description of their correlation to each other.

This framework offers two individual order parameters to probe the phase

3. Theoretical Framework

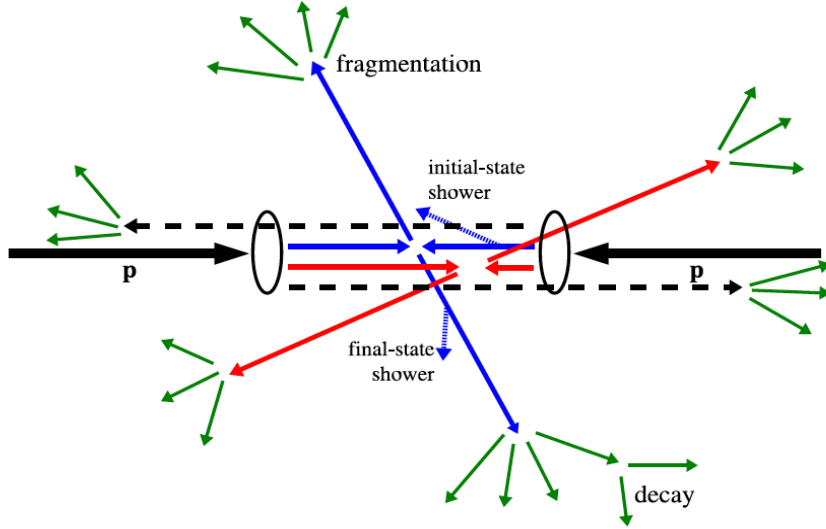


Figure 3.2.: Schematic view of high-energy collisions. Taken from [Gro09].

transition. One indicator of a transition is a signature of a large increase of $\xi(T)$ close to the critical temperature T_c . The other indicator is given by the product of the mediums susceptibility in the long wavelength limit and the systems temperature

$$\chi_{\omega=0}(T) \cdot T \propto \xi(T) \cdot G_2(0) \quad . \quad (3.14)$$

Their product should show a discontinuous behavior at a phase transition. That means the systems temperature T is $T \propto T_c$ close to the transition region.

As a consequence if one can observe strongly non-linear curve progression of the order parameters in both cases, a phase transition of second order took place. Therefore it is of key importance to measure density fluctuations via multiplicity distributions in a high precision.

3.5. Multiplicity Distribution

The charged particle multiplicity distribution $P(N_{ch})$ vs. N_{ch} is a key observable of high-energy collisions and used to explore multi-particle productions in hadron collisions. Matter which is produced in high-energy collisions expands longitudinally and cools after its initial thermalization [Adl07]. If this scenario takes place close to a critical point, large correlated density fluctuations will appear as the temperature T approaches the critical temperature T_c from above. If this process is rapid enough these fluctuations can potentially survive into the final state. The evolution to the final state of particles after the collision is illustrated in green in Figure 3.2 which shows a schematic view

of high-energy collisions.

The probability $P(n)$ to create n charged particles in the final state is connected to the particles production mechanism. If the multiplicity distribution follows a Poissonian form, particles in the final state are produced independently. Then the dispersion $D = \sqrt{\langle n^2 \rangle - \langle n \rangle^2}$ is related to the average multiplicity as $D = \sqrt{\langle n \rangle}$ [Gro10]. Hence, deviations from the Poisson distribution indicate correlations.

As a result spatial density fluctuations in longitudinal space z can be measured as density fluctuations in pseudo-rapidity η in the final state.

3.5.1. The Negative Binomial Distribution

In 1985 charged particle multiplicity distributions in high-energy collisions have found to be mathematically well described by the Negative Binomial Distribution (NBD) by the UA5 experiment² [Aln87]. The NBD is described by

$$P_{p,k}^{NBD}(n) = \binom{n+k-1}{n} (1-p)^n p^k \quad (3.15)$$

and provides the probability for n failures and $k-1$ successes in random order before the k 'th success occurs in an Bernoulli experiment with a success probability p . The commonly used form in high-energy physics though is

$$P = \frac{\Gamma(n+k)}{\Gamma(n+1)\Gamma(k)} \left(\frac{\langle n \rangle}{1 + \frac{\langle n \rangle}{k}} \right)^n \left(\frac{1}{1 + \frac{\langle n \rangle}{k}} \right)^k \quad (3.16)$$

with

$$\Gamma(p) = \int_0^{\infty} e^{-y} y^{p-1} dy \quad , \quad p > 0 \quad . \quad (3.17)$$

The k_{NBD}^{-1} parameter of Eq. 3.16 describes the difference between the width of the distribution and the width of the Poisson mean where $\langle n \rangle$ is the mean of the distribution. In Figure 3.3 it is shown that for $k_{NBD} \rightarrow \infty$ the NBD coincidences with the Poisson distribution and for $k_{NBD} = 1$ with a simple Bose-Einstein or geometrical distribution. As declared before on the one hand a Poissonian form would mean no correlation between produced and already existent particles. On the other hand a Bose-Einstein distribution would indicate that all produced particles are in the same state and dependent on each other. Thus k_{NBD} directly reflects the degree of correlation between the particles produced in the examined spatial phase space. Furthermore, k_{NBD} is

²The CERN UA5 Experiment at the SPS $p\bar{p}$ Collider

3. Theoretical Framework

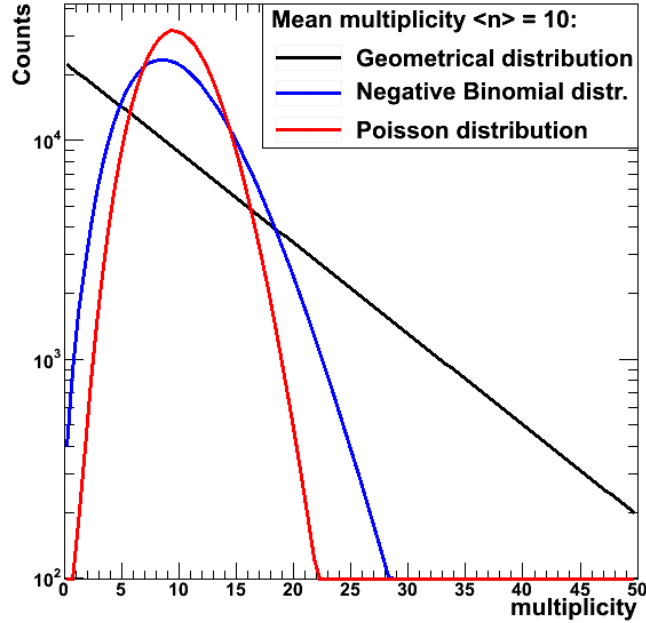


Figure 3.3.: The NBD and its relations to other distributions

associated with the correlation between the phase space densities in different pseudo-rapidity windows η .

Mathematically, k_{NBD} is related to the integrated second-order factorial moment F_2 of the NBD,

$$\frac{1}{k_{NBD}} = F_2 - 1 \quad , \quad (3.18)$$

where F_2 estimates the strength of the correlation between two particles. This gives rise to two possible methods to determine k_{NBD} .

One possibility comes with the direct measurement of F_2 through

$$F_2 = \frac{\sum P_n(n)n(n-1)}{\langle n \rangle^2} \quad (3.19)$$

with $P_n(n)$ being the probability of multiplicity n and $\langle n \rangle$ the mean multiplicity. In the other method one simply applies a fit with a NBD to the corrected spectrum and extracts the fit parameter k_{NBD} . Both procedures will be applied in this analysis.

A different approach concerning the form of the Negative Binomial Distribution was made from Giovannini and Van Hove in 1986. They summarized the possible interpretations of the negative binomial shape of multiplicity distributions. One interpretation was a stochastic cell model based upon 'stimulated

emission of identical bosons by identical cells' [Gio86]. The other explanation assumed that the shape was given by cascading and fragmentation processes which were studied before in cosmic ray experiments (see Section 3.5.5). Their approach characterises the multiplicity distribution through an intermittent correlation between $P(n)$ and $P(n+1)$. $P(n)$ is the probability to have a multiplicity of n and $P(n+1)$ to have a multiplicity of $(n+1)$ in a large ensemble of collisions. The particles which form the distribution are mostly identical but are distinguishable through their momenta. As a result one can relate a collision of multiplicity $n+1$ to $n+1$ collisions of multiplicity n through the removal of any one of the $n+1$ particles of a given collision. This leads to the functional form of

$$g(n) = (n+1) \frac{P(n+1)}{P(n)} \quad (3.20)$$

In the case of independent emission of particles one is dealing with a Poisson distribution $P(n) = \lambda^n e^{-\lambda}/n!$ and Eq. 3.20 turns out to be constant. Connecting this recurrence relation $g(n)$ to a negative binomial it can be written as

$$g(n) = a + bn \quad (3.21)$$

with

$$k_{NBD} = \frac{a}{b} \quad \text{and} \quad \langle n \rangle = \frac{a}{1-b}. \quad (3.22)$$

Further interpretations of $g(n)$ are given in the Paper of Giovannini concerning partially stimulated emission [Gio86].

3.5.2. The NBD k parameter and the Ginzburg-Landau framework

In order to connect the k_{NBD} to the Ginzburg-Landau framework [Adl07] one takes advantage of the relation between the normalized two-particle density correlation function C_2 to F_2 which is dependent on the pseudo-rapidity window size $\delta\eta$:

$$F_2(\delta\eta) = \frac{1}{(\delta\eta)^2} \int \int^{\delta\eta} \frac{C_2(\eta_1, \eta_2)}{\bar{\rho}_1^2} \delta\eta_1 \delta\eta_2 + 1 \quad (3.23)$$

with

$$\bar{\rho}_1 = \frac{1}{\delta\eta} \int^{\delta\eta} \rho_1(\eta) d\eta \quad (3.24)$$

3. Theoretical Framework

being the average density per unit length within $d\eta$ and

$$C_2 = \rho_2(\eta_1, \eta_2) - \rho_1(\eta_1)\rho_2(\eta_2) \quad (3.25)$$

the two-particle density correlation where η_i represents the pseudo-rapidity of a single particle. Due to this connection one can achieve a good approximation of F_2 and therefore of k_{NBD} as well.

Looking to the one-dimensional form Eq. 3.10 from the GL framework C_2 can be rewritten as

$$\frac{C_2(\eta_1, \eta_2)}{\bar{\rho}_1^2} = \alpha e^{-\frac{\eta_1 - \eta_2}{\xi}} + \beta \quad , \quad (3.26)$$

where $\bar{\rho}_1 \propto \langle M \rangle$ corresponds to the mean multiplicity in each collision and α gives the strength of the correlations at zero separation. The β term is constant and represents all correlations which are independent of pseudo-rapidity η like the residual effect of the centrality binning [Adl07]. This effect is generated by finite binning which adds up fluctuations coming from other centrality classes with different numbers of participants. But those centrality correlated fluctuations are independent of spatial fluctuations which are based on the systems temperature.

Furthermore, the connection between the k_{NBD} and the pseudo-rapidity window size $d\eta$ can be acquired by substituting Eq. 3.26 into Eq. 3.23

$$k_{NBD}^{-1}(\delta\eta) = F_2 - 1 = \frac{2\alpha\xi^2 \left(\frac{\delta\eta}{\xi} - 1 + e^{-\frac{\delta\eta}{\xi}} \right)}{\delta\eta^2} + \beta \quad . \quad (3.27)$$

If the experimental windows are much larger than the correlation length ξ Eq. 3.27 can be approximated as

$$k(\delta\eta) = \frac{1}{\frac{2\alpha\xi}{\delta\eta} + \beta} \quad (\xi \ll \delta\eta) \quad . \quad (3.28)$$

The limitation of the description lies in the resolution of the $\alpha\xi$ product. The parameters α and ξ cannot be resolved separately but their product can be determined. As already stated, this product is linked to the medium's susceptibility in the long wavelength limit derived by the GL free energy with Eq. 3.1. Therefore one gets for a given T

$$\alpha\xi \propto \bar{\rho}_1^2 \frac{1}{|1 - \frac{T_c}{T}|} \quad . \quad (3.29)$$

Since $\bar{\rho}_1$ is a monotonic function of the temperature T (Eq. 3.24) in the limit of T far away from the critical temperature T_c , the $\alpha\xi$ product should also

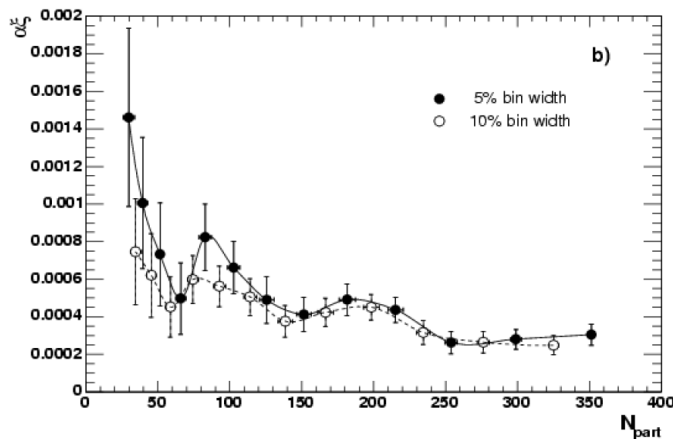


Figure 3.4.: $\alpha\xi(N_{part})$ from Au+Au collisions at $\sqrt{s_{NN}} = 200$ GeV taken from PHENIX [Adl07].

vary monotonically as a function of T . When the temperature of the system approaches the critical temperature, this product will show a singular behavior. Then the singularity can be interpreted as the signature of a possible phase transition. Furthermore, if one would even exclude correlations which are independent of pseudo-rapidity, the slope in the k_{NBD} parameter contains information about the order of the phase transition! This result implies that in the GL framework ξ and $\chi_{\omega=0}$ diverge at the same temperature.

The Ginzburg-Landau framework was already tested by the PHENIX experiment. Scientists were able to extract the $\alpha\xi$ parameters from charged-particle multiplicity distributions of Au+Au collision systems at $\sqrt{s_{NN}} = 200$ GeV in different centralities. Figure 3.4 shows their results. It depicts $\alpha\xi$ in relation to the number of participating nucleons N_{part} , which will be explained in section 3.6, with a 10% and 5% bin width. Caused by the slightly non-linear behaviour of the curve with 5% bin width, it is possible that $\alpha\xi$ is indeed capable of probing a phase transition. Although this fluctuation around roughly 90 participants is far from being significant it is interesting if it is possible to observe a similar behaviour for Pb-Pb collisions at $\sqrt{s_{NN}} = 2.76$ TeV with ALICE.

3.5.3. Convolution property of the NBD

The relation of multiplicity distributions to the NBD gives the opportunity to investigate a variety of different effects. The convolution property will be introduced at this point in order to get a tool to examine the correlation strength between different experimental windows.

A probability distribution function like the NBD can be expressed by the sum of n independent NBD's which equals the n -fold convolution of a NBD [Tan04].

3. Theoretical Framework

The resulting NBD has a mean

$$\tilde{\mu} = n \cdot \mu \quad \text{and a parameter} \quad \tilde{k} = n \cdot k, \quad (3.30)$$

for which the ratio of the parameters

$$\frac{\tilde{\mu}}{\tilde{k}} = \frac{n\mu}{nk} = \text{const.} \quad (3.31)$$

i.e. that the ratio for all distributions is the same. Following that

$$\sum P(\mu_i, k_i) = P\left(\sum_i \mu_i, \sum_i k_i\right) \quad (3.32)$$

leads to the conclusion that the convolution of n identical probability distributions are of the form

$$\sum_{i=1}^n P(\mu, k) = P(n\mu, nk) \quad . \quad (3.33)$$

This special property of the NBD allows to test if the extracted multiplicity distributions for the various $\delta\eta$ -window are correlated with each other or if not. Considering this relation one can exemplarily pick the $\delta\eta = 1.2$ window for further illustration. This window can be defined as the convoluted distribution of the sum of two identical distributions of $\delta\eta = 0.6$. Therefore if their ratios hold the following relation

$$\frac{\mu_{\delta\eta=0.6} + \mu_{\delta\eta=0.6}}{k_{\delta\eta=0.6} + k_{\delta\eta=0.6}} = \frac{\mu_{\delta\eta=1.2}}{k_{\delta\eta=1.2}} \quad (3.34)$$

it would mean that there is no correlation between the experimental window $\delta\eta = 0.6$ and $\delta\eta = 1.2$ so that the particles inside them are emitted statistically independent. In turn if the ratio does not hold the experimental windows are correlated with each other.

3.5.4. Clan Model

The connection between the charged particle distribution and the negative binomial distribution is not fully understood. The so called clan model [Ada08] was developed to interpret the relationship of these distributions. It describes the hadron production by cascades of particles. Particles and their offsprings can be grouped into hadronic clusters N_c . Their development can be described by a cascade. In particle collisions several of those hadronic clusters are created and independently emitted. Each individual cluster contains a mean number of hadrons \bar{n}_c and is produced independently. Therefore the independent emission of ancestors/clans are described by a Poisson distribution with an average

clan multiplicity \bar{N}_c . After their emission the clans fragment into their final state hadrons. Sometimes clusters are thought to correspond to jets or mini-jets.

The measured mean charged multiplicity μ_{ch} is related to the clan multiplicity as $\mu_{ch} = \bar{N}_c \bar{n}_c$. This multiplicity distribution within a cluster is also a logarithmic distribution. Concerning this matter k_{NBD}^{-1} refers to the probability that two particles originate from one clan in comparison to the probability that they come from two clans [Kit05].

In order to determine \bar{N}_c and \bar{n}_c one takes advantage of the simple relationship between the cluster multiplicity parameters and the NBD parameters of the measured multiplicity distribution. So that one gets for the average number of clusters \bar{N}_c

$$\bar{N}_c = k_{NBD} \ln\left(1 + \frac{\mu_{ch}}{k_{NBD}}\right) \quad (3.35)$$

and for the average number of particles per cluster \bar{n}_c

$$\bar{n}_c = \frac{\frac{\mu_{ch}}{k_{NBD}}}{\ln\left(1 + \frac{\mu_{ch}}{k_{NBD}}\right)} \quad (3.36)$$

By plotting \bar{N}_c vs. \bar{n}_c for pp and Pb–Pb collisions the average correlation of the clan model parameters can be visualized.

3.5.5. Intermittency and Multifractality

Intermittency and multifractality are interrelated interpretations of the appearance of large multiplicity fluctuations in the JACEE event [Kit05]. This event was measured by a cosmic ray experiment done by the JACEE Collaboration and shows a multiplicity distribution over pseudo-rapidity. Figure 3.5 shows this multiplicity distribution where the expected multiplicity distribution was already subtracted. Therefore the plot exhibits large unexpected fluctuations in multiplicity which go up to ~ 300 . This circumstance gives rise to the question if the origin of those fluctuations is of statistical or dynamical nature.

If we assume that the fluctuations in the multiplicity distribution are of dynamical nature, then one has to assume further that they have to have a typical minimal size $\delta\eta_o$ in the phase space. So that the experimental windows which are investigated need to be larger than the expected $\delta\eta_o$ in order to gain reliable results. To investigate these potential fluctuations in multiplicity it is valuable to make use of the moments of a distribution. They reflect local characteristics and contain the whole information of the distribution. The reduced

3. Theoretical Framework

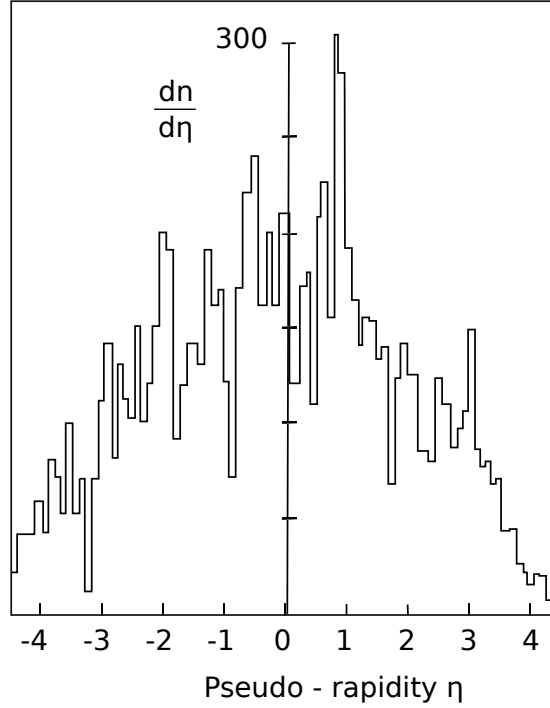


Figure 3.5.: JACEE event [Kit05]

C-moment

$$C_q = \frac{\langle n^q \rangle}{\langle n \rangle^q} = \frac{\sum n^q P_n}{\left(\sum_n n P_n \right)^q} \quad (3.37)$$

contains the probability P_n of producing n charged particles. Whereas the factorial moment F_q comprehends in integrated form the correlation of q particles

$$F_q = \frac{\langle n(n-1)\dots(n-q+1) \rangle}{\langle n \rangle^q} \quad (3.38)$$

If those exemplary moments represented in Eq. 3.37 and 3.38 rise with decreasing bin size in $\delta\eta$ with the side constrain that $\delta\eta > \delta\eta_o$ and self-similar fluctuations exist on several level, the moments should exhibit a power law behaviour.

Figure 3.6 visualizes exemplary self similarity as a consequence of gluon radiation. The gluon which was emitted from the proton decays into an $q\bar{q}$ -pair which itself radiates two gluons itself and so on. The recurrent structure in this process therefore is the gluon radiation and the emittance of a minijet on several levels.

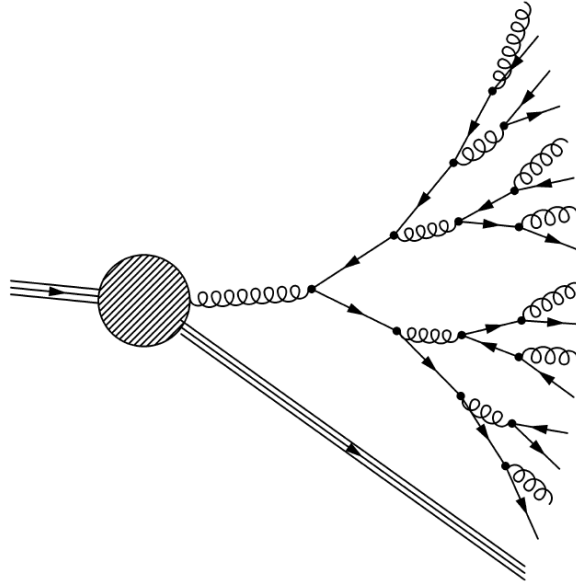


Figure 3.6.: Self similarity shown on several levels via gluon radiation and mini-jets

3.6. Collision centrality in nucleus-nucleus collisions

In high energy nuclear collisions the initial system which is brought to collision has tremendously different prerequisites compared to elementary systems. The fact that nuclei are composite systems out of nucleons and therefore receive geometric quantities force a remarkable particle multiplicity and particle diversity in the outcome due to multi-particle scattering. Following this, techniques like the Glauber Monte Carlo Calculation were created in order to estimate the already mentioned geometric quantities like the impact parameter b and the number of participating nucleons N_{part} which will be explained in the next section. Furthermore, this provides the possibility to make predictions about the charged-particle multiplicity and to apply similar centrality cuts to real data samples.

3.6.1. The Glauber Monte Carlo Calculation

The Glauber MC Calculation [Mil07] [Eli11] is based on simple assumptions and therefore turns into a very powerful tool. In this approach the two colliding nuclei are each built randomly out of a number of nucleons. This three dimensional concept is visualized in Figure 3.7 where the nuclei are positioned with an offset perpendicular to each other. Given that one can illustrate the

3. Theoretical Framework

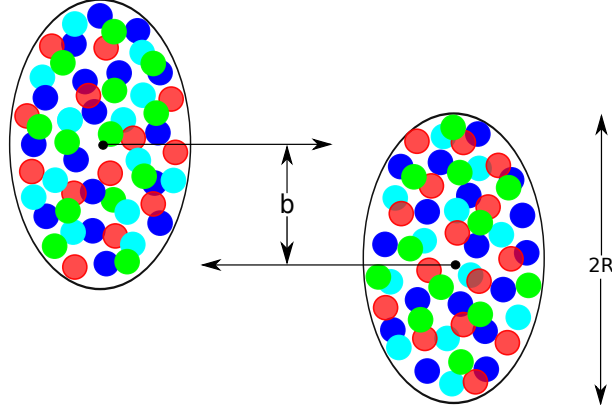


Figure 3.7.: Schematic view of two Lorentz contracted, colliding nuclei in the Glauber model

impact parameter b as the distance between the two centroids. This leads to the possibility to estimate the interaction probability of the nuclei by the use of this relative distance b .

The random location of the nucleons in the nucleus can be simulated through the nuclear charge density distribution. Hence, the nucleon density can be described by a Fermi distribution

$$\rho(r) = \rho_o \frac{1 + s\left(\frac{r}{R}\right)^2}{1 + \exp\left(\frac{r-R}{a}\right)} \quad (3.39)$$

with ρ_o being the nucleon density in the center of the nucleus, R being the nuclear radius, s being the skin-depth and a being a factor which represents the difference of the shape to a spherical form. Important for the systems characteristics is the nuclear radius

$$R \approx r_o \cdot A^{1/3} \quad \text{with} \quad r_o = 1.2 \text{ fm} \quad (3.40)$$

which depends on the mass number A . Taking all these assumptions into account one uses the Monte Carlo technique to be able to draw a random impact parameter b from the distribution which connects the center of the two colliding nuclei

$$\frac{d\sigma}{db} = 2\pi b \quad . \quad (3.41)$$

Eq. 3.41 is illustrated in Figure 3.8 where $b_{max} \approx 2R$ is the maximum value of the impact parameter which is marked by a red line.

It is necessary to verify that a collision took place. This is done by using the inelastic nucleon-nucleon cross section which is assumed to be constant independent of how many collisions a nucleon has undergone so far. The

3.6. Collision centrality in nucleus-nucleus collisions

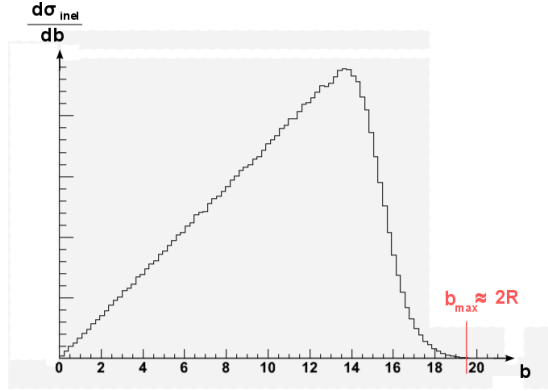


Figure 3.8.: Impact parameter b in relation to $\frac{d\sigma_{inel}}{db}$

relation

$$d \leq \sqrt{\frac{\sigma_{inel}^{NN}}{\pi}} \quad (3.42)$$

has to be satisfied where d corresponds to the orthogonal distance of the centres of two nucleons.

Figure 3.9 shows that the nucleons in the area between the two centroids take part in the collision whereas for the other nucleons called spectators the remaining part of the nuclei is invisible.

As a result one is able to classify collisions in central and peripheral ones. Central collisions have an impact parameter close to $b = 0$ and a small fraction of the inelastic cross section. This leads to many produced particles and almost no spectators. In contrast, peripheral collisions have the largest fraction of the cross section, only a small number of produced particles and many spectators.

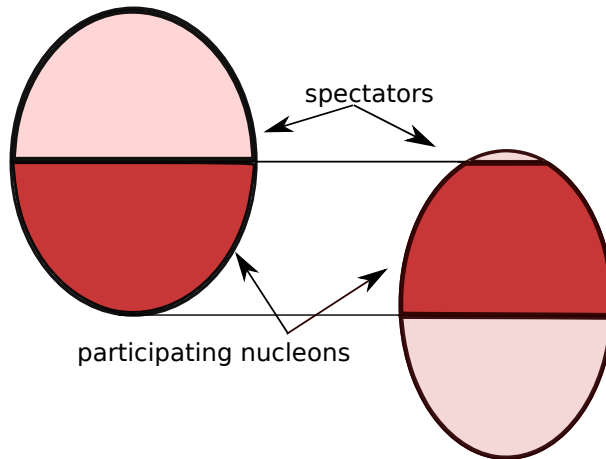


Figure 3.9.: Difference between the number of participating nucleons N_{part} and spectators

4. Data Analysis

This chapter describes the data analysis of pp collisions at a center-of-mass energy of $\sqrt{s} = 7$ TeV as well as of Pb–Pb collisions at $\sqrt{s_{NN}} = 2.76$ TeV taken with the ALICE detector. It first gives an overview over the trigger and event selection which were applied for pp and Pb–Pb collisions, it will address the centrality selection in Pb–Pb collisions and will further discuss the correction methods of the measured multiplicity distributions. In pp collisions these methods are the χ^2 - and Bayesian unfolding. Whereas in Pb–Pb collisions an estimation of fake tracklets and an acceptance correction were done. Afterwards the different techniques to extract the NBD k parameter (see Chapter 3.5) from the data will be addressed.

4.1. Proton-Proton collisions

4.1.1. Trigger and Event selection

The readout of all ALICE detectors is triggered with the SPD and the V0 detectors. If either V0A or V0C or the SPD detects the collision, all sub-detectors start to take data. The SPD triggers in pp whenever a Fast-Or signal is introduced by a signal in at least one pixel in one of the 1200 chips. With this online trigger selection it is possible to identify beam-gas, beam-halo and beam-beam interactions in order to select only the beam-beam interactions for physics analysis. Beam-beam interactions are collisions inside the fiducial region of $z_{vtx} = \pm 10$ cm from the nominal vertex whereby beam-gas interactions are collisions inside the central barrel but outside this fiducial region. Beam-halo interactions are collisions between particles and residual gas outside the central barrel which are still able to produce hits in the detector. For background studies also these events are recorded. Those collisions can be identified by the use of the time condition of the V0 detectors. The SPD, V0A and V0C form together a so called minimum bias trigger because they introduce the least possible bias to the recorded data sample. Besides the above mentioned trigger condition many more trigger schemes are available within ALICE.

In order to analyse the data from high-energy collisions one has to make specific choices to reduce the data sample corresponding to the aim of the analysis. The online trigger selection described above determines which events of a col-

4. Data Analysis

lision are stored and hence has a great impact on the recorded data sample. In addition to the online trigger selection it is possible to replay offline the trigger selection. By doing an offline trigger class selection it is feasible to choose a smaller and more specific set of triggers. Those sets need to be present among others in the online trigger selection. This procedure is done by using the stored information of the sub-detectors and query offline the trigger decisions to select events. Therefore it is important to know which trigger selection sorts out which class of events. Otherwise the analysis is biased from the beginning through a wrong setup.

For this analysis the pp data was analysed with three different offline trigger sets. The different trigger possibilities were chosen in order to get a deeper understanding of the underlying production mechanism of the particles.

Offline trigger selection

The AliRoot class (see Section 2.3) *AliTriggerAnalysis* was used to reproduce the online trigger choice for the offline selection. It basically provides the information from ESDs if certain trigger bits of the trigger detectors are set and which trigger input class was used.

Trigger condition A The offline trigger condition A selects all minimum bias triggered events for which online a trigger bit was fired. This selection is further constraint by a requirement on the hadronic level. Only events are taken which have at least one SPD tracklet in $|\eta| < 1$.

Trigger condition B Offline Trigger condition B uses the information that the event had been triggered offline and uses the introduced minimum bias trigger. Compared to condition A no further constraints were made. This selection triggers on all inelastic collisions and has the smallest impact on the sample because no additional η -requirement was made compared to trigger condition A.

Trigger condition C Offline trigger condition C utilizes the information of the V0 detectors through the V0AND choice. This requires hits from particles in both V0A and V0C which are connected with a logical AND. No SPD Fast-OR trigger was used. By choosing this setup one can diminish the influence of single-diffractive events¹.

¹In single diffractive events only one system evolves and decays whereas the other collision system stays intact. Those events have a much higher charged particle density in either the forward or the backward hemisphere.

Event selection

The events which passed the various offline trigger selections still need to be filtered in order to match the requirements for an analysis of charged-particle multiplicity distributions. Caused by the fact that the analysis is based upon SPD tracklets it is necessary to demand that the chosen event has to have a reconstructed primary vertex. The reconstruction procedure was already introduced in Section 2.2.2. The vertex condition leads to the fact that events without a reconstructed primary vertex will not be processed through the analysis. Additionally a $|\Delta\varphi|$ -cut is applied on the tracklets which takes out all tracklets with clusters which have an azimuthal separation of $|\Delta\varphi| > 0.05$ rad. This cut guarantees that only high quality tracklets are used. The remaining tracklets then consist out of 99 % reconstructed tracklets from primary particles.

Besides the mentioned cuts a cut in z -direction, which means along the beam pipe, is applied too. The z -cut is needed due to the asymmetric pseudo-rapidity coverage in z -direction of the SPD. Figure 2.4 justifies that for different experimental windows in pseudo-rapidity it is necessary to adjust the z -range in order to take out tracklets that are outside the fiducial region. Table 4.1 displays the applied z -cuts.

$\delta\eta$ - range	z - range
0.2 - 1.0	± 10.0 cm
1.2 - 2.2	± 5.5 cm
2.4 - 2.6	± 4.0 cm
2.8	± 2.0 cm

Table 4.1.: Table of applied z -cuts regarding to the pseudo-rapidity range η of the experimental window

Datasets

The used datasets in the pp analysis are

- Data: LHC10b pass 2, run 114931 with 250000 events
- MC 1: LHC10b4, run 114931 - 114936 with 2 million events
- MC 2: LHC10b2, with 3.9 million events

The mentioned number of events is the number of events after the application of the trigger selection. MC 1 corresponds to a MC production with a flat multiplicity distribution whereas MC 2 has no special features. Further details about the flat multiplicity distribution are given below in section 4.1.3.

4. Data Analysis

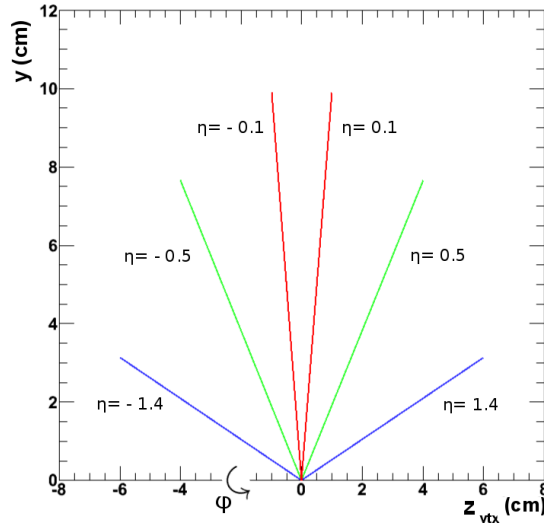


Figure 4.1.: Coverage of different experimental windows with respect to the nominal vertex position in a selected azimuthal plane

4.1.2. Measurement of multiplicity distributions

The introduced analysis in this thesis is based upon the measurement of charged-particle multiplicity distributions which are basic properties of high-energy collisions. Multiplicity distributions were measured for 14 experimental windows going from $|\eta| < 0.1$ to $|\eta| < 1.4$ with a step size of 0.1 in each direction. Figure 4.1 illustrates exemplarily the pseudo-rapidity range in three used windows in one azimuthal plane. The complete coverage is given with the rotation of the isochromatic lines around the z_{vtx} -axis which corresponds to the beam axis. This rotation is indicated with the φ -arrow in the picture. The blue lines enclose the largest pseudo-rapidity window of $|\eta| < 1.4$, the light green lines a window of $|\eta| < 0.5$ and the red lines the smallest experimental window of $|\eta| < 0.1$. The experimental windows will be labelled like $\delta\eta = 0.2$ in the following which corresponds to $|\eta| < 0.1$ because each $\delta\eta$ -window has its center at $\eta = 0$. At the reference point $z_{vtx} = 0$ the nominal vertex is located. The measured distributions are corrected via one of the unfolding methods which will be discussed in the next section. Afterwards the NBD k parameter was extracted through different techniques as it will be explained in section 4.1.4 and plotted as k vs. $d\eta$.

4.1.3. Correction through unfolding methods

The measured multiplicity distributions are probability distributions and are corrected through unfolding. Unfolding is the estimation of a probability dis-

tribution for which normally no parametric form is available [Cow02]. This method needs to be applied if the data incorporates non-specific fluctuations caused by the limited resolution of the detector. Therefore a measured distribution $f_m(x)$ always contains the detector response $R(x|y)$

$$f_m(x) = \int R(x|y) f_{true}(y) dy \quad (4.1)$$

where f_{true} is the true distribution. With a finite binning one can establish a matrix notation of the measured distribution M with

$$M = R \cdot T \quad (4.2)$$

where R is the response matrix and T is the true distribution. The aim is to extract the true multiplicity distribution out of the given data which corresponds to a corrected distribution. Große-Oetringhaus [Gro09] expressed that this cannot be done by simply weighting and assuming that the measured multiplicity is mostly caused by the true multiplicity. An option out of this dilemma is a model independent way which is exclusively determined by detector simulations and evaluates the impact of the detector material on a generated event.

This gives a possibility to understand to what extend and how true events which hit the detector are transformed. The response matrix R describes the detector behaviour with the aid of the matrix element R_{mt} . This element gives the probability that a 'collision with the true multiplicity t is measured as an event with the multiplicity m ' [Gro09]. As stated before this matrix is created with a detector simulation with the event generator PYTHIA (see Chapter 2.3) for certain pseudo-rapidities η and vertex z -ranges. These mentioned constraints arise out of the acceptance of the SPD detector.

Figure 4.2 depicts the detector response of a pp collision at 7 TeV in a pseudo-rapidity window of $|\eta| < 1$. It shows the true versus the measured multiplicity. Both multiplicity distributions have their origin in Pythia MC simulations which have a flat multiplicity distribution. In this simulation the high multiplicity bins were artificially enhanced. Thus allowing to correct the experimental spectra also in higher multiplicity bins caused by the reduction in the loss of information in those bins. The displayed MC multiplicities differ from each other because the true distribution reflects the input in the detector and the so called 'measured' but still simulated distribution displays what is reconstructed out of this MC sample. One can conclude from Figure 4.2 that the average measured multiplicity is roughly 0.7 times the true multiplicity in this exemplary chosen pseudo-rapidity range.

On that account the true distribution for real data can be determined by

$$T = R^{-1} \cdot M \quad (4.3)$$

4. Data Analysis

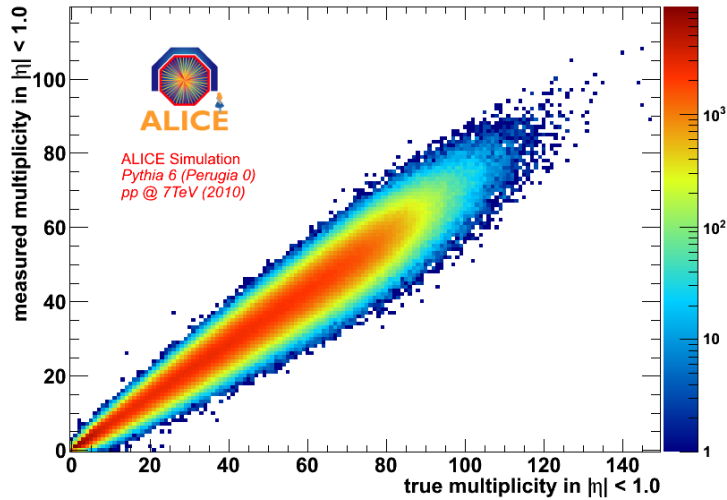


Figure 4.2.: Response matrix for the pseudo-rapidity window $|\eta| < 1$

which is the goal of the correction procedure. By doing so several problems might occur. It is possible that the response matrix R cannot be inverted which means R^{-1} could get singular. This could happen when two rows of the matrix are identical as a consequence of a poor detector resolution. To avoid this situation an appropriate binning is necessary, for example by combining the identical entries. Although R^{-1} exists another issue usually occurs. The result which is achieved by Eq. 4.3 contains intense oscillations that arise due to statistical fluctuations. These fluctuations are more precisely descendants from the limited number of 'measured' (but still generated) events and used to create the response matrix. The limit in the resolution ends up in a loss of information. As an effect the unfolded spectrum is affected by large non-physical fluctuations which therefore cannot correspond to the true spectrum. These difficulties with non-physical fluctuations can be circumvented by constraining the result with an a priori knowledge about the smoothness of the function which allows to recover the true distribution T . Exactly this challenge is the assignment of the two independent unfolding methods, the χ^2 -minimization with regularization and the Bayesian unfolding method, which will be introduced below. Further details of the following description can be found in [Gro09] to which is related to.

χ^2 unfolding

The χ^2 unfolding method is a numeric approach to unfold a measured distribution M via the minimization of a χ^2 -function with a regularization term to receive the true spectrum T . This χ^2 -function is minimized by the MINUIT [Jam75] program. It gives a measure of the coincidence of the measured

spectrum with the product from the unfolded spectrum with the response matrix. $\hat{\chi}^2$ is defined as

$$\hat{\chi}^2(U) = \sum \left(\frac{M_m - \sum R_{mt} U_t}{e_m} \right)^2 . \quad (4.4)$$

The measured distribution is represented by M_m , the response matrix by R_{mt} , the guessed spectrum by U_t and the error stemming from the measurement by e_m . Thereby U_t corresponds to an estimate of the true spectrum.

Because the number of events which are included are always finite no solution will ever satisfy $\hat{\chi}^2(U) = 0$. For this reason Eq. 4.4 has more than one minimizing true spectrum. Many other solutions exist but are mainly unfeasible due to the appearance of large fluctuations. Therefore no obvious proper corrected spectrum exists. To avoid large fluctuations in the solution spectrum the bin size for the response matrix has to be chosen carefully. Is its size smaller than the detector resolution events with a true spectrum T are smeared over several multiplicity bins in the unfolded spectrum. To work around this issue, a side condition is applied to the χ^2 -function in order to get an impact on the shape of the unfolded spectrum. Thus, the function changes by

$$\chi^2(U) = \hat{\chi}^2(U) + \beta P(U) \quad (4.5)$$

where the second term is the so called penalty term. The penalty term is the product of the weighting factor β and the regularization term which only depends on the guessed spectrum U . By changing the value of β one can influence the solution space. If β has a high value, $\hat{\chi}^2$ increases accordingly and the solution space is wider than with a smaller weighting factor. That means it is of key importance to optimize the β -factor. Mostly the error which is introduced by the β term is smaller than the statistical error of the measurement. Finally the regularization schema reduces fluctuations in the unfolded spectrum by favouring solutions with small sums of 1st and 2nd order derivatives or by maximizing the entropy. Consequently the influence needs to be investigated to keep the bias on the unfolded spectrum as small as possible.

Bayesian method

The Bayesian unfolding is an iterative method which was first introduced by D'Agostini [Dag95] and is based on the Bayes' theorem. The theorem states that the probability of an event A conditional on another event B is generally different from the probability of B conditional on A :

$$P(A|B) = \frac{P(B|A)P(A)}{P(B)} \quad (4.6)$$

In terms of unfolding A equals the true event or true multiplicity and B the measured event or multiplicity. $P(A|B)$ is the conditional probability of A

4. Data Analysis

given the fact that B is true and is known as the smearing matrix, $P(B|A)$ is identified as the detector response, $P(B)$ is the measured and $P(A)$ the true distribution.

The goal is the determination of $P(A)$, the true distribution, which is impractical to be gained directly out of Eq. 4.6 because this equation has two unknown parameters: $P(A|B)$ and $P(A)$. Therefore $P(A)$ has to be guessed in order to be obtained correctly via an iterative method:

The unfolded spectrum $P(A)$ or U_t is governed by

$$U_t = \sum_m \tilde{R}_{mt} M_m \quad (4.7)$$

where M_m is also an a priori distribution of the measured one in this analysis and \tilde{R} the response matrix. Taking Eq. 4.3 and the Bayes' theorem in Eq. 4.6 into account, the response matrix should be of the form

$$\tilde{R}_{mt} = \frac{R_{mt} P_t}{\sum_{t'} R_{mt'} P_{t'}} \quad (4.8)$$

In this formula P_t corresponds to the predisposed distribution of the true distribution. If P_t is completely unknown it is set to a flat distribution. One has found the true spectrum if $U_t = P_t$ else wise the solution is in-between P_t and the true distribution. That being the case a next iteration follows where U_t is the predisposed probability P_t . This iteration process is stopped whenever U_t , which is not normalized, converges. The convergence is probed by a χ^2 -test between U_t and P_t . The iteration procedure is terminated if this χ^2 is smaller than 10^{-6} times the bin quantity. Another way of stopping the iteration is the selection of the number of iterations. By applying this limitation there is automatically a regularization applied to the solution, like in the χ^2 -unfolding method. Besides this it is possible to employ additional smoothing to reduce the statistical fluctuations by using

$$\hat{U}_t = (1 - \alpha) U_t + \frac{1}{3} \alpha (U_{t-1} + U_t + U_{t+1}) \quad (4.9)$$

Here α represents the weighting factor like β did in the χ^2 unfolding. If $\alpha = 0$ it follows that $\hat{U}_t = U_t$ and for that reason the optimal value needs to be calculated. Executing this smoothing between the iteration steps, each time a new a priori distribution \hat{U}_t is found. When approaching the last iteration no smoothing is applied.

4.1.4. Extraction of NBD k parameter

This analysis aims at the extraction of the k parameter of the negative binomial distribution in various η windows from charged-particle multiplicity distributions of pp collisions. The determination of k can be approached differently. Four possible procedures were applied and their results will be compared in chapter 5. More specific k was estimated via the second-order factorial moment F_2 , through the fit of a NBD to the unfolded multiplicity distribution, with a fit of a folded NBD to the raw multiplicity spectrum and also via a linear fit to a special form of the NBD invented by [Gio86]. All those techniques which theoretical background was addressed in Chapter 3.5 will be explained in the following.

Estimation of F_2 from the unfolded spectra

The second-order factorial moment F_2 estimates the strength of the correlation between two particles and is related to k_{NBD} (see Eq. 3.18). F_2 can be calculated directly from the corrected multiplicity spectra because it is dependent on the probability of the multiplicity of each unfolded bin n . One has to start from bin $n=2$ because otherwise the ratio would turn zero and one would get a non-physical result. The moment F_2 is determined via Eq. 3.23 for each experimental window. The error bars of F_2 are calculated by the Gaussian error propagation. It contains the error of the mean multiplicity $\Delta\mu$ as well as the error of the unfolded multiplicity bins.

Linear Fit to probability functions

The concept of Giovaninni and Van Hove which interprets the multiplicity distribution as an intermittent correlation of two adjacent multiplicity bins was utilized as well in this analysis. The corrected spectra through unfolding were used and the correlation of the adjacent multiplicity bins were calculated with Eq. 3.20. Errors of the different multiplicity bins were taken into account via error propagation. The resulting $g(n)$ relation was fitted with a linear fitting function (Eq. 3.21). The fitting parameter a of Eq. 3.21 is the y -value at the origin and parameter b the slope of this linear function. As a result k_{NBD} and the mean multiplicity μ could be calculated with Eq. 3.22.

NBD Fit to unfolded spectra

A different approach was taken by fitting the unfolded distributions, which means corrected spectra, with a negative binomial distribution. Then the k_{NBD} parameter was extracted as a fitting parameter besides the mean multiplicity μ by the fitting routine. This method turned out to be very sensitive to the used fitting range. Therefore one had to make a great effort in order to rule

4. Data Analysis

out the 'bad' regions of the corrected spectra. Bad regions could be on the one hand easily marked by the area where non-physical oscillations due to too little statistics appeared. On the other hand one could use the previously described method to locate the multiplicity bin which is not in good agreement with the linear dependence of the rewritten NBD (Eq. 3.21). The applied errors are results out of the fitting process.

Fit folded NBD to raw spectra

The before described extraction procedure used the corrected multiplicity spectra. In contrast to that one can use the uncorrected spectrum and 'corrects' the negative binomial distribution. The correction of the spectra takes the detector response through the response matrix generated by MC simulations into account. Consequently it is possible to modify the NBD with the response matrix as well. This is called folding and is technically applied via a matrix multiplication. The folded NBD was used as the fitting function and fitted to the raw spectrum. As a result the k parameter as well as the mean multiplicity are received through the fitting parameters. The errors are obtained from the fitting procedure as well as from the variation of the fitting range and the there out resulting different fitting parameters.

4.2. Pb–Pb collisions

4.2.1. Event and Trigger Selection

For the analysis of the Pb–Pb collisions at a center-of-mass energy per nucleus of 2.76 TeV the reconstructed data of LHC10h.pass2 was used. The data was analysed with the minimum bias trigger of Pb–Pb, whose setup was changed during the data taking period. Compared to the pp minimum-bias trigger it was necessary to further constraint the Pb–Pb minimum bias trigger in order to reduce electromagnetic interactions (EMI) in the low multiplicity region. First it was assured that the two colliding beams intersect with each other plus 'no beam' condition did not occur. This circumstance was established with the combination of two of the three following options. The selection consisted out of the V0A, V0C and at least two chips firing in the outer SPD layer. With this selection data was recorded from which 99% of the total inelastic cross section could be reconstructed. To further suppress the EMI the trigger condition was later changed to the condition that both V0A and V0C need to detect signals in order to record data. This caused to reduce the background and it was possible to reconstruct the cross section up to 97%. In the end the trigger condition was a coincidence of both V0 detectors and the SPD with no further loss of the cross section measurement. In addition to that a high multiplicity

trigger was used which triggered only if the SPD detected a large number of hits. With this online trigger class one was able to diminish the EMI and still recorded a total of roughly 30 million events.

The event selection was done with the *Physics Selection* in combination with the *Centrality framework*, both classes implemented in AliRoot. The special analysis cuts for multiplicity distribution studies are identical to those in the pp analysis. This selection lead to a total of 4,9 million events for the following analysis with the Ginzburg-Landau framework (see Chapter 3).

Physics Selection In heavy-ion runs several possibilities occur that can induce background. Those are effects induced by the machine itself, parasitic collisions as well as electromagnetic interactions which need to be removed. The machine-induced background (MIB) originates on the one hand from beam ion interactions with beam-gas and on the other hand from the interaction of halo ions with material of the machine. Whereas parasitic collisions arise if de-bunched ions cross and cause a shift of the vertex position to a point outside of $z_{vtx} = \pm 10$ cm. Inside this so called fiducial region the vertex can be efficiently determined. The effects described so far can be removed by a timing coincidence cut of the Zero-Degree Calorimeter (ZDC). But the EMI which are generated by the fast movement of the heavy ions are more difficult to reject. They appear to have cross sections in the order of $kbarn$ and contribute the most to the physical background. These interactions are very soft lepton pairs (QED pair production), photonuclear reactions and electromagnetic dissociation. The EMI are removed as well with the ZDC calorimeters by applying a minimal threshold of 500 GeV. It was checked with the HIJING event generator [Wan91] that the ZDC cuts are working extremely well up to a centrality of 80%. Therefore the change of the minimum bias trigger during the data taking period does not introduce an additional bias. Further information can be found in [Eli11].

Event selection As mentioned before additional event selection was done by choosing SPD tracklets with a reconstructed primary vertex. Then z -cuts regarding to the experimental window in η as well as the $\Delta\varphi$ -cut were identical to the pp analysis applied.

4.2.2. Centrality selection

The measured multiplicity distributions in Pb–Pb collisions like in Figure 4.3 need to be classified after the event selection in terms of their interaction likelihood. This is done with the information of the V0 detectors in combination with the *AliCentrality* class in AliRoot.

This AliRoot class is in charge of the re-alignment of the V0 detectors and uses

4. Data Analysis

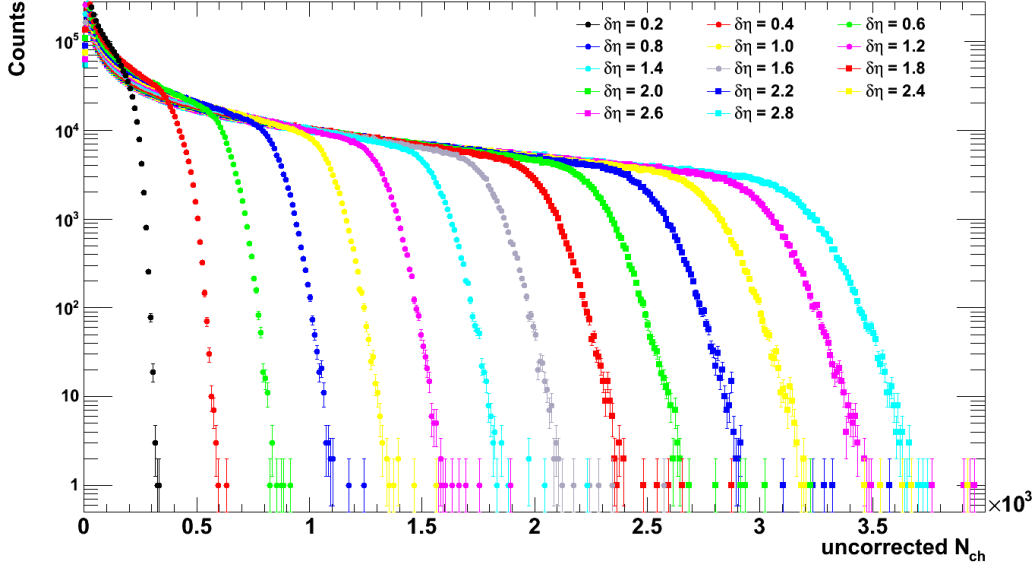


Figure 4.3.: SPD multiplicity distributions for various η -cuts

the amplitude of this detector in order to calculate the centrality classes [Eli11]. Basically a V0 signal is simulated with MC Glauber calculations to gain a simulated multiplicity distribution. With this simulated distribution one is able to make an estimation of the minimum bias cross section and to determine N_{part} as well as N_{coll} distributions.

The implemented model supposes that in each collision a number of ancestors are produced which equal

$$N_{ancestor} = \alpha \cdot N_{part} + (1 - \alpha) \cdot N_{coll} \quad . \quad (4.10)$$

The ancestors then decay independently from each other, which is given by a NBD. Again the k parameter of the NBD defines the width and constrains the fluctuations to large multiplicities. Therefore the simulated V0 multiplicity distribution contains $N_{ancestor}$ times a NBD in a MC event. In order to extract the optimal values for the parameters μ and k , with μ being the mean multiplicity per ancestor, the difference between the measured and simulated V0 distribution is minimized. So that the parameter set with the smallest χ^2 is chosen. After that the fit is used to evaluate the point that corresponds to 90% of the total inelastic Glauber cross section. With the exact location one is able to obtain the centrality information by integrating the measured distribution from the right with the needed percentage. Figure 4.4 gives an example of the result of this procedure. There one can see a multiplicity distribution in the pseudo-rapidity window of $\delta\eta = 2.6$ from the mid-centrality region. Through this method one is able to determine N_{part} and N_{coll} for a given centrality class like it will be done in this analysis in the following chapter. Alternatively these values can be extracted out of the calculation of the impact parameter b .

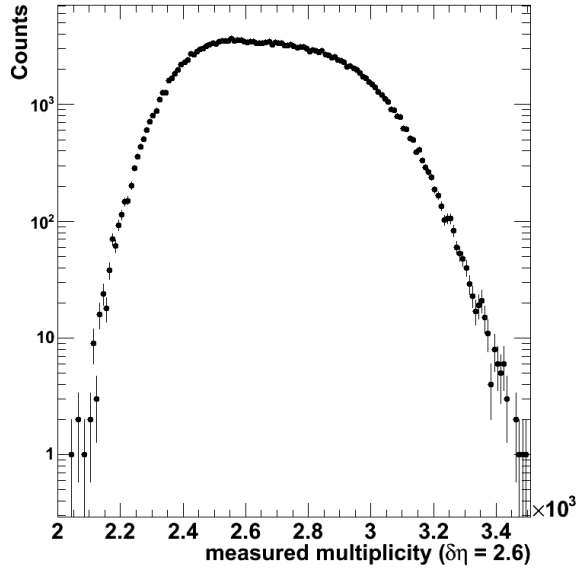


Figure 4.4.: SPD multiplicity distribution for $\delta\eta = 2.6$ for the centrality range 0-5%

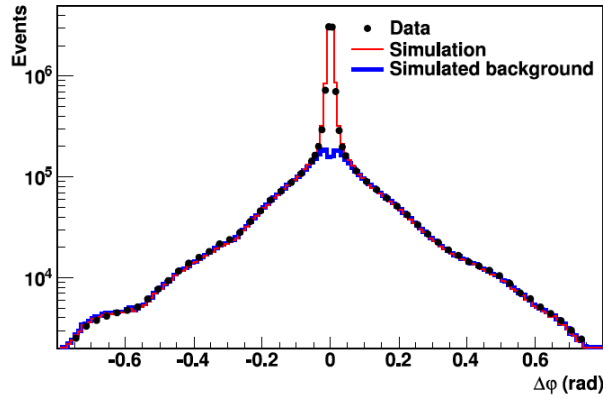


Figure 4.5.: Correction of Pb–Pb multiplicity distributions by tail matching: Distribution of azimuthal separation $\Delta\varphi$ of all candidate tracklets in data, simulation, and background contribution that is estimated from the simulation taken from [Aam11].

4.2.3. Correction

The obtained multiplicity distributions in Pb–Pb collisions in the various centrality classes are corrected with the framework provided by the *First Physics Working Group* [Eli11]. They were in charge of the analysis of the first Pb–Pb multiplicity papers [Aam10c], [Aam11]. Due to the fact that the present analysis only uses SPD tracklets the correction of the combinatorial background was done with MC labels of tracklets. Fake tracklets are the fraction of re-

4. Data Analysis

constructed tracklets which are artificially induced by random combinations of SPD clusters of the inner and outer layer or by the presence of background hits in the real event. By checking in the simulation if each cluster combination which forms a tracklet has the same MC label, it is possible to extract only the real simulated tracklets. The fraction of tracklets which are obviously assigned as 'fakes' can be evaluated by matching the tails of the $\Delta\varphi$ tracklet distributions of data, simulation and simulated background. $\Delta\varphi$ corresponds to the azimuthal difference of the combined clusters which form a tracklet relative to the reconstructed primary vertex (see Section 2.2.2). In Figure 4.5 an example of the matching of the tail with the MC label method is given. This correction technique was applied for the various pseudo-rapidity windows and the different centrality classes. It was found that differences in the percentage of fakes in the various experimental windows but within the same centrality class are negligible. As a result each bin was corrected down by for example 13.2% at mid-centrality (0-5% centrality) in order to account for the fakes. Furthermore, an acceptance correction was done which shifted the given multiplicity distribution by a factor of at most 1.77 to higher multiplicities (for 0-5% centrality).

4.2.4. Extraction of NBD k and $\alpha\xi$ parameters

The extraction of the NBD k parameter in Pb–Pb collisions was done with only one method. In the pp analysis various methods were used due to the fact that k_{NBD} was extremely sensitive to the fitting range. This circumstance is not present in the Pb–Pb analysis because of sufficient statistic. Thus, the determination of k_{NBD} was much more stable. The variable was determined through a NBD fit which was applied on the whole given multiplicity range for each pseudo-rapidity window in each determined centrality class. Afterwards the $k(\delta\eta)$ dependence of the various centralities were individually fitted with the Ginzburg-Landau approximation through Eq. 3.28. It was possible to extract the resulting products of the correlation strength and correlation length $\alpha\xi$ as well as the pseudo-rapidity independent correlation parameter β . Caused by the fact that those parameters are centrality dependent one can relate them to the number of participating nucleons N_{part} . This dependence was already measured at PHENIX. The accomplished ALICE results will be discussed and compared to the PHENIX results in the next chapter.

5. Results

5.1. Proton-Proton collisions

This section presents the results of the pp analysis described in the last chapter. It will first explore the difference in the measured multiplicity spectra caused by the three trigger selections. Afterwards the effect of the unfolding methods will be pointed out and compared to each other. The resulting NBD k parameters obtained with the various methods from the charged-particle multiplicity distributions and their physical message will be discussed. The convolution property, the clan model as well as the concept of intermittency and multifractality is examined. As a last step the results of the analysis of Pythia MC data completes the picture.

5.1.1. Measured distributions

The multiplicity distributions were measured in 14 different pseudo-rapidity windows for 3 individual trigger selections. Figure 5.1 (a) depicts the experimental window of $\delta\eta = 2.0$ which has its center at $\eta = 0$. This range was chosen to show the discrepancy in the different measurements which results from the trigger selection. In order to get a better understanding of their differences to each other the ratio to trigger condition C namely the V0AND trigger selection was calculated (see Figure 5.1). Especially in the lower multiplicity region from bin 1 to 10 condition B has a 26 % higher value than trigger selection C and decreases steeply up to multiplicity 6. At this point the difference to condition C is almost not existent. From there condition B drops to a 6 % lower value which stays constant from multiplicity bin 10 on. A similar scenario can be seen for trigger selection A except for the zero bin. There the difference amounts with a ratio of 0.1 to 90 %. The first bin shows a positive deviation of 20 % which decreases again steeply up to a multiplicity of 10. From this point on a variance of 2 %, with small oscillations around this value, to selection C can be observed.

Both trigger selections A and B which were compared to C indicate how single diffractive events have an impact on the obtained multiplicity spectrum because those events are diminished by C. Summed up, selection C is the most restrictive option followed by A and the loosest is B.

5. Results

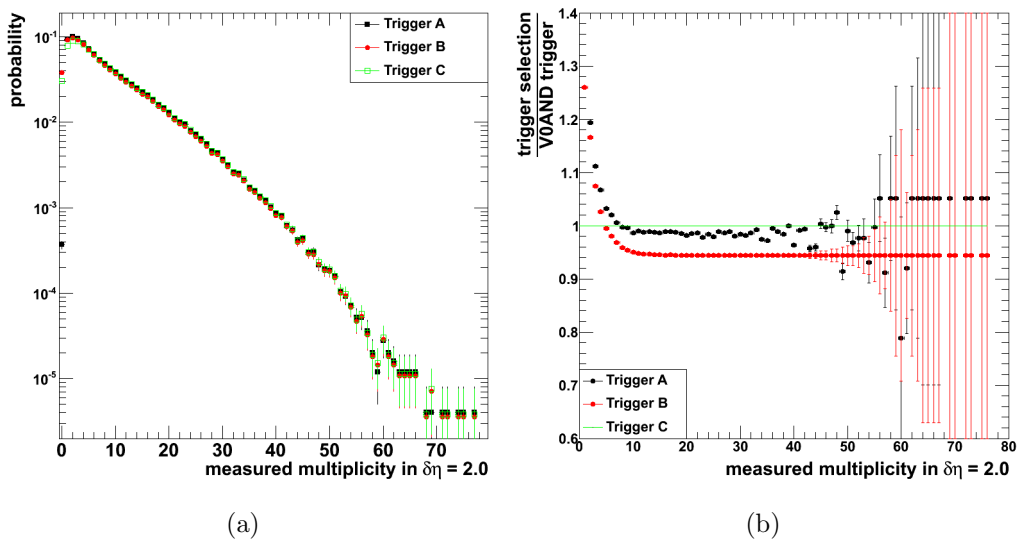


Figure 5.1.: (a) Measured multiplicity distributions in $\delta\eta = 2.0$ with the three introduced trigger conditions; (b) Ratio of the trigger selections to trigger selection C (V0AND)

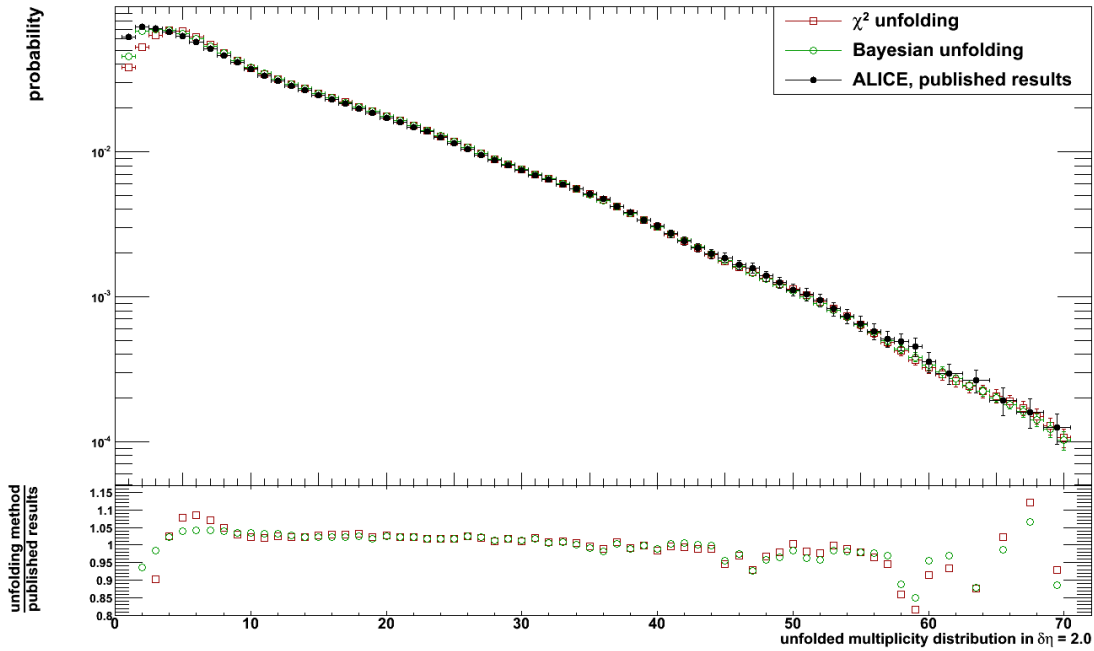


Figure 5.2.: Comparison of different unfolding methods with the published unfolded distribution taken from [Aam10b]

5.1.2. Corrected distributions

The correction of the raw multiplicity spectra was done separately by the χ^2 -unfolding and the Bayesian method for the three trigger selections. Especially the χ^2 -method was found to be enormously sensitive to the statistics of the response matrix. The response matrix was produced separately for the various pseudo-rapidity windows as well as for the trigger selections. Therefore a total of 84 different detector response matrices like the one shown in Figure 4.2 had to be produced. A flat multiplicity distribution was used to create the matrices and already reduced the bias in the higher multiplicity bins through the enhanced statistic in those bins.

The quality of the unfolding procedure was checked with two different techniques. The first technique tested if the obtained unfolded spectrum with trigger condition A in $\delta\eta = 2.0$ matched with the published results found in [Aam10b]. Figure 5.2 illustrates in the lower part with open red squares that the χ^2 -unfolding lies from bin 8 up to bin 56 within a 5 % band around the published results from the ALICE collaboration. From bin 56 on the deviation is between -21 % and +12 %. This can be caused by different weighting factors in the unfolding process as well as different statistics in the higher multiplicity bins. In open green circles the comparison with the Bayesian unfolding is depicted. It is observed that the Bayesian result also lies within a 5 % band around the published results. In contrast to the χ^2 -result it does not show oscillations to the same extent around the reference line of 1. The Bayesian solution starts with a -5 % deviation to the published results and evolves up to a multiplicity of 8 into a deviation of +5 %. From a multiplicity of 10 the Bayesian and the χ^2 -results match and their deviation to the published result decreases slowly up to a multiplicity of 45. Then they start to build out fluctuations which get bigger in the higher multiplicity bins. Both solutions start to vary more than 5 % from the published data from bin 58 on. The Bayesian unfolding does have with -15 % and +7 % a smaller deviation range than the χ^2 -unfolding.

In order to get an impression how the increasing pseudo-rapidity range effects charged-particle distributions, Figure 5.3 shows exemplary the results for the Bayesian unfolding in all fourteen pseudo-rapidity windows for trigger selection A. The broader η -windows show that the probability to obtain high multiplicities is much higher than for example in the smallest η -window.

Another way of checking the quality of the unfolding can be established by taking the unfolded distribution and multiply it with the corresponding response matrix. If the resulting spectrum matches with the measured spectrum, the unfolded spectrum is of high quality. It means that the procedure is reversible with the extracted correction as an input. This is displayed with red markers in Figure 5.4 (a). The black markers represent the measured spectrum. The

5. Results

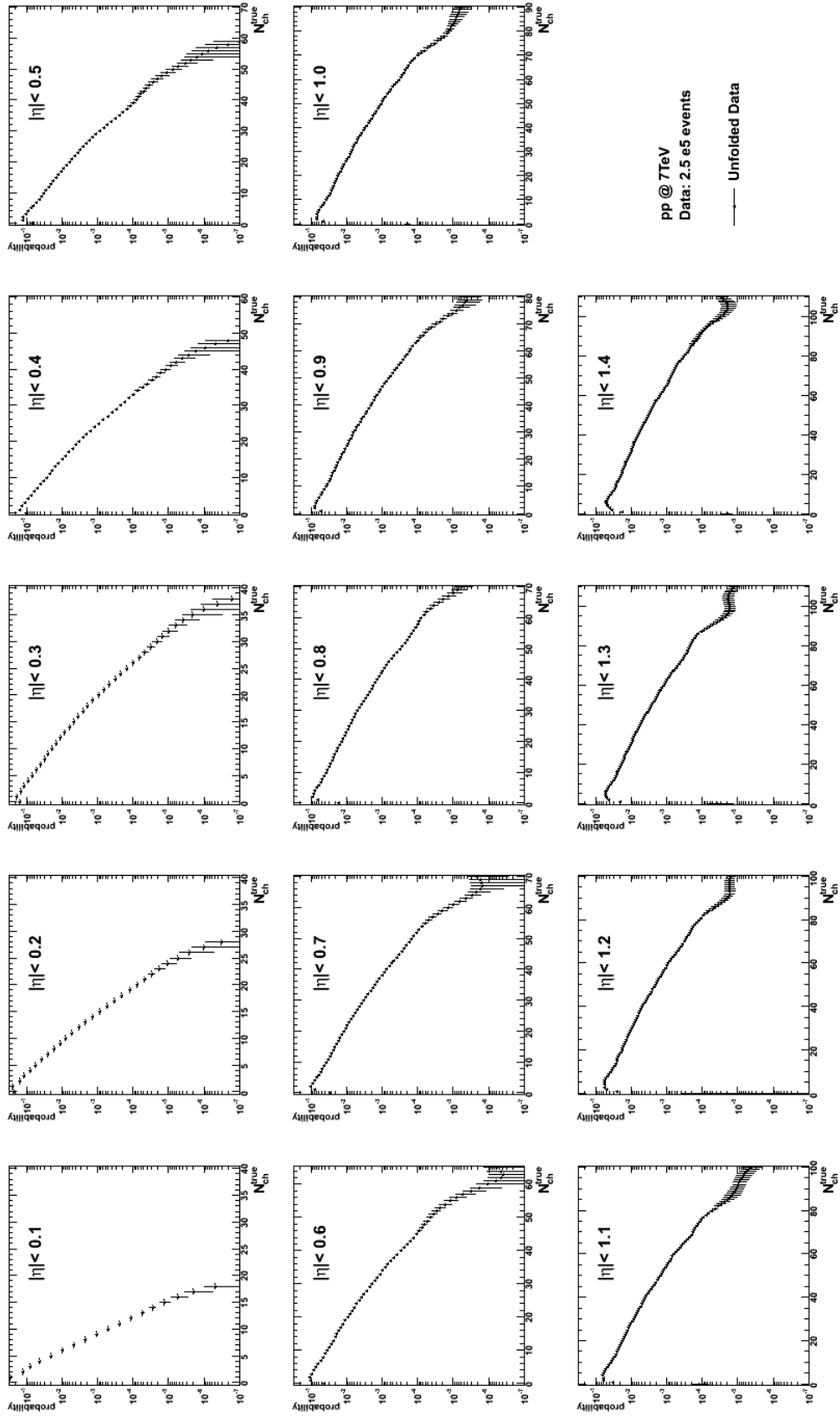


Figure 5.3.: Bayesian unfolding of fourteen pseudo-rapidity windows with Trigger selection A

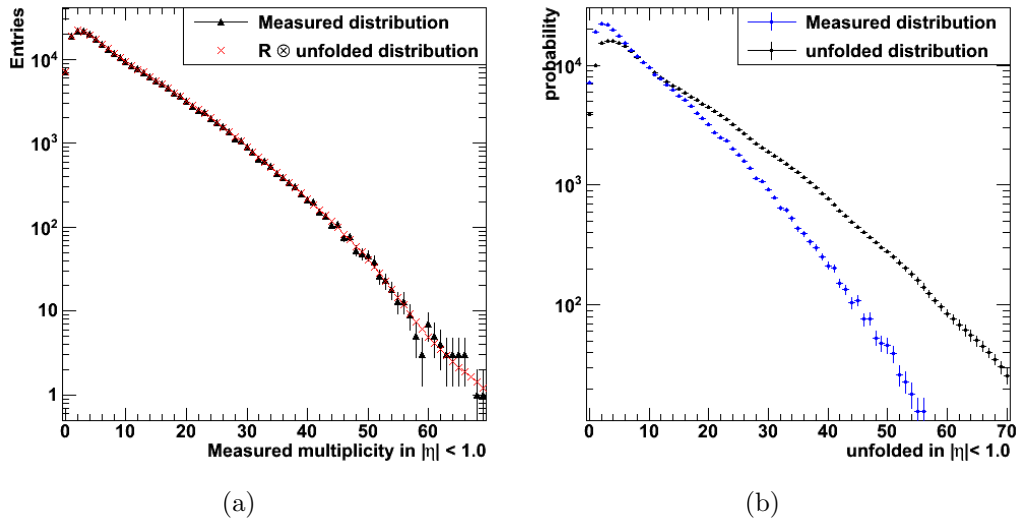


Figure 5.4.: (a) Evidence of the unfolding quality of Bayesian unfolding (Trigger C); (b) Measured and unfolded distribution of Bayesian unfolding (Trigger selection C)

deviation between the spectra is extremely small and can be noticed from a multiplicity of 56. The divergence from 56 on mirrors the observations from the comparison made with the published data.

Besides these quality checks it was observed, that the oscillations of statistical fluctuations are more visible in the χ^2 -unfolding than in the Bayesian unfolding. The Bayesian unfolding was done by applying the same weighting factor as in the other technique. But it followed that its solution needed less iterations than in χ^2 -unfolding before it converged to a result. In χ^2 -unfolding many iterations of TMinuit were done before the result with the smallest χ^2 by the minimizing program was found. This points towards the fact that the solution space there consists of a variety of local minima which complicates the fitting procedure.

Since two correction methods were investigated in this study it is of great interest, how much their results differ. Therefore the ratio of χ^2 to Bayesian result was taken. Figure 5.5 illustrates that the ratio lies within a 3% band in the lower and mid-multiplicity region. Up to higher n oscillations build up and cross the acceptable tolerance. This happens whenever the statistical errors from the unfolding process start to grow rapidly. Hence, these oscillations indicate the regions in which the unfolding process is not successful any more.

Given the corrected spectra it is interesting how much the correction had an impact on the different trigger selections. Therefore the ratios of the different

5. Results

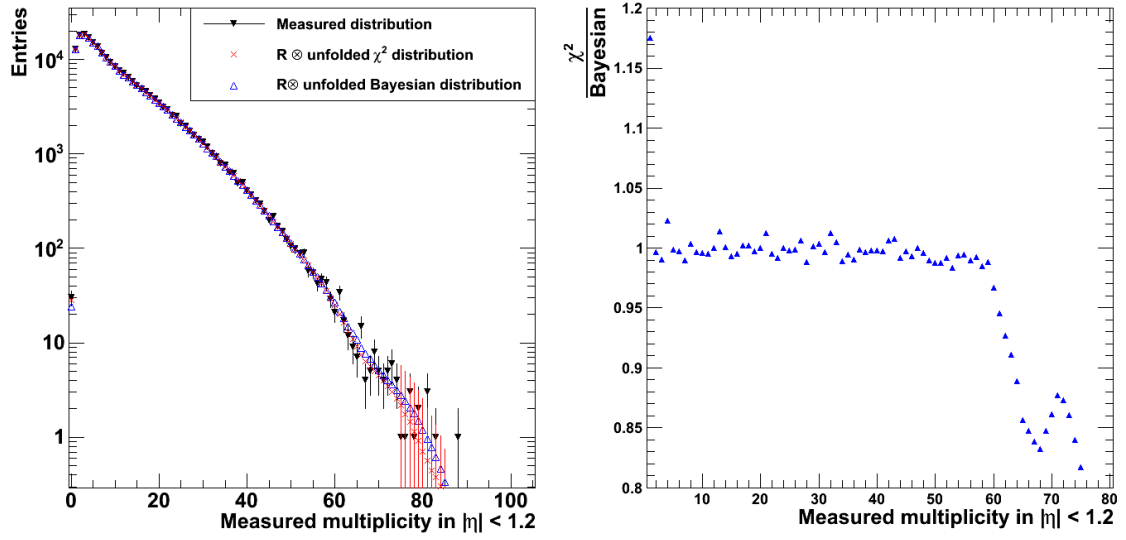


Figure 5.5.: Comparison of χ^2 and Bayesian unfolding and the χ^2 /Bayesian ratio

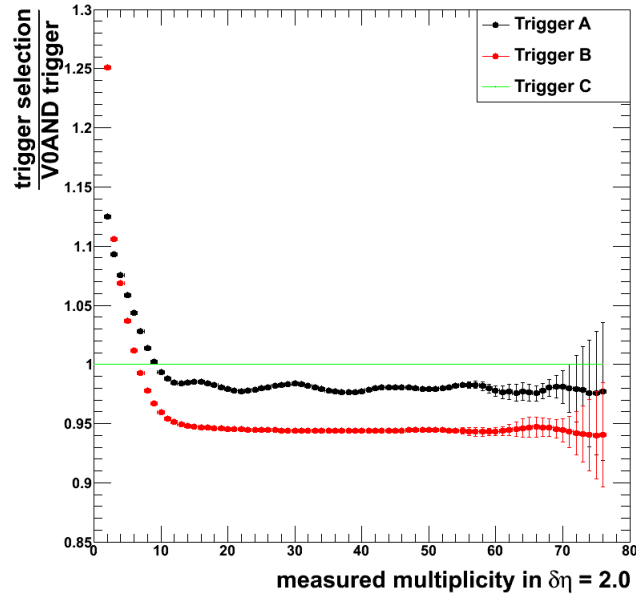


Figure 5.6.: Unfolded distributions of the three trigger selection (Bayesian method)

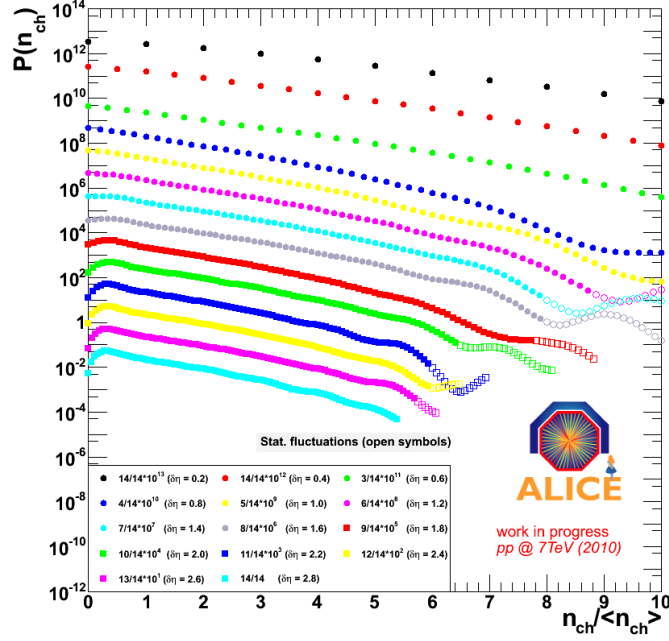


Figure 5.7.: KNO form of pp at 7 TeV

trigger selections to the reference of selection C, namely the V0AND offline trigger, was estimated. Their results are shown in Figure 5.6. Compared to Figure 5.1 (b) it is obvious that the unfolding had a positive effect especially on the higher multiplicities. The results do not fluctuate in the same manner as the results of the measured trigger ratios. In addition, the errorbars from multiplicity bin 45 on and growing are drastically reduced through the unfolding process. The difference from trigger selection A to reference C has not changed and has from bin 10 on a roughly 2% lower value. The same can be observed for the ratio of selection B to C, where B is around 6% lower than reference C. As a conclusion one can state, that the overall behaviour of the trigger selection does not change with the correction process which is expected and that unfolding removes the effects coming from the measurement of the detector.

Koba-Nielsen-Olesen form Another way to illustrate multiplicity distributions is to investigate their Koba-Nielsen-Olesen (KNO) form. In order to do so the multiplicity distributions of the individual pseudo-rapidity windows are multiplied with the inverse of their mean multiplicity. For illustration purpose each distribution is additionally scaled by a factor to shift the different spectra over the available y -range. The result is shown in Figure 5.7 where the spectra increase in their pseudo-rapidity size from top to bottom. The smallest pseudo-rapidity window of $\delta\eta = 0.2$ is pictured with black dots and has the broadest distribution compared to the biggest window of $\delta\eta = 2.8$

5. Results

depicted with cyan squares. The open symbols in the individual distribution indicate the statistical fluctuations which are introduced through the unfolding process. These distributions do not satisfy the so called KNO scaling which would correspond to an universal curve on which all distributions would match without their scaling factor in y -direction. KNO scaling would indicate that the moments of the distributions are independent of the beam energy as well as the factorical moments F_q (Eq. 3.38) [Gro10].

5.1.3. NBD k parameter versus $\delta\eta$

The aim of the presented analysis is the extraction of the NBD k parameter from the different corrected experimental windows in order to understand the underlying process of particle production. In Chapter 4 the extraction methods were introduced. Their results are shown individually in Figure 5.8 and combined for one trigger selection in Figure 5.9. They will be discussed below.

Estimation via F_2 The estimation of $k_{NBD}(\delta\eta)$ by using the second order factorial moment of the distribution turned out to be a very stable method. Figure 5.8 (a) shows the obtained results. Trigger selection A and C agree within 2% with each other. Whereby for selection B an offset of -0.1 which correspond to 8 % to the other methods is observed. This is caused by the applied trigger selection and reflects the divergence of those in the measured as well as in the unfolded distributions in the first 10 multiplicity bins. Physically it shows that the event selection which is the loosest one has the lowest k values.

The applied technique uses moments of a distribution which always describe a local property of it. In this case F_2 represents in integrated form the correlation strength between two particles. Since it uses the full information of the bin content over the available range of multiplicity bins it turns out that it statistically smoothens the existing fluctuations. By using a linear extrapolation of the NBD k parameter which relates it with F_2 , it turns out to be a very stable extraction method. Therefore it is used as the main method in the following analysis procedure for pp.

Linear fit to a probability function Another technique uses the NBD form of Giovannini. It was noticed that this method, illustrated in Figure 5.8 (b), showed the expected linear behaviour of $g(n)$. The fitting procedure with a linear function was applied but showed that the containing statistical fluctuations or oscillations around a fictional linear line through the data points affected the fit. Therefore the smallest pseudo-rapidity windows are problematic because only a few points could be used. This has a dramatic effect at $\delta\eta = 0.4$ where it produces a local maximum. Although this method has some difficulties in

the first few pseudo-rapidity windows it still shows that the general trend of the k -slope is increasing like in the F_2 -method.

Fit with the NBD The approach of fitting an NBD to a corrected spectrum was found to be highly sensitive to the applied fitting range. Figure 5.8 (c) depicts the result out of this procedure. The NBD overestimated the multiplicity distributions in the higher multiplicity bins. The bigger the experimental windows grows the more the NBD overestimates the corrected spectrum. This effect can be owed to the beam energy. As published in [Aam10b] at 900 GeV only a slight deviation from the fitted distribution is seen and from 2.36

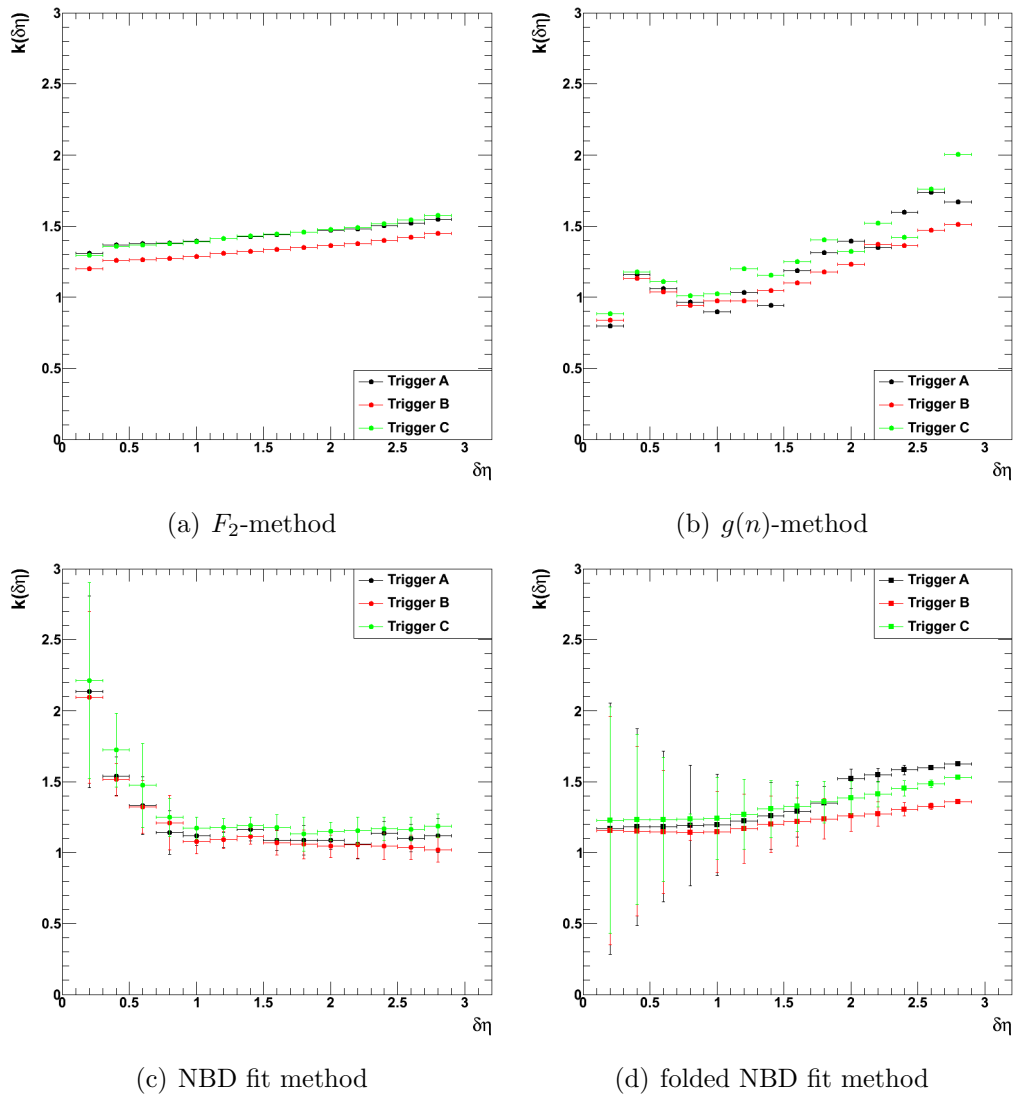


Figure 5.8.: (a),(b),(c): Extracted $k(\delta\eta)$ from corrected spectra using Bayesian unfolding; (d): Extracted $k(\delta\eta)$ from measured spectra

5. Results

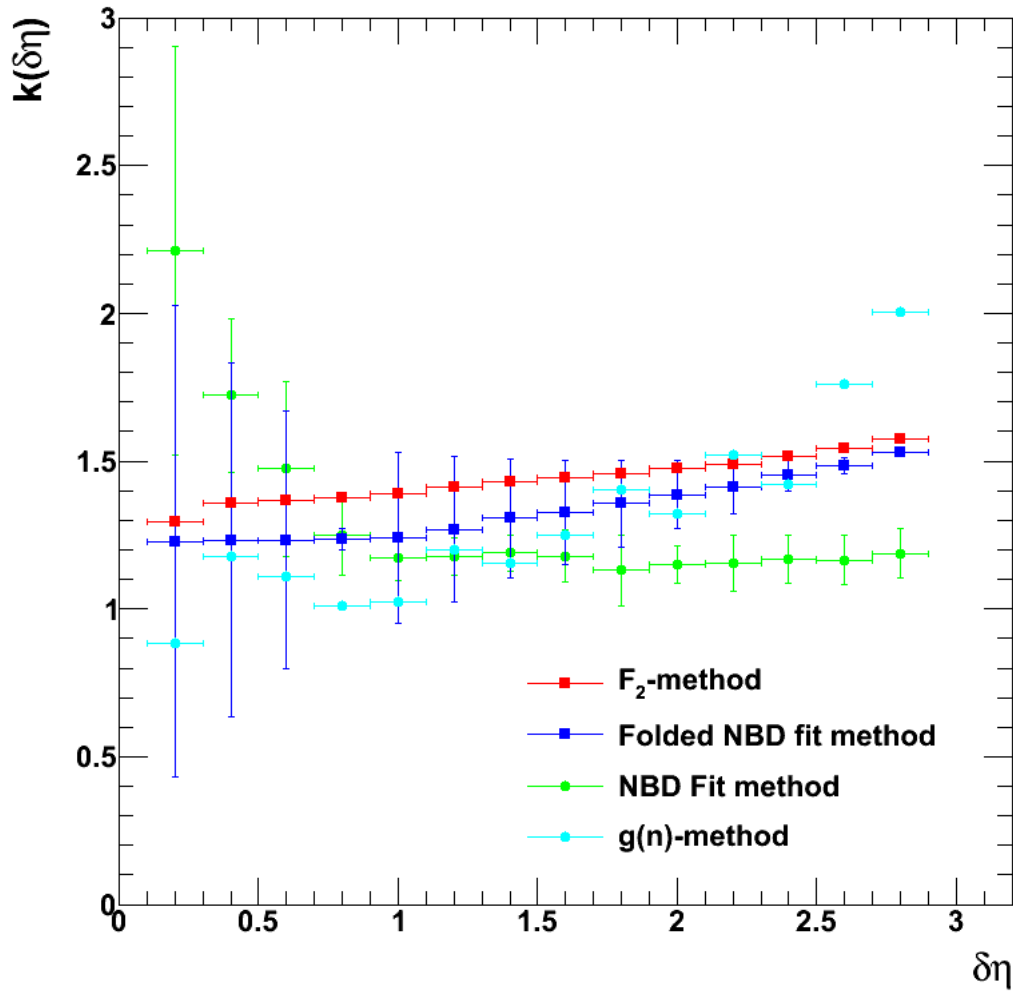


Figure 5.9.: Results of the four extraction methods of k_{NBD} of trigger selection C: F_2 -method, NBD Fit method and $g(n)$ -method used corrected spectra from Bayesian unfolding. The Folded Fit method used the measured spectra.

TeV on a shoulder builds up. This deviation evolves with the rise in beam energy. Another reason why the results of the fitting do not match with the other methods can be the fact, that the errors of the multiplicity spectrum are correlated with each other and can as a result effect the fitting parameters and quality. Therefore many reasons can be found why this method is not as optimal as the already discussed ones.

Fit with the folded NBD This fitting method goes the other way around as the latest introduced fitting technique. It fits a NBD which was folded with the detector response to the measured spectrum. By doing so the problem of

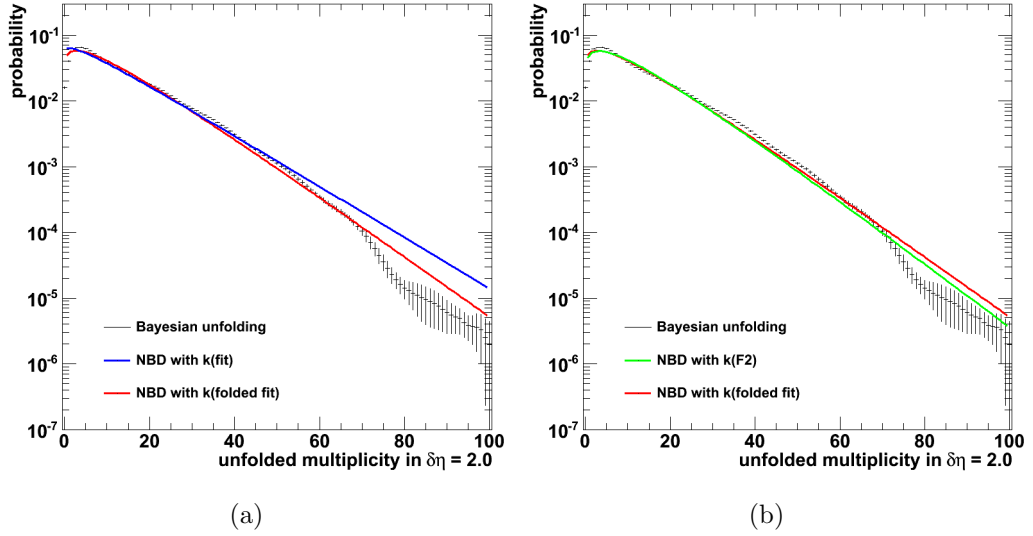


Figure 5.10.: (a) Comparison of the 'NBD fit' and the 'folded NBD fit' to the corrected spectrum; (b) Comparison of the 'folded NBD fit' and the F_2 -method to the corrected spectrum

correlated errors due to unfolding vanishes and it turns out, as can be seen in Figure 5.8 (d), that the overall slope slightly rises for all trigger selections with enlarged experimental windows as in (a) and (b). The results of the different trigger selections differ from 7 % in the smaller experimental windows to 16% in the largest windows at most. It is observed that the error is fairly big in the pseudo-rapidity range from $\delta\eta = 0.2$ to 1. The same behaviour of the errors can be found in the conventional NBD fitting procedure discussed before.

Interpretation of the different extraction methods The shape of the multiplicity distribution contains as aforementioned the correlation strength of the produced final-state particles. This is expressed through the shape of the negative binomial distribution which if wider than a Poisson distribution states to contain positive correlated particles and if narrower than Poissonian to contain negative correlated particles. However, as stated before, the NBD builds up a shoulder at high multiplicities with rising beam energy. The obtained results of k_{NBD} which are fitted with a single NBD like the 'NBD fit method' shown exemplary in blue and the 'folded NBD fit method' depicted in red in Figure 5.10 (a) mirror the mentioned deficits. Either the slope in the first bins is not sufficiently described and/or the tail of the distribution is overestimated. As a consequence the four different extraction methods of k_{NBD} show diverging results. However, it seems that the F_2 -method illustrated in green in Figure 5.10 (b) reflects the unfolded distribution best because it resolves the first bin

5. Results

as well as the tail of the multiplicity distribution fairly good and is therefore used to examine further models who investigate particle properties in the following.

The fact that the multiplicity distributions are not perfectly described by one NBD at LHC energies in pp collisions indicate that the multiplicity distributions should be fitted with a combination of two NBDs which can describe the appearing difference at high n . One NBD would reflect the soft physics and the second the QCD semi-hard mini-jets [Kit05] in this picture. This corresponds to take multiparton collisions as well as multichain production into account.

According to [Kit05] there are many interpretations about the relationship of the NBD and multiplicity distributions. The most probable ones are (partial) stimulated emission and cascading. The cascading effect will again be addressed below in the Clan model.

Comparison to published data In the eighties the $k_{NBD}(\delta\eta)$ values in various pseudo-rapidity windows were already determined in $p\bar{p}$ collisions at $\sqrt{s} = 900$ GeV by the UA5 experiment. Figure 5.11 depicts the result of this analysis and compares it with the 7 TeV results obtained in pp collisions with ALICE. In UA5 the k parameter rises linearly with rising pseudo-rapidity range which can be seen for the ALICE results as well. A difference is visible in the slope. The shape of UA5 $k_{NBD}(\delta\eta)$ is much steeper than the one of ALICE. Taking this observation into account the produced final-state particles are correlated stronger with each other in higher beam energies.

Convolution property

The convolution property (section 3.5.3) of the negative binomial distribution is a tool to display the correlation of particles in the different experimental windows and is used as a check if correlation between them exist. This is done by the determination of the ratio of the mean μ and the k parameter of the probability distribution. If the ratio of the individual η ranges are equal to each other it would mean that there is no correlation between the enlarging windows, so that only the particles in the smallest window can be correlated. Figure 5.12 (a) confirms that it is not the case by showing a linear rise in μ/k . The value of the convolution ratio increases in a step size of 0.9 going from $\delta\eta = 0.2$ up to 2.8 which means that for each additional 0.2 η the correlation between the particles rises linearly too.

Clan model

The clan model interprets the particle production mechanism by a pure cascading process. In Figure 5.12 (b) the extracted average particles per clusters \bar{n}_c and the average number of clusters \bar{N}_c are presented. The obtained results

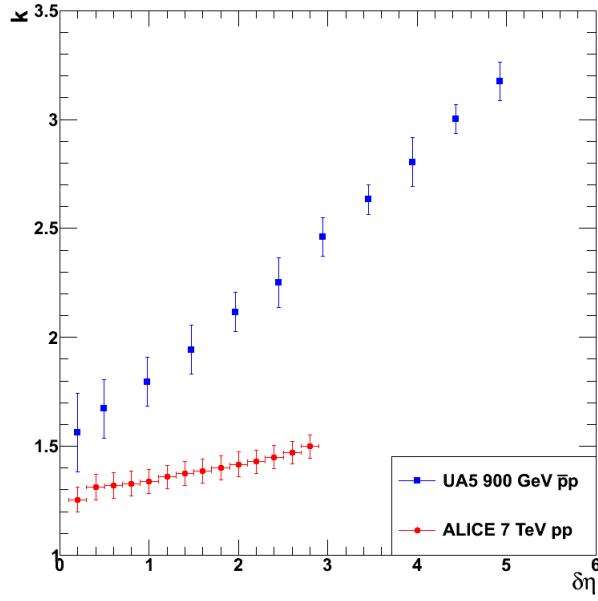


Figure 5.11.: The NBD k parameter determined with the CERN UA5 [Aln87] and ALICE experiment

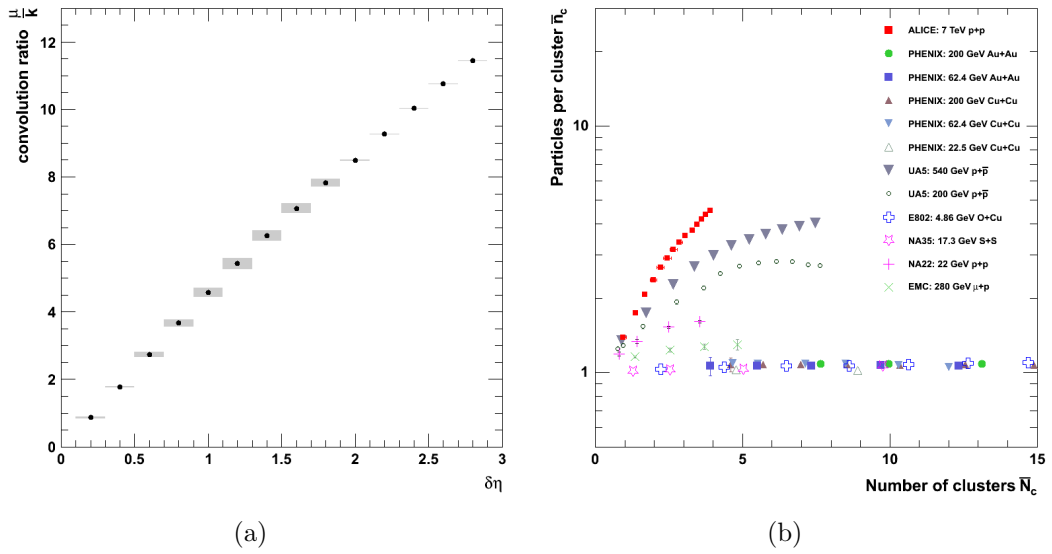


Figure 5.12.: $\delta\eta$ -distributions determined with the k_{NBD} : (a) Convolution property of the NBD with systematic error from unfolding methods; (b) Correlation of the Clan parameters: ALICE results in comparison with world data (taken from [Ada08])

5. Results

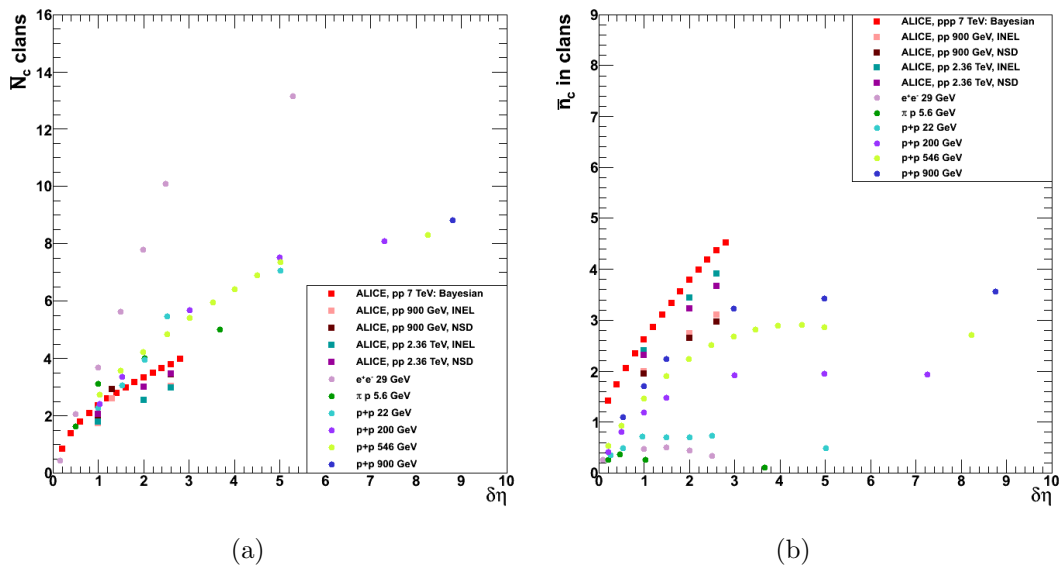


Figure 5.13.: Clan parameters in relation to pseudo-rapidity: ALICE 7 TeV of this analysis, ALICE 2.36 TeV and 900 GeV where the multiplicity distributions were taken from [Aam10a] in comparison to different other experiments where the clan parameters were taken from [Kit05].

for ALICE at 7 TeV are shown with red squares. First of all, this graphic can be split into two groups, namely the results given by elementary collisions and the results from heavy-ion collisions. In elementary collisions the particles per cluster increase with rising number of clusters. Furthermore it is observed that the particles per cluster from all shown elementary results increases with growing beam energy as well. The ALICE results beyond roughly 5 clusters cannot be shown because of the limited pseudo-rapidity coverage of the SPD with $|\eta| < 1.4$ at most. This is equal to the largest experimental window of $\delta\eta = 2.8$ of the presented analysis.

The data points of the group of heavy-ion collisions is behaving differently than the ones of elementary collisions. It can be seen that the clustering in heavy-ion collisions is very weak compared to elementary collisions [Ada08]. But as a consequence of having roughly one particle in each cluster the number of clusters is much higher compared to pp collisions. In contrast to this it is also observed that the beam energy does not seem to have an impact on the number of particles per cluster in heavy-ion collisions.

Figure 5.13 shows the results of the individual clan parameters in relation to the pseudo-rapidity range. The red squares represent the 7 TeV results of the unfolded multiplicity distributions of the presented analysis. The other ALICE results with different center-of-mass energies are obtained by the use of the published multiplicity distributions in [Aam10a] and are illustrated in squares too. It can be seen that for 7 TeV the average number of clans as well

as the average number of particles in a clan is greater than for 2.36 and 0.9 TeV. This mirrors the before observed energy dependence. This is contrary to the other results taken from [Kit05]. Guided by the pale lilac dots of the e^+e^- collision system at 29 GeV it is observed that going to lower beam energies the number of clans is getting bigger but at the same time the number of particles in a clan is getting dramatically smaller than the corresponding value of the ALICE 7 TeV parameters.

The determined clusters can be interpreted as the sources of semi-hard processes, namely mini-jets, as well as for multiple parton interactions [Ada08].

Intermittency and Multifractality

The measurement of charged-particle multiplicity distributions can be probed if they contain event-to-event fluctuations which are of dynamical nature. It is interesting to investigate if these fluctuations originate from non-statistical sources. Therefore the corrected spectra were used to determine the reduced C-moment of the distributions as well as the factorial moment F_q up to the 5th order. This technique is known to separate fluctuations of statistical origin from dynamical fluctuations of the underlying particle densities.

It was stated in section 3.5.5 that self-similar fluctuations are present if the extracted moments increase with decreasing bin size in $\delta\eta$ which equals the given experimental windows. The necessary side condition was fulfilled with experimental windows which are bigger than the expected minimal size of such a fluctuation.

Figure 5.14 shows that self-similar fluctuations exist because the individual filled data points of the different orders follow individually a power law. This leads to a scale invariance of moments in high energy multiparticle production processes with respect to the phase space bins. Therefore the particle density shows fractal behaviour.

Multifractal behaviour was also tested with a Pythia MC sample and is depicted with open symbols and the corresponding color of the different orders. It was found that the event generator PYTHIA describes these fractal properties surprisingly well. However, the real moments are underestimated in the MC samples but the different slopes of the presented quantities in Figure 5.14 are crucial and converge with the corresponding slopes of the extracted real data. A possible origin of these multifractal and periodic characteristics in the event generator is the implemented parton shower evolution in jets.

5.1.4. Comparison to MC predictions

The results of the $k(\delta\eta)$ extraction were presented in the last sections. It is now of great interest in which way they are conform with Pythia MC predictions. Figure 5.15 shows two applied methods of extraction. The black points are the

5. Results

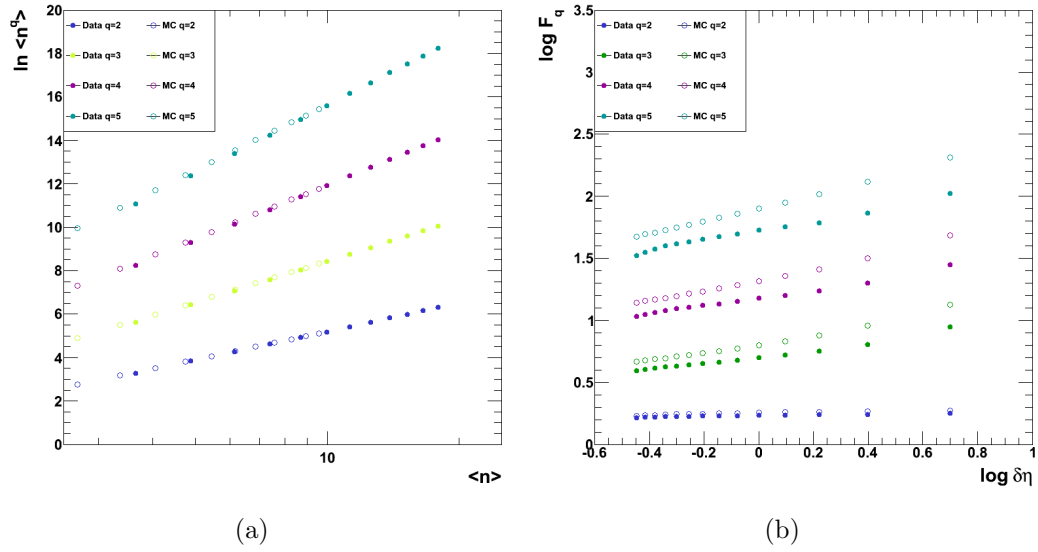


Figure 5.14.: (a) q^{th} orders of the reduced C-moment; (b) q^{th} orders of the factorial moments

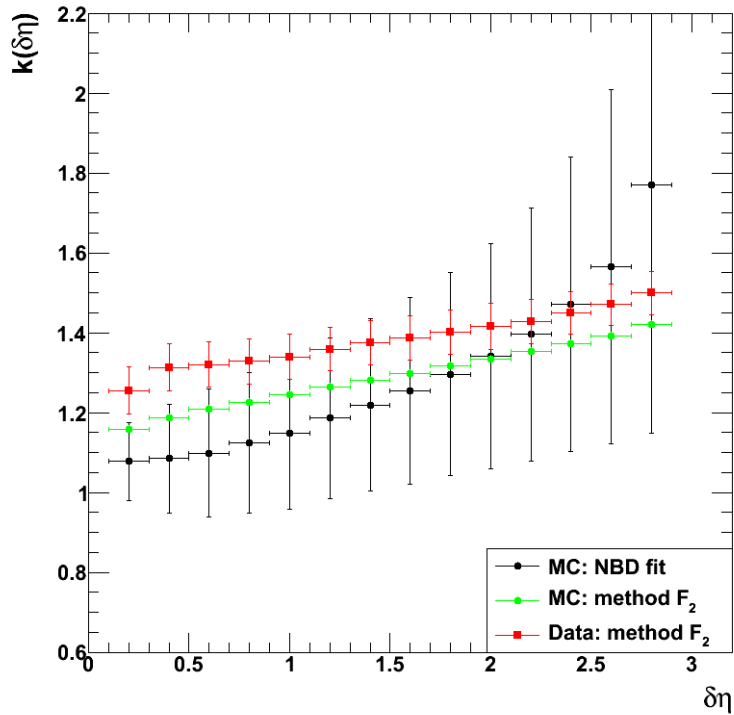


Figure 5.15.: k_{NBD} extracted out of MC simulations of LHC10b.pass2 (Trigger V0AND) and data

product of fits with the NBD to the measured spectra. It was perceived that the fitting range in the pp analysis had a great impact on the extracted parameter like in real data. This can be seen again in the result of the simulation. The green points are coming from the extraction of k_{NBD} through the second-order factorial moment F_2 . The error bars are so small that they are within the markers. Both methods are agreeing with each other within the error bars. The red data points show the results of the real data obtained by F_2 . They are roughly 5 % higher than the MC predictions of the F_2 method but agree in the assigned error region.

5.2. Pb–Pb collisions

This section presents the results of the heavy-ion analysis carried out with Pb–Pb data recorded at $\sqrt{s_{NN}} = 2.76$ TeV with the ALICE detector. It will give an overview of the measured multiplicity spectra in the different centrality classes and will introduce the correction for centrality ranges in a step size of 10%. Moreover, it will show the fitting results with the negative binomial distribution and the individually received centrality dependent $k(\delta\eta)$ distributions for the various centrality ranges. The clan model was examined with the obtained results of $k(\delta\eta)$ in order to estimate the clustering strength in Pb–Pb collisions. Furthermore, the Ginzburg-Landau theory was applied to the $k(\delta\eta)$ distributions through a fit which extracts the pseudo-rapidity dependent and independent parameters $\alpha\xi$ and β . Finally, the role of $\alpha\xi$ as an indicator of a phase transition will be discussed.

5.2.1. Measured multiplicity distributions

In Pb–Pb collisions the particle density is much higher than in pp collisions. It turns out that the particle density is $dN_{ch}/d\eta = 1600$ at (0-5)% centrality [Aam10c] and is below the design value of $dN_{ch}/d\eta = 4000$ for which ALICE was optimized.

This analysis was done for different centrality ranges with a step size of 1%, 5% and 10%. First 10% centrality step sizes were examined. It turned out that a more precise centrality classification helps to improve the resolution of possible multiplicity fluctuations. Therefore it will be possible to distinguish the difference between the results obtained from the 3 different centrality class selections. Furthermore, this analysis is based on fourteen multiplicity distributions like in pp (see Section 4.2.1). However, in contrast to pp the Pb–Pb spectra have a more Gaussian shape as can be seen exemplarily in Fig. 5.16. This is implied by a k_{NBD} parameter between 10 and 200 for Pb–Pb where the pp k values were in the range of 1 to 2 in the same pseudo-rapidity bins. Figure 5.16 shows as an example in green and blue two extracted multiplicity spectra in the centrality range of 10-15% and 15-20% for $\delta\eta = 2.0$. The fits with a NBD are shown in similar colors too. It can be seen that the NBD fits well to the measured spectra. The fits turned out to be much more stable than in pp.

Another possibility to investigate multiplicity spectra is to transform them into the Koba-Nielsen-Olesen (KNO) form and to check if the KNO scaling is satisfied. The KNO form is illustrated in Figure 5.17 for 0-5% most central events. The individual probability distributions are multiplied with a scaling factor in order to distinguish them better from each other. Going from top to

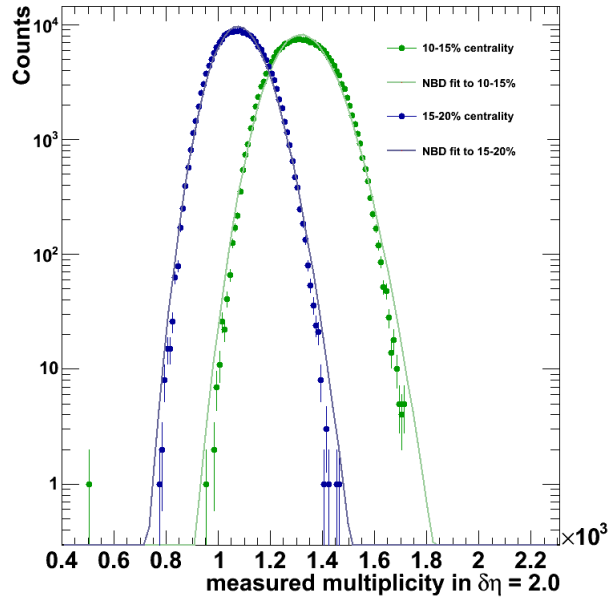


Figure 5.16.: Measured multiplicity distributions for the centrality range 10-15% and 15-20% for $\delta\eta = 2.0$, fitted with negative binomial distributions

bottom the pseudo-rapidity range increases where at the same time the width of the multiplicity spectra decreases. If the KNO scaling would be fulfilled in this energy regime for Pb–Pb then there would be a universal curve on which all other probability distributions lie on top. It was found that the KNO scaling does not hold in Pb–Pb collisions at 2.76 TeV.

5.2.2. Correction of multiplicity distributions

The correction of measured multiplicity distributions in the various centrality classes was done for the 10% centrality bin width. A multiplicity measurement in Pb–Pb with tracklets always needs to be corrected for combinatorial background. In this analysis the method of tail matching with MC labels was used. In order to apply corrections, 3 dataset had to be produced. A set of raw data, a MC raw data set generated with in the same manner as for the raw data and a set of MC data which represents the combinatorial background. Tracklet reconstruction in the MC raw data set was done by checking the MC labels of each cluster in both layers. Real tracklets were found if the MC labels of combined clusters from the different layers matched. This suppressed the reconstructed fake tracklets which basically have just one cluster or which have a cluster combination were the MC labels do not match. In order to extract information from the different data sets it is necessary to match the tails of the Δ -distributions of each dataset. These Δ -distributions contain the infor-

5. Results

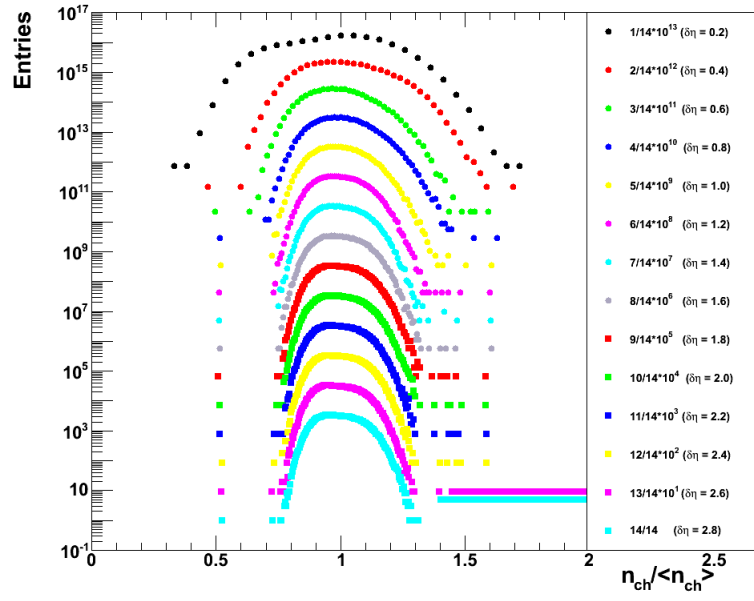


Figure 5.17.: KNO form of multiplicity distributions in 14 pseudo-rapidity windows for the 0-5% most central events

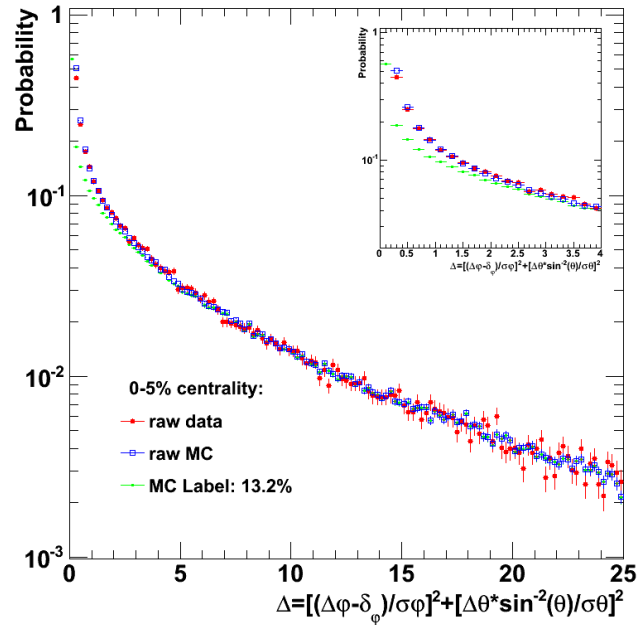


Figure 5.18.: Correction of fake tracklets through tail matching

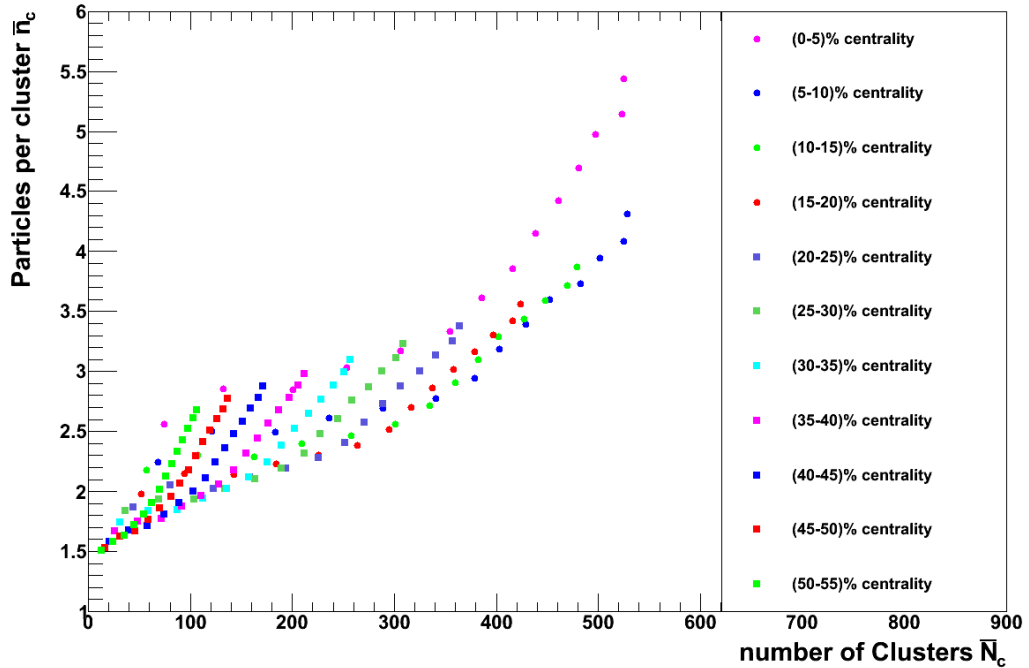


Figure 5.19.: Clan model in Pb–Pb collisions in various centrality classes

mation of $\Delta\varphi$ and $\Delta\theta$, i.e. the azimuthal and polar variance of the combined clusters, which form tracklets, relative to the primary vertex. The percentage of fake tracklets in the raw spectrum can be determined from the matching of the tails with MC data and the combinatorial background. Therefore it is possible to correct for fakes in the raw spectrum by simply subtracting them from the distribution. The procedure of tail matching is shown for 0-5% centrality in Figure 5.18. The inlay of this plot shows a zoom of the region where the spectra start to match.

5.2.3. Clan model

The clan model in the context of heavy-ion collisions was already briefly addressed in the result section of the pp analysis. It was found that in Cu+Cu the correlation among clusters was weak, i.e., their distributions were close to a Poissonian. This was shown through the number of particles per cluster n_c which were in the region of $\bar{n}_c \approx 1$ over a large number of clusters \bar{N}_c . The number of clusters in a Cu+Cu system with a center-of-mass energy of 200 GeV from PHENIX [Ada08] went up to 60. In Pb–Pb collisions measured with ALICE at a center-of-mass energy of $\sqrt{s_{NN}} = 2.76$ TeV, 531 clusters with at most 5.5 particles for most central collisions were found. Figure 5.19 shows the rise of the clan parameters in various centrality classes. This rise in the number of particles in a cluster as well as in the number of clusters indicate

5. Results

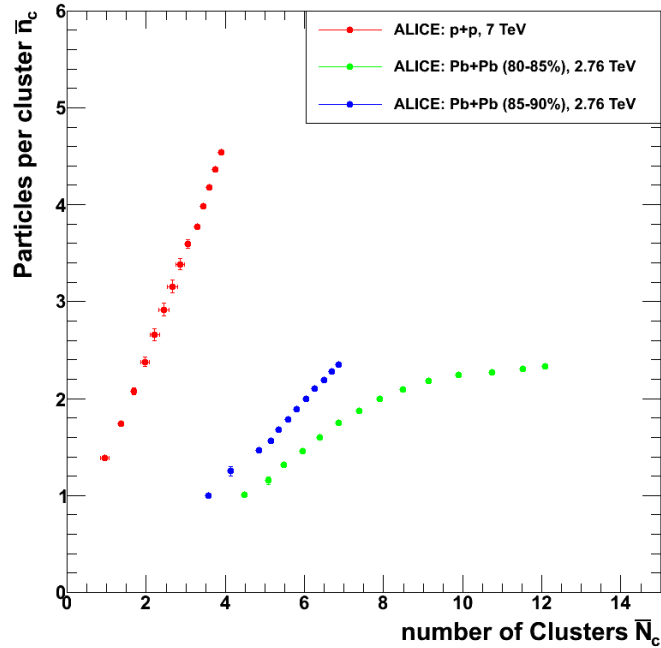


Figure 5.20.: Comparison of centrality 80-85% and 85-90% of Pb–Pb collisions with ALICE data from pp collisions at 7 TeV

that the cascading behaviour increases with increasing beam energy as well as growing centrality in heavy-ion collisions.

Figure 5.20 illustrates the comparison of clan results from pp in red and from peripheral Pb–Pb collisions in green and blue. This comparison was made because it was observed by [Aam10c] that $(dN_{ch}/d\eta)/(\langle N_{part} \rangle/2)$ in relation to N_{part} of peripheral centrality bins in Pb–Pb are similar to pp collisions. In combination with Figure 5.19 it can be concluded that going from central (0-5%) to peripheral (85-90%) the clan parameters, more precisely the average number of clusters and the average number of particles in a cluster, begin to behave similar to the pp results.

5.2.4. The Ginzburg-Landau Fit

The Ginzburg-Landau framework was already introduced in Section 3.5.2 with its relation to the NBD. The extracted k_{NBD} of the available different centrality classes and ranges, namely 10%, 5% and 1%, were individually fitted with Eq. 3.27. Figure 5.21 shows results exemplary for the uncorrected 5% centrality classes with the corresponding GL-fits in the same color as their markers. The errors of the $k(\delta\eta)$ -distributions are tiny and within the markers. It can be observed that the GL-fits work well from centrality class 15-20% on. In the most central collisions the fit has some difficulties. The fitting parameters

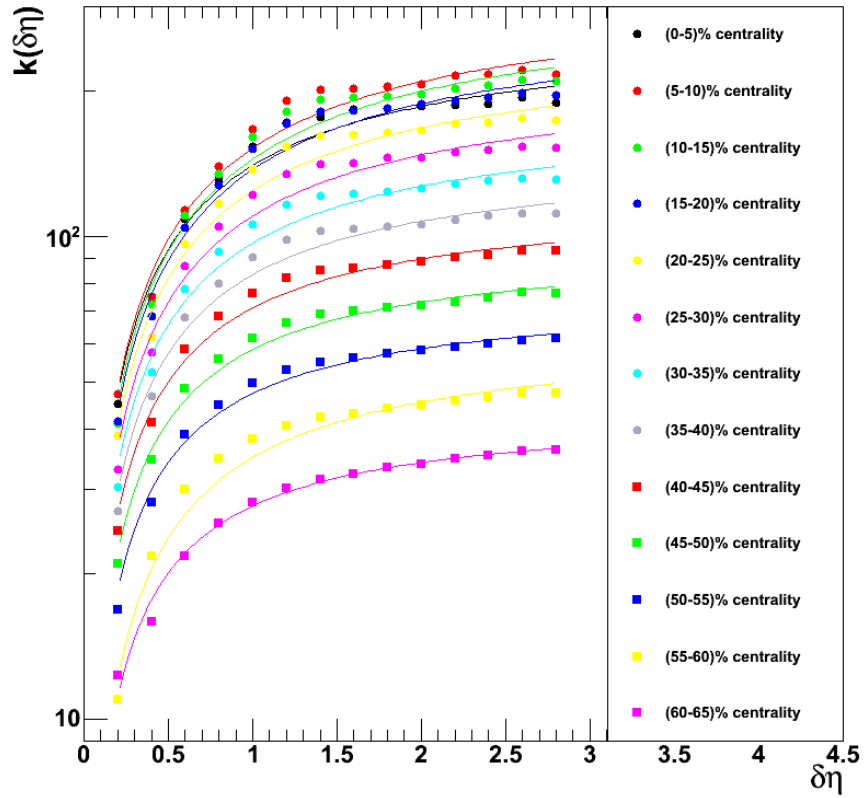


Figure 5.21.: $k(\delta\eta)$ distributions of different centralities in a step size of 5% with their corresponding Ginzburg-Landau fits

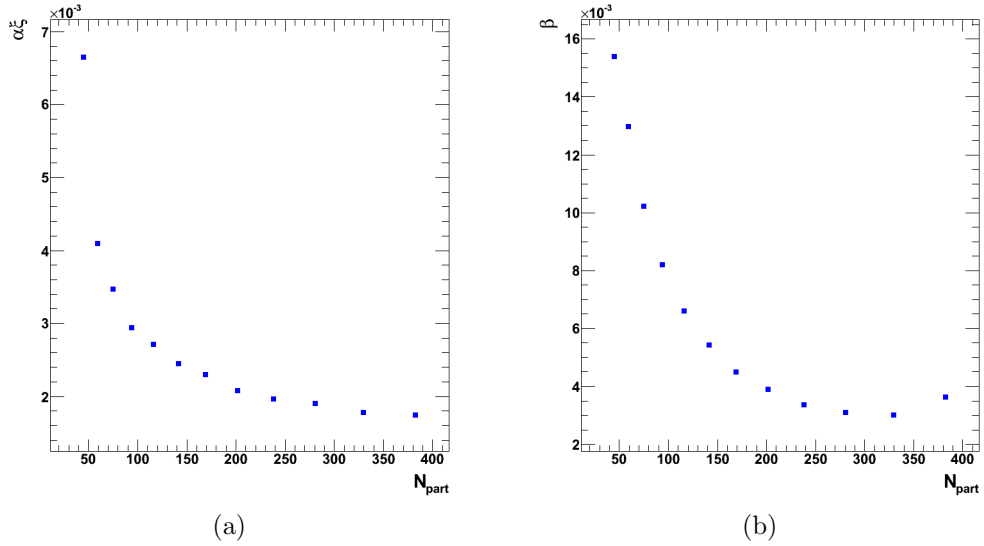
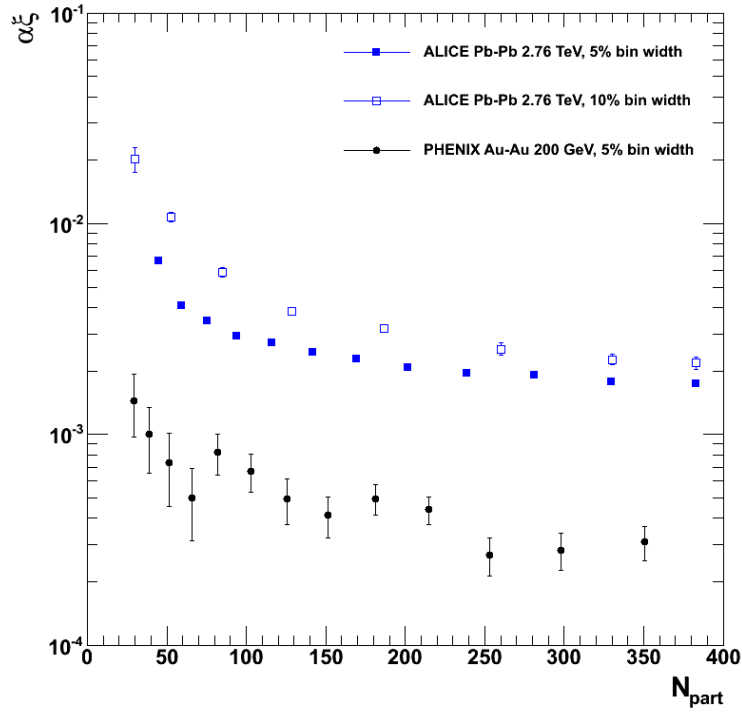
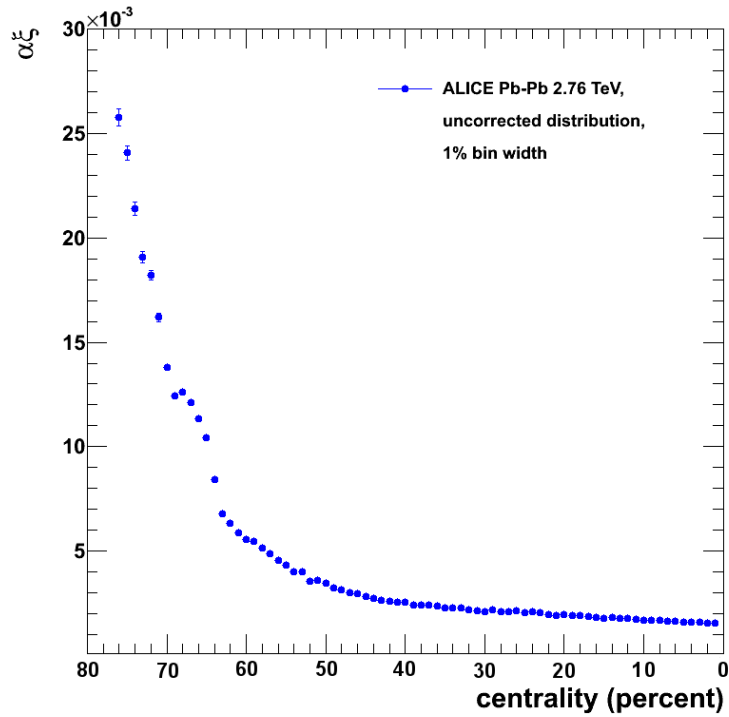


Figure 5.22.: The Ginzburg-Landau parameters $\alpha\xi(N_{part})$ (a) and $\beta(N_{part})$ (b) in a centrality step size of 5%

5. Results



(a)



(b)

Figure 5.23.: Ginzburg-Landau order parameter $\alpha\xi$ vs. N_{part} or centrality in different centrality binning compared to PHENIX data. PHENIX data taken from [Adl07]

are $\alpha\xi$ and β and correspond to the Glauber model to assigned numbers of participants N_{part} in the collision. The parameters with their corresponding N_{part} are shown in Figure 5.22 for the selection with 5% bin width. It is observed that the pseudo-rapidity dependent parameter $\alpha\xi$ and the independent parameter β decreases with growing N_{part} without an interesting feature. The corresponding result with the corrected multiplicity distributions for the 10% centrality ranges for $\alpha\xi(N_{part})$ are depicted in Figure 5.23 (a) with the ALICE 5% results and the PHENIX results at $\sqrt{s_{NN}} = 200$ GeV/c from Au+Au collisions. PHENIX observed indications for an increase in the product of correlation length and correlation strength. One can speculate about the origin of the feature at 90 participating nucleons. The aim of the analysis with ALICE data was to investigate if the ALICE data also exhibits this behaviour. This analysis described in this thesis does not show fluctuations in the same manner as in PHENIX in the corrected 10% and the uncorrected 5% results. Therefore a further investigation was done and the centrality binning was decreased to a 1% centrality binning. The output of a 1% centrality binning is shown in Figure 5.23 (b) where, although the result is for uncorrected multiplicity distributions, the $\alpha\xi(\text{centrality})$ -distribution is decreasing extremely smooth to more central events. Taking everything into account one can summarize that no fluctuations in $\alpha\xi$ were observed in the various centrality selections. This circumstance supports two conclusions. Either the theory does not hold in the context of relativistic heavy-ion collisions or the multiplicity fluctuations did not survive into the final state. Then one would not be able to detect those fluctuations. Therefore it is unfortunately not possible to make a statement if $\alpha\xi$ is a possible observable to probe the Quark-Gluon Plasma.

6. Summary and Outlook

The measurement of charged particle multiplicity distributions is a key observable in relativistic high-energy particle physics. In the presented analysis multiplicity distributions of pp and Pb–Pb collisions in limited pseudo-rapidity windows were investigated to gain a deeper understanding of the underlying particle production mechanism.

The fourteen windows used had its center at the pseudo-rapidity of $\eta = 0$. The window with the smallest range was $\delta\eta = 0.2$ and the biggest one had a range of $\delta\eta = 2.8$. The measured multiplicity spectra in pp were corrected by two unfolding methods, namely the χ^2 - and the Bayesian unfolding. It was found that the unfolding procedure introduces statistical fluctuations in higher multiplicity bins also observed in [Gro09]. In order to investigate the obtained corrected spectra the negative binomial distribution was used to examine the particle correlation in each window individually. It was found by the CERN UA5 experiment that the negative binomial distribution describes multiplicity distributions fairly well. The k parameter of the NBD is of great importance because it gives a measure of the particles correlation in a single window. This is possible because k_{NBD} estimates the difference between the width of the obtained distribution and that width of a Poisson distribution. A Poisson distribution would indicate that no correlation between the individual particles exist.

The k_{NBD} was extracted with four different techniques from the corrected multiplicity spectra: by using the integrated second-order factorial moment F_2 , by fitting the NBD to the corrected spectra, by transforming the NBD in a different shape and fitting the new shape with a linear function and by folding the NBD and fitting the result to the measured, thus uncorrected, spectra. It was found that the extraction with the F_2 -method was the most stable one because it describes the high multiplicity bins best.

Due to the fact that the emphasis was put on particle correlations in the different windows it was checked if correlations between the individual windows exist. This check was done with the convolution property of the negative binomial distribution which uses the k_{NBD} parameter. It was found that the individual windows are correlated with each other.

Furthermore, cascading, intermittency and multifractality were examined. The average number of particles in a cluster and the average number of clusters were found to be strongly depend on the beam energy. The intermittency anal-

6. Summary and Outlook

ysis showed that the measured multiplicity distributions are consistent with a self-similar particle production mechanism.

Multiplicity distributions in Pb–Pb were examined, too. It was observed that heavy-ion multiplicity distributions have a completely different shape than pp distributions in the central regions. Going to more peripheral centralities the shape starts to converge. This feature is supported by the extracted k_{NBD} parameter through the fitting method with the NBD. Those k_{NBD} values are one order of magnitude bigger in central regions than in peripheral centrality regions. Like in the pp analysis the clan model, i.e. the cascading behaviour was investigated. Contrary to the results obtained by PHENIX [Ada08] it was found that Pb–Pb collisions at $\sqrt{s_{NN}} = 2.76$ TeV per nuclei exhibit a clustering behaviour which depends on centrality. The average number of clusters was found to be up to 531 in 0-5% centrality with an average number of about 5.5 particles. As observed in the shape of peripheral multiplicity distributions the clan parameters start to converge at 85-90% centrality with the pp results. Unfortunately, it is not possible to resolve more peripheral centralities.

Furthermore, the relation of the NBD to the multiplicity distribution gave the opportunity to test the Ginzburg-Landau framework in the context of heavy-ion collisions. It was predicted that this theory provides a possible indicator to probe the Quark-Gluon Plasma and would be able to pin down the number of participants at the phase transition by measuring multiplicity fluctuations. This analysis was done for three different centrality selections which are a 10% study with corrected spectra, a 5% and a 1% study with uncorrected spectra. Contrary to PHENIX [Adl07] no interesting increase was found in the examined $\alpha\xi$ order parameter. Therefore it is not possible to make a statement if a phase transition happened or if just the theory does not hold. As a result it is not obvious that $\alpha\xi$ is a good experimental observable to probe the Quark-Gluon Plasma.

As a prospective it would be interesting to run the pp analysis with the 2.76 TeV run of 2011. This would round over the picture of $k(\delta\eta)$ becoming flatter with higher beam energies. This would indicate and further proof an energy dependent correlation strength of the particles. Furthermore, the presented concepts of the clan model, intermittency and multifractality could be presented in their evolution with increasing beam energies. However, it was stated that the NBD does not fit perfectly to the multiplicity distributions in the given energy regime therefore it would be interesting how a fit with two combined NBDs would describe the distributions and what could be learned from this. A possible approach for the Pb–Pb analysis would be the correction of the 5% and the 1% analysis in order to be able to confirm the results of $\alpha\xi$ with uncorrected spectra.

A. Acronyms

ALICE	A Large Ion Collider Experiment
AliROOT	Alice ROOT
ACORDE	ALICE Cosmic Ray Detector
ATLAS	A Toroidal LHC ApparatuS
CERN	Conseil Européen pour la Recherche Nucléaire
CEP	Critical End Point
CMS	Compact Muon Spectrometer
EMCAL	Electromagnetic Calorimeter
EMI	Electromagnetic Interactions
ESD	Event Summary Data
FMD	Forward Multiplicity Detector
GEANT	Geometry And Tracking
GL	Ginzburg-Landau
HIJING	Heavy Ion Jet Interaction Generator
ITS	Inner Tracking System
IP	Interaction Point
KNO	Koba-Nielsen-Olesen
LEP	Large Electron-Positron Collider
LHC	Large Hadron Collider
LHCb	Large Hadron Collider beauty experiment
LINAC	Linear Accelerator
MC	Monte Carlo
MIB	Machine-Induced Background
MINUIT	Minimization and Error Analysis program
NBD	Negative Binomial Distribution
PBS	Proton Synchrotron Booster
PHENIX	Pioneering High Energy Nuclear Interactions eXperiment
PHOS	Photon Spectrometer
PID	Particle Identification
PMD	Photon Multiplicity Detector
PS	Proton Synchrotron
QCD	Quantum Chromodynamics
QGP	Quark-Gluon Plasma
RHIC	Relativistic Heavy Ion Collider
SPD	Silicon Pixel Detector

A. *Acronyms*

SPS	Super Proton Synchrotron
TOF	Time-of-Flight detector
TPC	Time-Projection Chamber
TRD	Transition Radiation Detector
ZDC	Zero-Degree Calorimeter

B. Multiplicity Distributions

In the following the different unfolding methods, more precisely the χ^2 - and the Bayesian unfolding, are shown for the 3 different offline trigger selections. The difference in the offline trigger selection is described in section 4.1.1 . The cross-check of the unfolding process will be shown as well for each individual pseudo-rapidity window.

B. Multiplicity Distributions

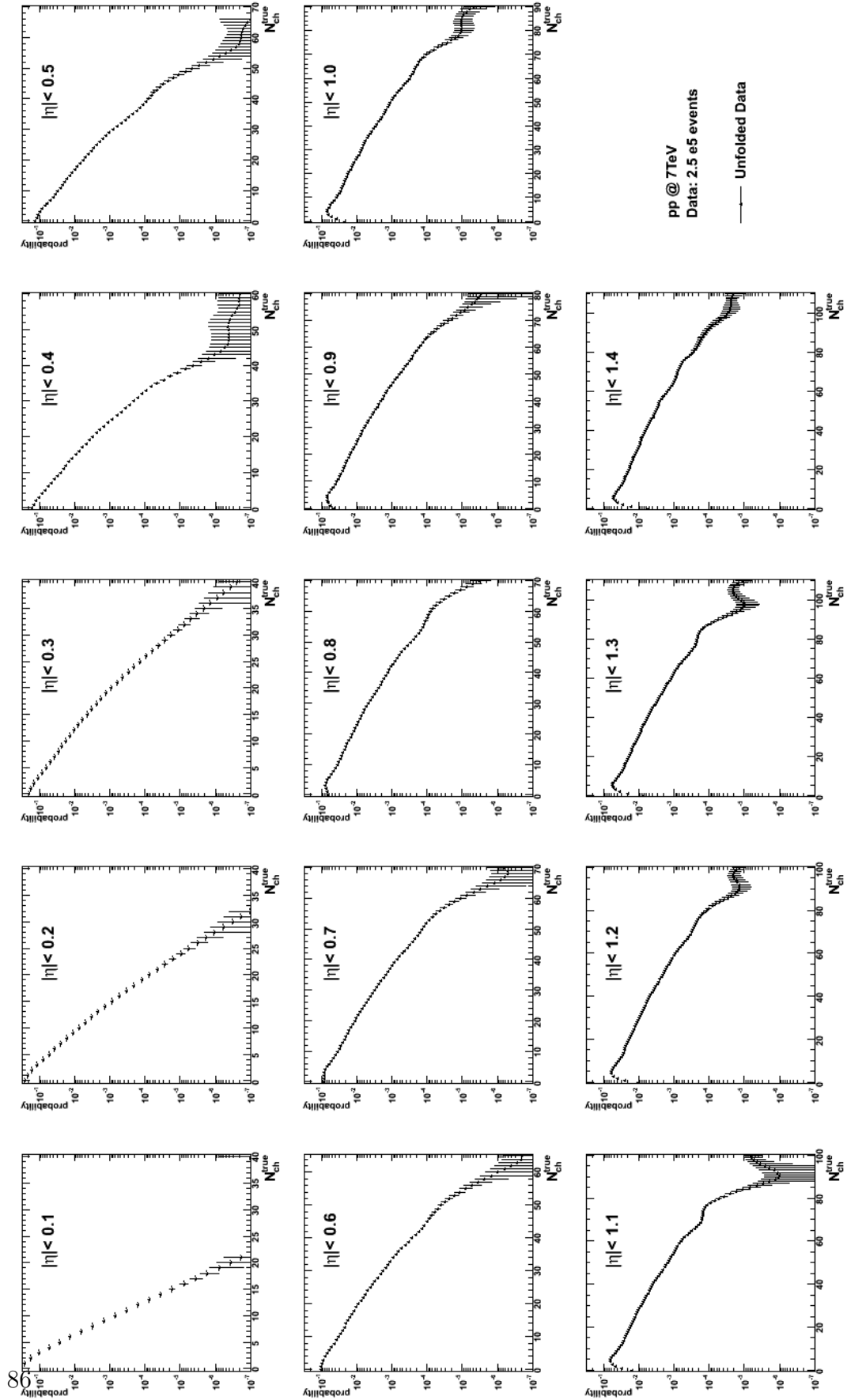


Figure B.1.: Multiplicity distributions corrected through χ^2 unfolding, Trigger
A

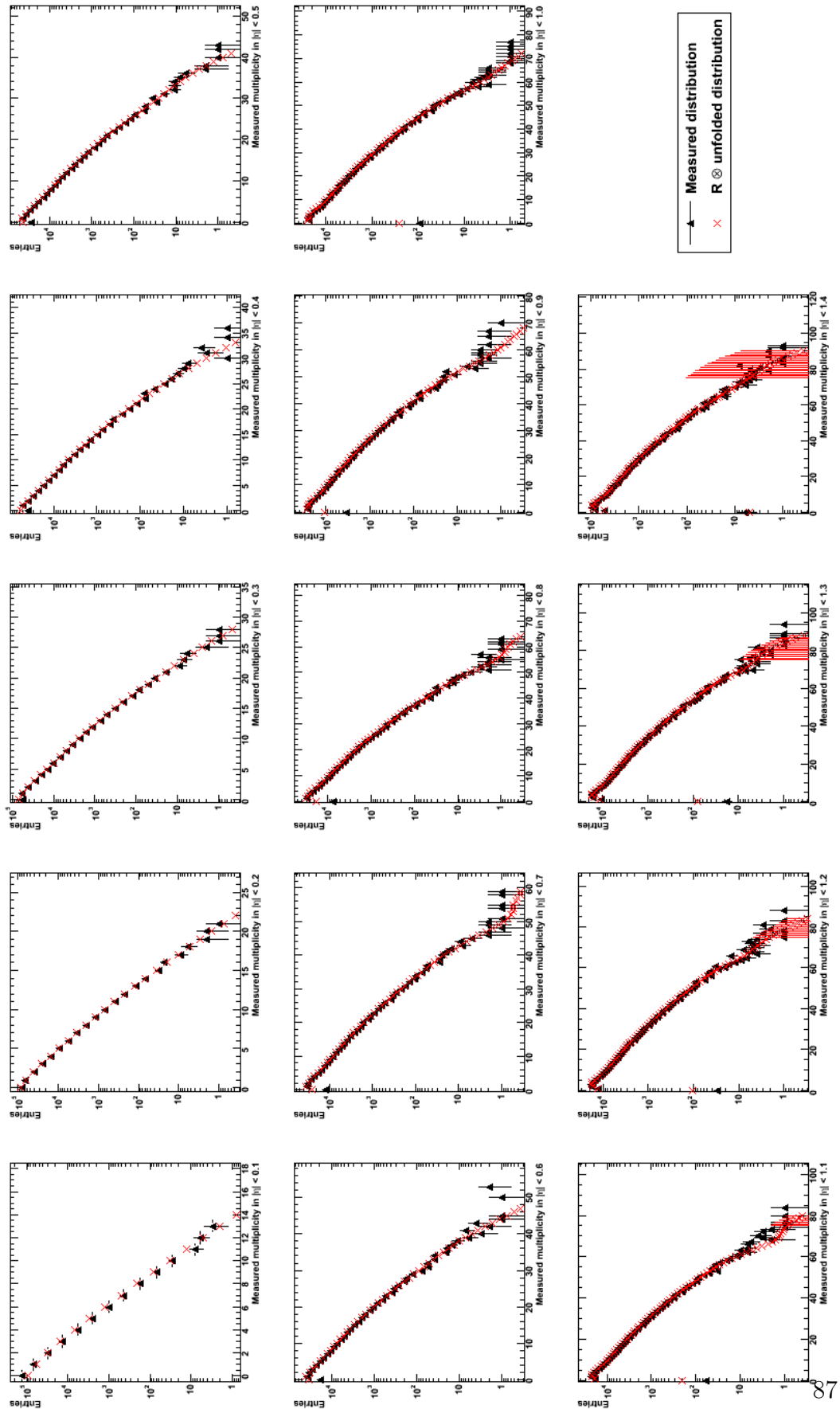


Figure B.2.: Measured multiplicity distributions and Response Matrix \otimes unfolded distributions (χ^2 unfolding, Trigger A)

B. Multiplicity Distributions

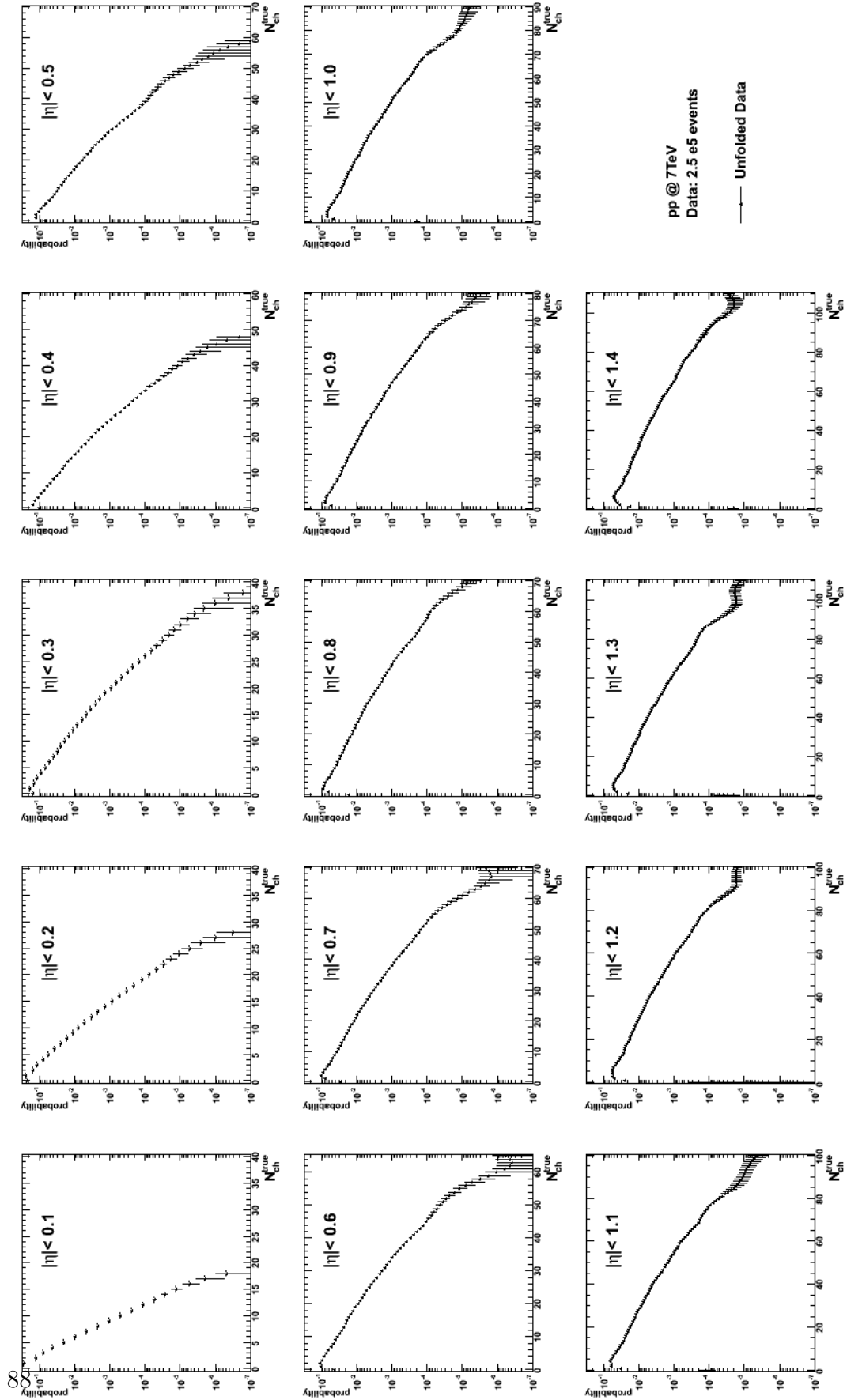


Figure B.3.: Multiplicity distributions corrected using the Bayesian unfolding, Trigger A

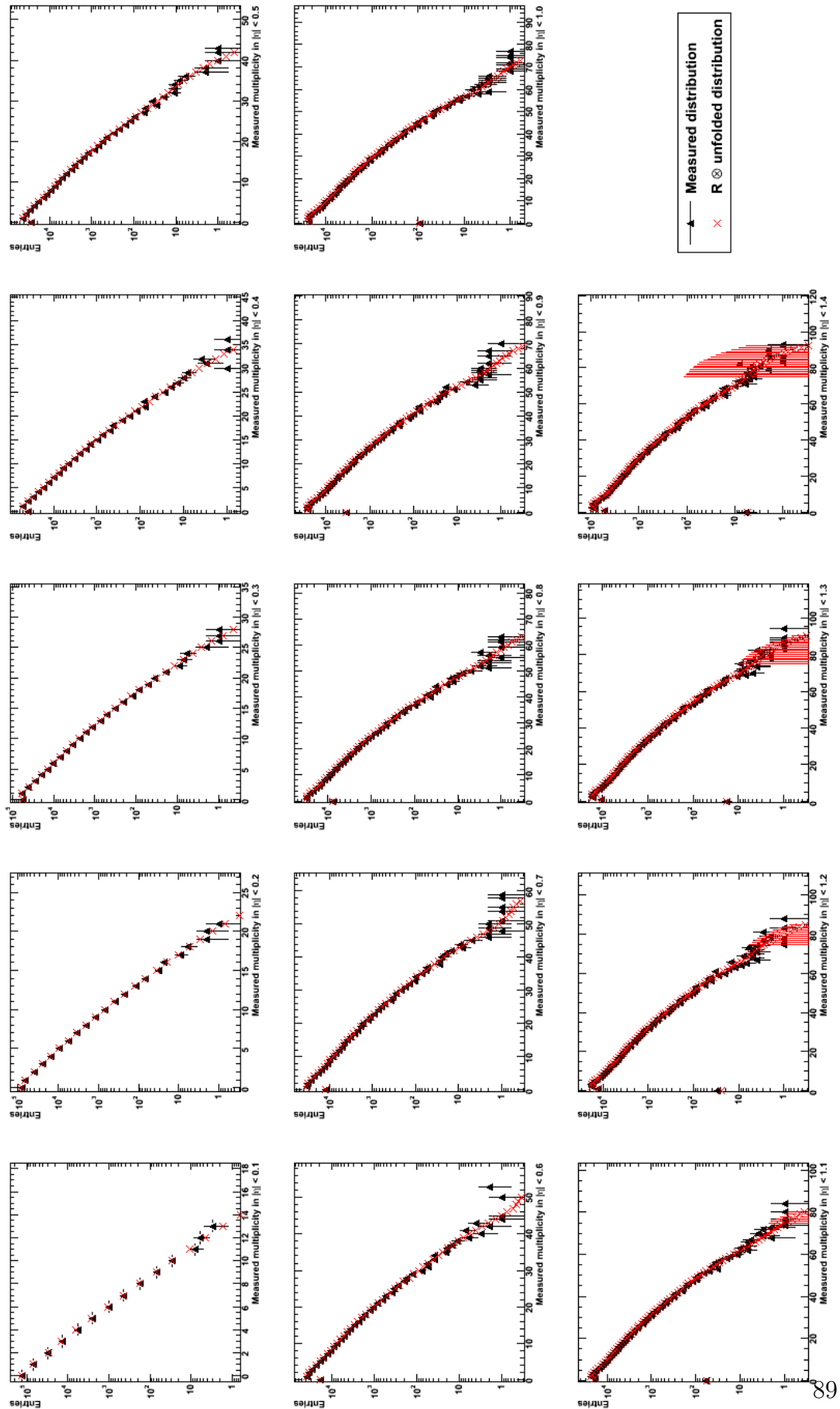


Figure B.4.: Measured multiplicity distributions and Response Matrix \otimes unfolded distributions (Bayesian unfolding, Trigger A)

B. Multiplicity Distributions

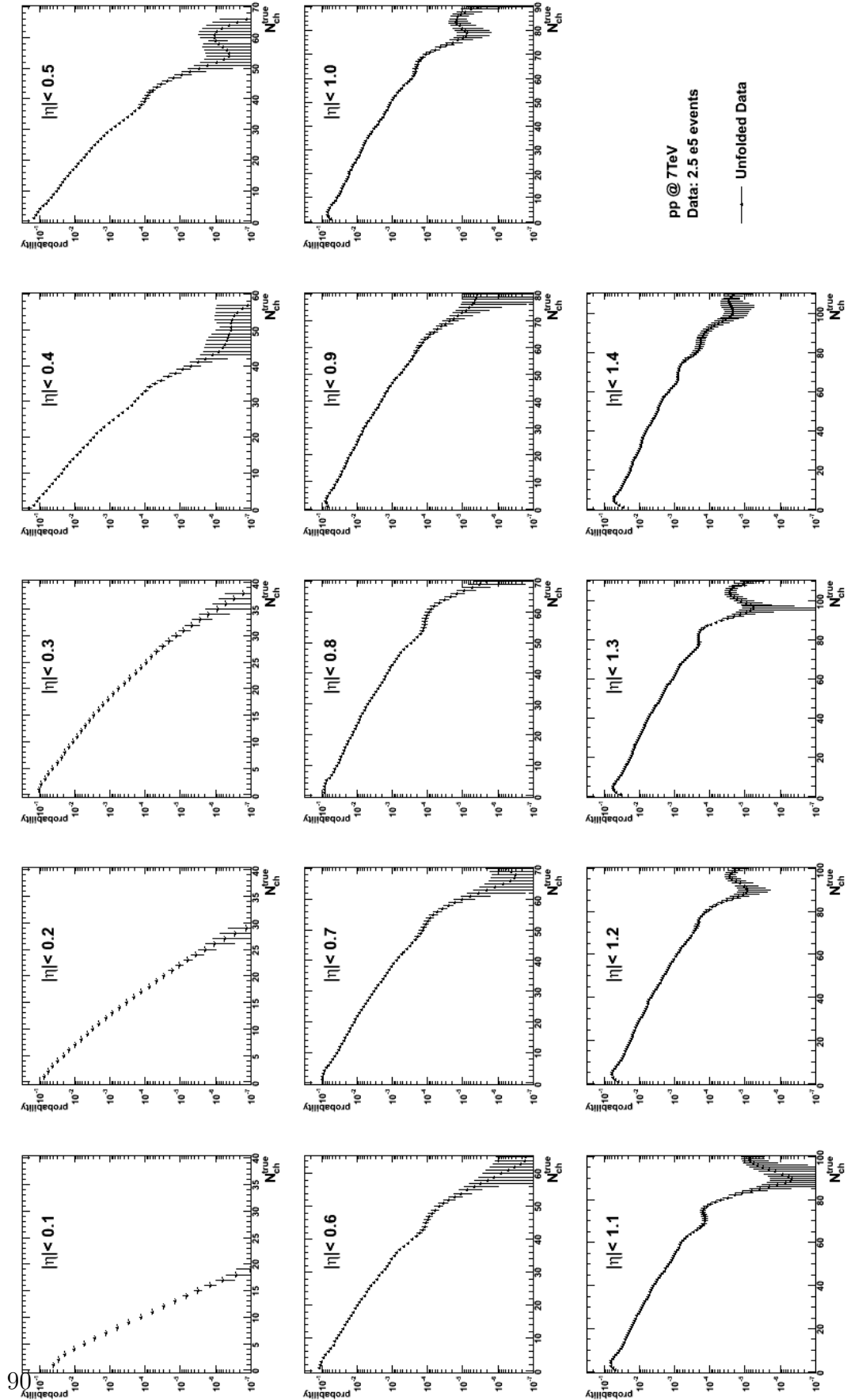


Figure B.5.: Multiplicity distributions corrected using the χ^2 unfolding, Trigger B

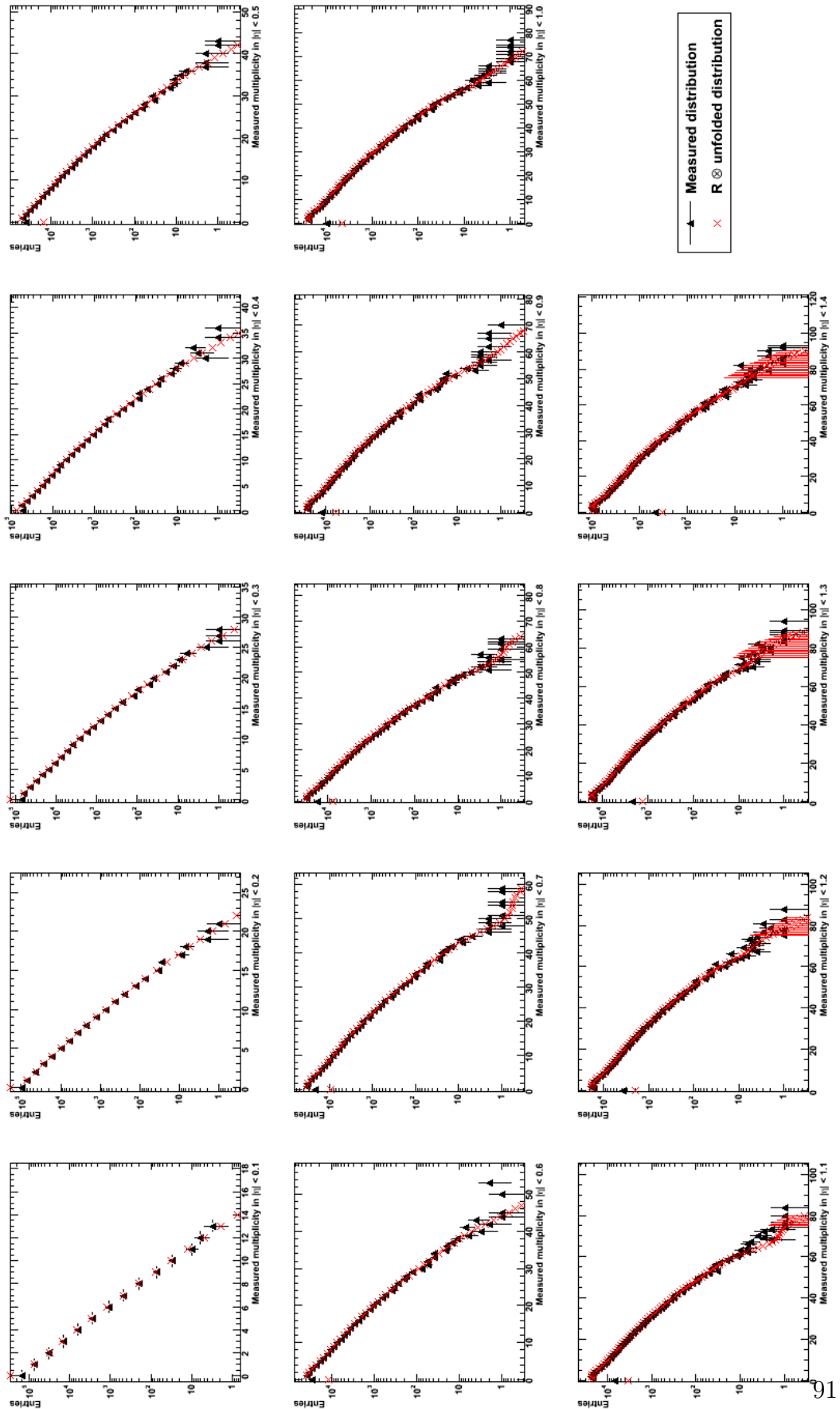


Figure B.6.: Measured multiplicity distributions and Response Matrix \otimes unfolded distributions (χ^2 unfolding, Trigger B)

B. Multiplicity Distributions

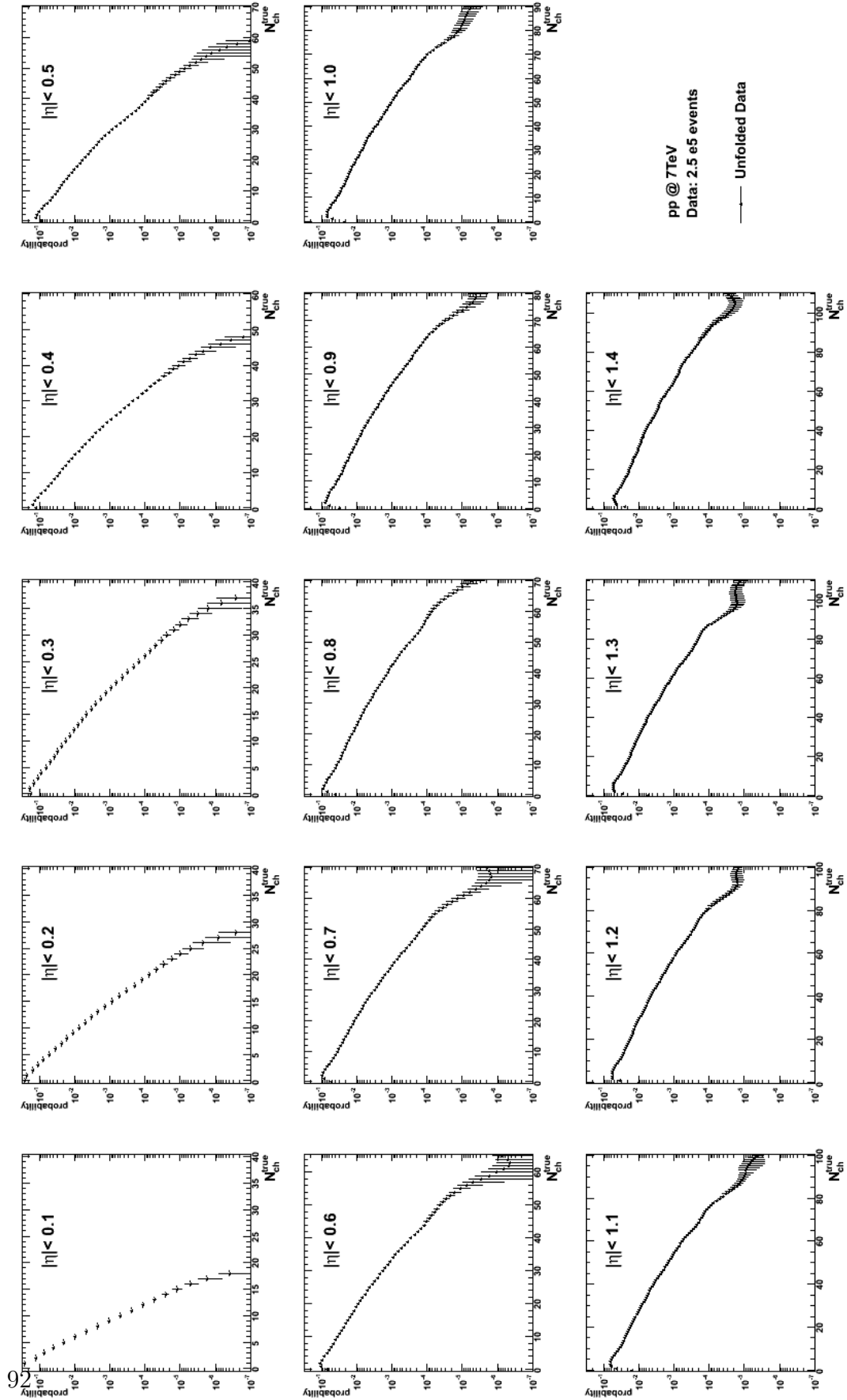


Figure B.7.: Multiplicity distributions corrected using the Bayesian unfolding, Trigger B

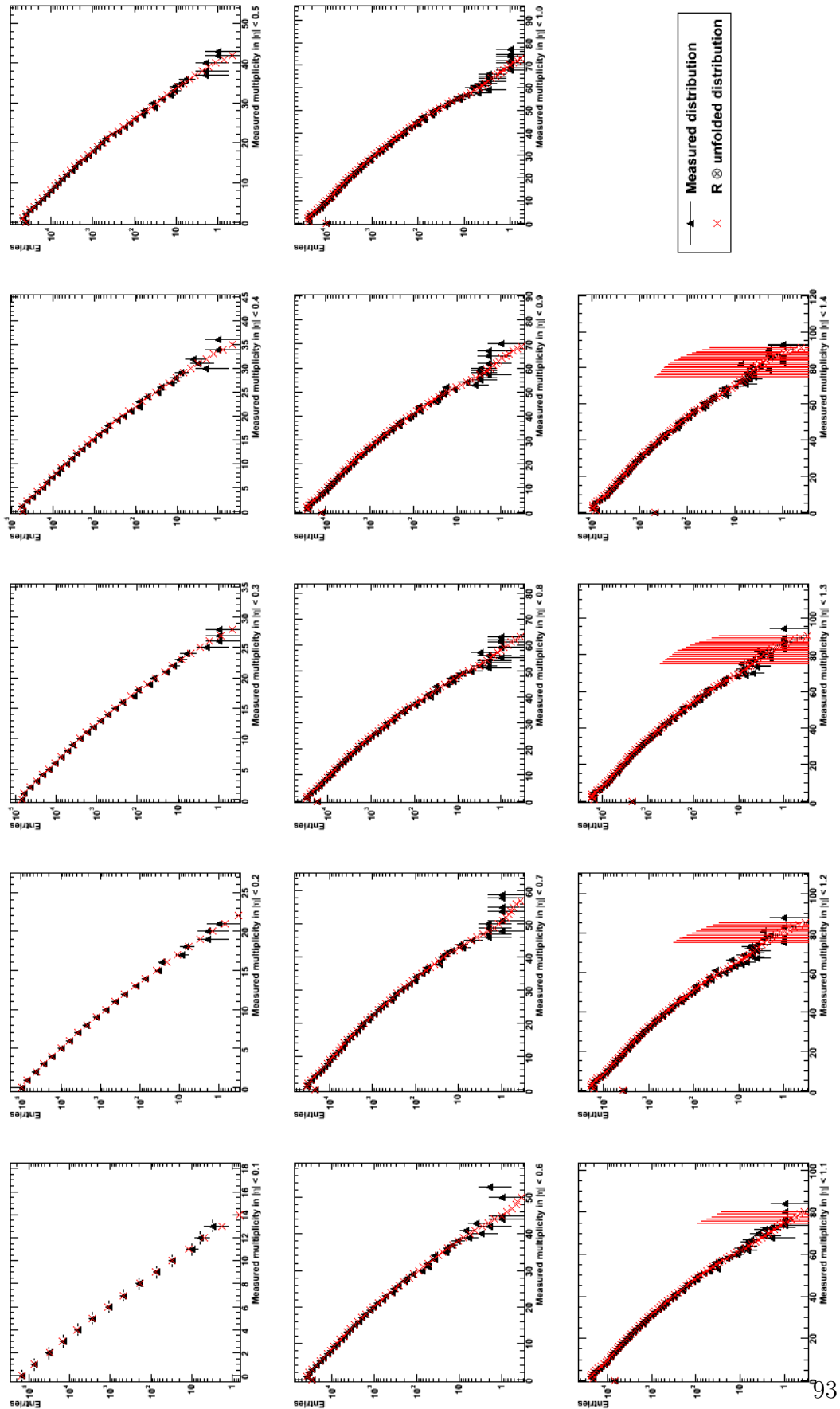


Figure B.8.: Measured multiplicity distributions and Response Matrix \otimes unfolded distributions (Bayesian unfolding, Trigger B)

B. Multiplicity Distributions

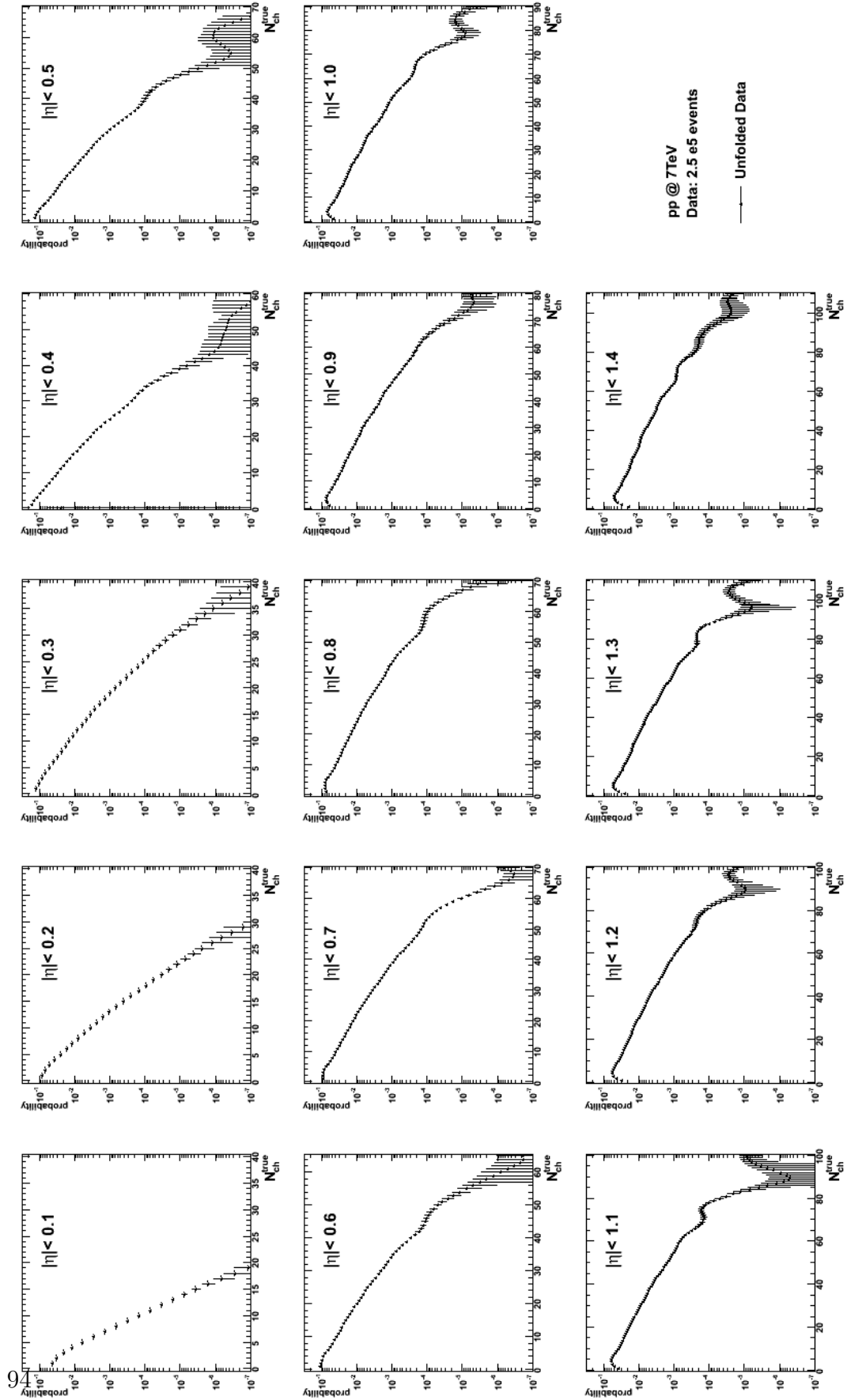


Figure B.9.: Multiplicity distributions corrected using the χ^2 unfolding, Trigger C

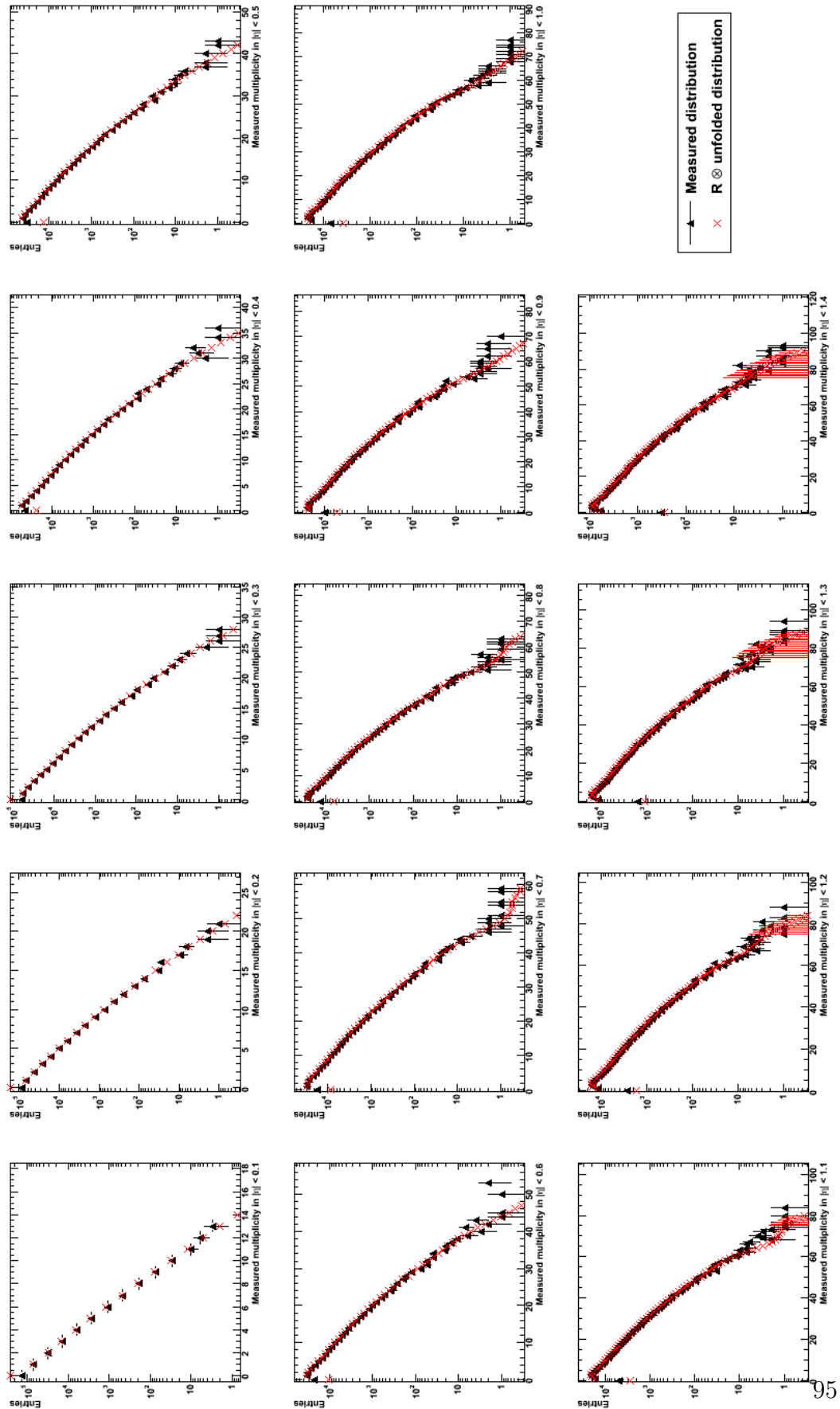


Figure B.10.: Measured multiplicity distributions and Response Matrix \otimes unfolded distributions (χ^2 unfolding, Trigger C)

B. Multiplicity Distributions

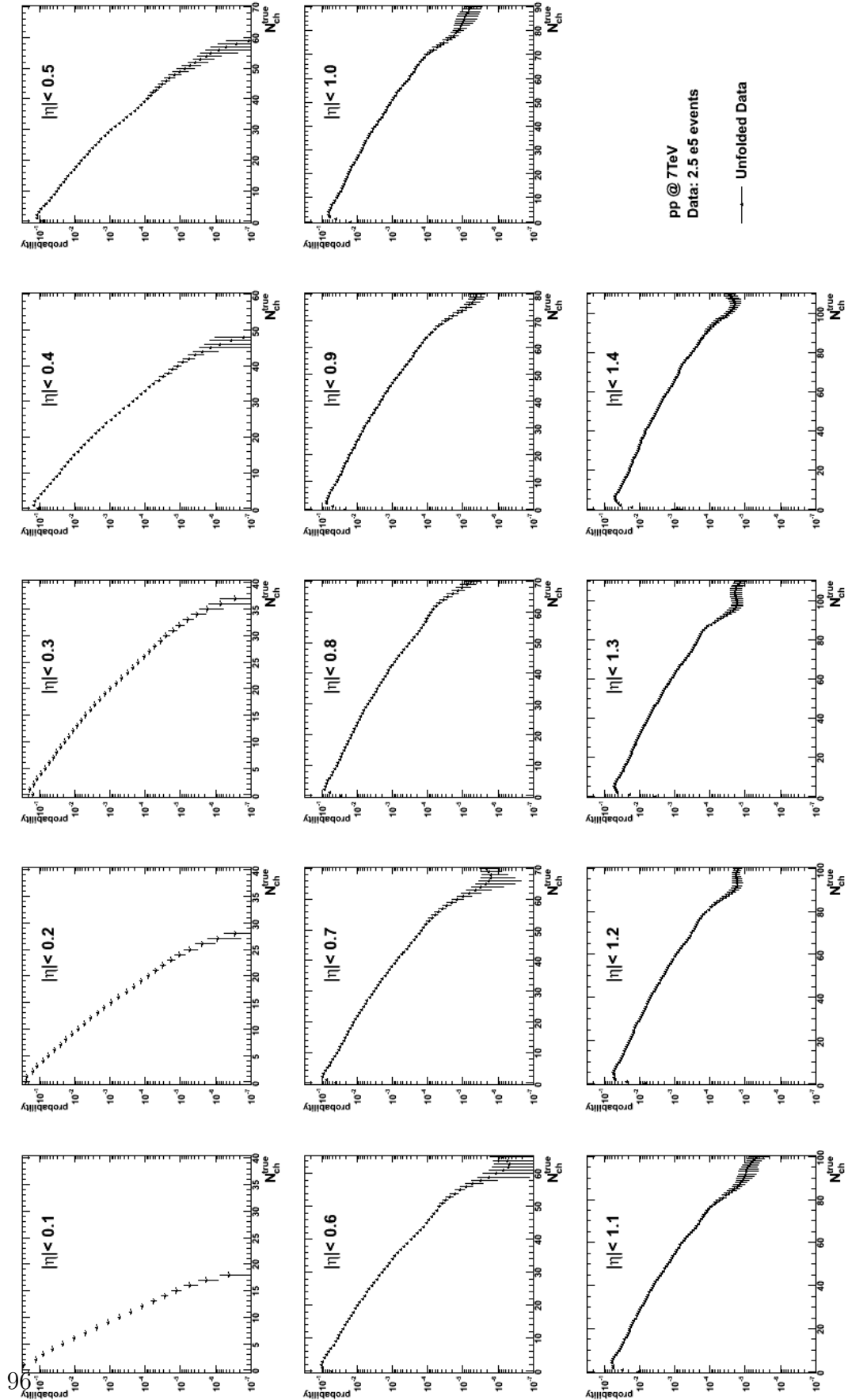


Figure B.11.: Multiplicity distributions corrected using the Bayesian unfolding, Trigger C

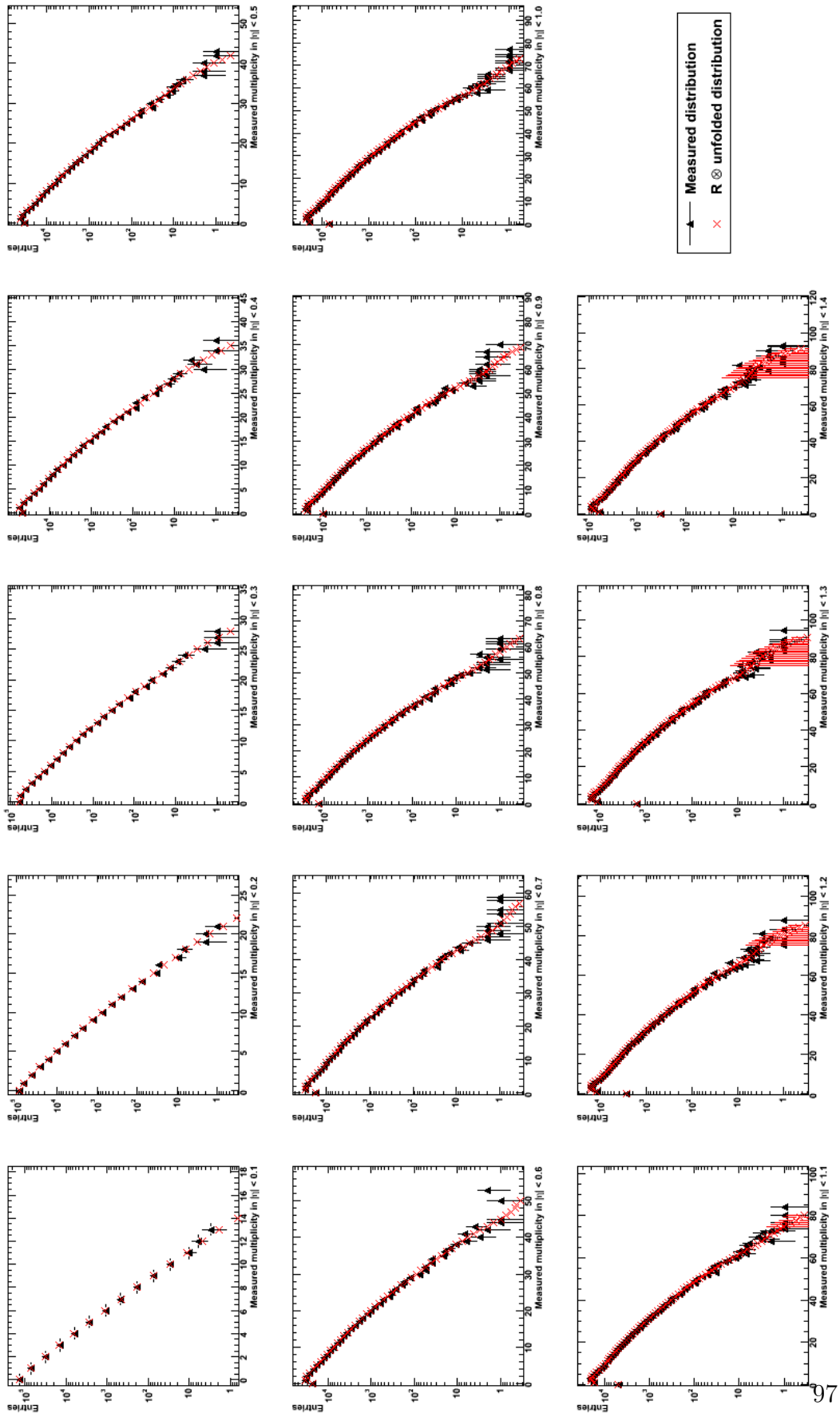


Figure B.12.: Measured multiplicity distributions and Response Matrix \otimes unfolded distributions (Bayesian unfolding, Trigger C)

Acknowledgements

Special thanks goes to PD Dr. Klaus Reygers for giving me the opportunity to carry out my diploma thesis, for his supervision and inputs concerning multihadron dynamics. Furthermore, I would like to give my gratitude to my group leader Prof. Dr. Johanna Stachel who made it possible that I could get an insight view into particle physics as well as giving me the opportunity to work at such a unique experiment.

I would like to thank Prof. Dr. Norbert Herrmann for reading and evaluating my thesis.

I would like to give a special thanks to Dr. Yvonne Pachmayer for advice and assistance in AliRoot, for the fruitful discussions about the Pb–Pb centrality framework and for proof reading. Besides them, I would like to express my gratitude to Kathrin Koch, Friederike Bock and Felix Reidt with whom I discussed my analysis and coding issues and many more things.

I am very grateful for the supervision of Dr. Jan-Fiete Große-Oetringhaus concerning the unfolding of multiplicity spectra in pp. Thanks goes to Xianguo Lu for the interesting discussions about the negative binomial distribution and special fitting procedures.

For providing the opportunity to work with the GSI batchfarm, I would like to thank Dr. Silvia Masciocchi, Dr. Jens Wiechula and the rest of the people involved in the GSI ALICE group. I further like to thank Jochen Thäder for helping me with AliRoot problems and introducing me to Dr. Ruben Shahoyan, who I thank for his help concerning the correction of my Pb–Pb analysis.

I would like to thank Dr. Rainer Schicker, Sara Vallero, Johanna Gramling, Radoslav Rusanov, Johannes Stiller, Michael Winn, Benjamin Hess and many more for providing such a kind working atmosphere.

A very special thanks goes to my parents, Ben and my friends for their support during my studies.

Bibliography

- [Aam08] K. AAMODT, ET. ALL (ALICE COLLABORATION), **The ALICE Experiment**, JINST 3 S08002 (2008)
- [Aam10a] K. AAMODT, ET. ALL (ALICE COLLABORATION), **Charged-particle multiplicity measurement in proton-proton collisions at $\sqrt{s} = 0.9$ and 2.36 TeV with ALICE at LHC**, arXiv:1004.3034 [hep-ex] (2010)
- [Aam10b] K. AAMODT, ET. ALL (ALICE COLLABORATION), **Charged-particle multiplicity measurement in proton-proton collisions at $\sqrt{s} = 7$ TeV with ALICE at LHC**, arXiv:1004.3514v2 [hep-ex] (2010)
- [Aam10c] K. AAMODT, ET. ALL (ALICE COLLABORATION), **Centrality dependence of the charged-particle multiplicity density at mid-rapidity in Pb-Pb collisions at $\sqrt{s_{NN}} = 2.76$ TeV**, arXiv:1012.1657 [nucl-ex] (2010)
- [Aam11] K. AAMODT, ET. ALL (ALICE COLLABORATION), **Charged-particle density at mid-rapidity in central Pb-Pb collisions at $\sqrt{s_{NN}} = 2.76$ TeV**, arXiv:1011.3916v3 [nucl-ex] (2011)
- [Abb95] T. ABBOTT, ET. ALL (THE E-802 COLLABORATION), **Multiplicity distributions from central collisions of $^{160}\text{O}+\text{Cu}$ at 14.6A GeV/c and intermittency**, PHYSICAL REV. C, VOL. 52 Number 5 (1995)
- [Ada08] A. ADARE, ET. ALL (PHENIX COLLABORATION), **Charged hadron multiplicity fluctuations in Au+Au and Cu+Cu collisions from $\sqrt{s_{NN}} = 22.5$ to 200 GeV**, PHYSICAL REV. C 78, 044902 (2008)
- [Adl07] S.S. ADLER ET. ALL (PHENIX COLLABORATION), **Measurement of density correlations in pseudorapidity via charged particle multiplicity fluctuations in Au+Au collisions at $\sqrt{s_{NN}} = 200$ GeV**, arXiv:0704.2894v1 [nucl-ex], 2007

Bibliography

- [Ali08] THE ALICE COLLABORATION, **The ALICE Experiment**, <http://aliceinfo.cern.ch/Public/en/Chapter2/Chap2Experiment-en.html>
- [Aln87] G.J. ALNER, ET. ALL (UA5 COLLABORATION), **UA5: A General Study of Proton-Antiproton Physics at $\sqrt{s} = 546$ GeV**, PHYSICS REPORTS 154, Nos. 5 & 6 (1987) 247-383
- [Baz10] A. BAZAVOVA AND P. PETRECZKYB (THE HOTQCD COLLABORATION), **Deconfinement and chiral transition with the highly improved staggered quark (HISQ) action**, arXiv:1005.1131v1 [hep-lat] (2010)
- [Bra07] P. BRAUN-MUNZINGER, J. STACHEL, **The quest for the quark?gluon plasma**, Nature 448, 302-309 (2007)
- [Bru97] R. BRUN, F. RADEMAKERS, **ROOT - An Object Oriented Data Analysis Framework**, PROCEEDINGS AIHENP'96 Workshop, Lausanne, Sep. 1996, Nucl. Instr. and Meth A 389 (1997)
- [Car08] F. CARMINATI AND THE ALICE COLLABORATION, **The ALICE Offline Bible**, Rev. 22 (2008)
- [Col77] P.D.B. COLLINS, **An Introduction to Regge Theory & High-Energy Physics**, Cambridge University Press (1977)
- [Cow02] G. COWAN **A Survey of Unfolding Methods for Particle Physics**, Proceedings of the IPPP Workshop "Advanced Statistical Techniques in Particle Physics" in Durham (2002); www.ippp.dur.ac.uk/Workshops/02/statistics/proceedings/cowan.pdf
- [Dag95] G. D'AGONSTINI, **A multidimensional unfolding method based on Bayes theorem**, NIM A 362 (1995), P. 487-498
- [Eli11] D. ELIA, M. FLORIS, M. NICASSIO, C.LOIZIDES, M. POGHOSYAN, R. SHAHOYAN, A. TOIA, **Analysis note for first Pb-Pb multiplicity papers**, ALICE Internal Note, Rev 422 (2011)
- [Eva08] L. EVANS AND P. BRYANT (EDITORS), **LHC Machine**, JINST 3 S08001 (2008)
- [Hom06] K. HOMMA AND THE PHENIX COLLABORATION, **Search for critical points by measuring spatial correlation length via multiplicity density fluctuations**, Int. Workshop 'The Critical Point and Onset of Deconfinement' (2006)

- [Jam75] F. JAMES AND M. ROOS, **MINUIT: a System for Function Minimization and Analysis of the Parameter Errors and Correlations**, Comput. Phys. Commun. 10 (1975) 343
- [Kit05] W. KITTEL, E.A. DE WOLF, **Soft Multihadron Dynamics**, World Scientific (2005)
- [Kle04] C. KLEIN-BÖSING, **Production of Neutral Pions and Direct Photons in Ultra-Relativistic Au+Au Collisions**, PhD. Thesis, 2004
- [Gio86] A. GIOVANNINI AND L. VAN HOVE, **Negative Binomial Multiplicity Distributions in High-Energy Hadron Collisions**, Z. Phys. C - Particle and Fields 30 (1986) 391-400
- [Gro09] JAN FIETE GROSSE-OETRINGHAUS, **Measurement of Charged-Particle Multiplicity in Proton-Proton Collisions with the ALICE Detector**, CERN-THESIS-2009-033
- [Gro10] JAN FIETE GROSSE-OETRINGHAUS, KLAUS REYGERS, **Charged-Particle Multiplicity in Proton-Proton Collisions**, arXiv:0912.0023v2 [hep-ex], 24 Feb 2010
- [Mal95] S. MALIK, S.K. SONI, R.K. SHIVPURI, **Negative binomial distributions in different pseudorapidity windows in 800 GeV proton-nucleon interactions**, Z.PHYS. C 67, 239-244 (1995)
- [Mil07] M.L. MILLER, K. REYGERS, S.J.SANDERS, P. STEINBERG, **Glauber Modeling in High Energy Nuclear Collisions**, arXiv: [nucl-ex] 0701025v1 (2007)
- [Sne03] R. SNELLINGS, **Heavy Ion Collisions**, arXiv: [nucl-ex] 0310019v2 (2003)
- [Sjö06] T. SJÖSTRAND, S. MRENNNA, P. SKANDS, **PYTHIA 6.4 - Physics and Manual**, [hep-ph] 0603175, LU TP 06 13, FERMILAB-PUB-06-052-CD-T
- [Ste06] M. STEPHANOV, **QCD phase diagram: an overview**, arXiv: [hep-lat] 0701002v1 (2006)
- [Shu04] E. SHURYAK, **The QCD vacuum, hadrons, and superdense matter**, World Scientific (2004)

Bibliography

- [Tan04] M.J. TANNENBAUM, **Some Probability Distribution Functions and Their Relation: Originally part of T.Abbott, et. al., Phys. Rev. C52, 2663 (1995)**, REVIEW, BNL (2004), <http://www.phenix.bnl.gov/phenix/WWW/publish/sapin/internal/memos/SomeProbabilityDistributions.pdf>
- [Wan91] X.-N. WANG, M. GYULASSY, **hijing: A Monte Carlo model for multiple jet production in pp, pA, and AA collisions**, Phys. Rev. D 44 (1991)
- [Wik11a] WIKIPEDIA (ENGLISH), **Large Hadron Collider**
- [Wik11b] WIKIPEDIA (ENGLISH), **QCD, QCD matter, Lattice QCD**
- [Zap05] K. ZAPP, **The Soft Scattering Contribution to Jet Quenching in a Quark-Gluon Plasma and General Properties of Partonic Energy Loss**, arXiv:0511141 [hep-ph] (2005)

Erklärung:

Ich versichere, dass ich diese Arbeit selbständig verfasst habe und keine anderen als die angegebenen Quellen und Hilfsmittel benutzt habe.

Heidelberg, den 31. Mai 2011

Unterschrift:
Maren Hellwig